Short Term Regulation of Aquaporin 4 and its Role in the Transportation of Water Across Astrocytic Basolateral Membrane

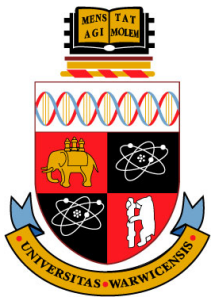

Luke Taylor

MOAC, Department of Chemistry and Division of Metabolic & Vascular Health, Warwick Medical School

A thesis submitted for the degree of

Philosophy Doctor (PhD)

2014, July

1. Reviewer: Name

2. Reviewer:

Day of the defense:

Signature from head of PhD committee:

To my Mum.

I dedicate this thesis to you. We have been through a lot over the past 4 years, and I am so proud of how you coped with your fight against cancer. You showed me to never give up, and always fight to survive, and without you this thesis and PhD would not have been possible, as it is through your support, finances and personal sacrifice, I have got to where I am today.

I hope you are proud and I look forward to celebrating the end of this chapter of our lives WHEN I graduate.

I love you more than words,

Your proud son,

Luke

Acknowledgements

I would like to acknowledge a variety of individuals who have helped me academically and personally complete this PhD and thesis.

Initially I would like to thank my family (Rosemary and Ian Taylor, and Hannah Chandler) for the continual support you have given me throughout my academic career. There is no way on earth that I would have been able to get to where I am today without your emotional and financial support. For this I am eternally grateful.

I would next like to thank my Supervisor, Alex Conner, for helping me develop my ideas and produce this piece of work. Without you this would not have been possible. You made sure that my project was continually moving forward, whilst continually challenging my ideas and assumptions at every step. You have not only enabled me to suceed and publish my work but you also helped me develop many essential transferable skills, which I will take with me in my future career.

I would like to thank the huge number of people from MOAC who have helped me through the long late nights in MOAC office (Evyenia Shaili, Kate Meadows and Vicky Marlow). I would especially like to thank Prof. Alison Rodger, for always finding time to meet, speak with me and discuss the any issues, problems, or ideas I had. You always made my position seem stronger than I ever could and you helped me find a new way forward. Without You I would not have done as well as I have.

There are four other people I owe particular thanks to.

Firstly, Mike Wooley and Holly Baum, thank you for all of your help navigating my way around the world of biology. At the start of my PhD, Biology was my least competent science, and now I feel very comfortable and capable when confronted with any biological conundrum, even co-immunoprecipitation. Good luck finishing your own PhDs and I wish you both the best for the future.

Secondly, Phil Kitchen for the work you did alongside me during your MSc project. You are a very competent scientist and challenged my knowledge and work throughout the time we worked together. I hope that the work I have done will help you develop our ideas into an excellent PhD and thesis for you in a few years time.

Thirdly, Chris Unsworth. I want to thank you for the meals, and the large number of evenings you spent helping me choose the images for my thesis. You have been instrumental in the completion of this work, and therefore my PhD. I hope that this aknowledgment will help make your efforts worthwhile. I wish you all the best with your own PhD where I hope to return the favour in 3-4 years time, York University is exceptionally lucky to have you.

Declaration

I herewith declare that I have produced this paper without the prohibited assistance of third parties and without making use of aids other than those specified; notions taken over directly or indirectly from other sources have been identified as such. This paper has not previously been presented in identical or similar form to any other British of foreign examination board.

The thesis work was conducted from 2009 to 2014 under the supervision of Alex Conner at Warwick Medical School, The University of Warwick, and Alison Rodger of MOAC, Department of Chemistry, at The University of Warwick

Coventry, United Kindom

Abstract

Aquaporin 4 (AQP4) is a tetrameric water channel protein with a pore in each monomer. AQP4 is the most abundant water channel protein in the brain, highly expressed in astrocytes. AQP4 knockout mice are protected against cytotoxic brain oedema. A cytotoxic brain oedema is where the blood brain barrier remains intact and the oedema is thought to form as a result of deterioration of cellular metabolism. There is no generally accepted current therapy for cytotoxic oedema, in part due to a lack of understanding surrounding the cellular signaling events. Work from our laboratory on a novel trigger for sub-cellular redistribution of the homologous AQP1 kidney protein has allowed us to investigate this phenomena in AQP4.

GFP tagged aquaporin constructs were created by inserting the Vector-N75 in the PcDNA-DEST47, by swapping out the ccdB gene which kills *E.coli*. The Vector-N75 doesn't contain a stop codon and is instead followed byattb attachment sites then the GFP tag sequence. The cellular relocalisation of GFP-tagged AQP4 was exposed to a hypotonic extracellular environment transfected into a live Human Embryonic Kidney (HEK293) cell line using confocal microscopy. Relative membrane expression (RME) of the AQP-GFP was measured by comparing the fluorescence intensity profiles of GFP tagged proteins across lines drawn using the image analysis software which bisect the membrane and cytosol of cells exposed to isotonic and hypotonic extracellular environments. These lines were drawn across the membrane, cytosol and opposite membrane, without bisecting the nucleus. These profile intensities were calculated using the software ImageJ. Cell volume was estimated by converting the image, in ImageJ, to a binary form, then, using the analyse particle function the cell was scanned to find the edge, an

outline drawn and the area calculated.

AQP4 rapidly and reversibly translocated to the cell surface in response to hypotonicity increasing RME from 29.3% ± 6.4% to 54.9% ± 6.6% ($p<0.05$; N=3). The cellular signaling required for this translocation response was investigated by exhibiting cells to different activation inhibitors. PKAi, Cytochalasin D, and extracellular calcium-free media were found to fully prevent the translocation and functional swelling response of HEK293 cells transfected with AQP4 (p

Motif and conservation analysis was used to identify potential PKA activation sites. These sites were substituted from serine to both alanine and aspartic acid using site-directed mutagenesis (SDM). One, highly conserved serine residue of transmembrane region 1 (TM1) at position 52, when mutated to aspartic acid (S52D) lost the hypotonicity-induced translocation and cell volume increase ($p<0.01$; N=3 in all cases). The alanine substitution (S52A) was unaffected. Molecular modeling of AQP4 and the mutant suggest a potential hydrostatic interaction with nearby cysteine and serine residues of TM2. Consequently the S52 residue was mutated to leucine, which has a similar size but no charge to form the potential hydrostatic interactions with neighboring residues. S52L also removed the translocation and functional swelling in response to hypotonicity, suggesting steric hindrance as the most likely factor inhibiting the translocation process rather than the interaction with neighboring residues.

This study demonstrates that a cellular signaling response to a change in tonicity of the cellular environment leads to AQP4 translocation to and from the cell surface. This involves the influx of extracellular calcium, the activation of PKA and cytoskeletal reorganization.

Contents

List of Figures

LIST OF FIGURES

List of Tables

LIST OF TABLES

1

Introduction

This introduction describes the different water transportation methods within the human body, how they are regulated, and what specific physiological processes they are involved in. This will identify specific mechanisms, and transportation proteins playing key roles in maintaining homeostasis. There are a specific class of proteins involved in the transportation of water in plants and mammals called aquaporins. All 13 aquaporins will be described and the research into them summarised.

1.1 Transportation of Water and Solutes Around the Human Body

Water is involved in many vital functions within the human body, which can be characterised into 5 different functions:

1. Cell life: - water is a carrier, distributing essential nutrients to cells, such as minerals, vitamins, and glucose.

2. Chemical and Metabolic Reactions: - water removes waste products including toxins that the organs' cells reject, and removes them through urine and faeces.

3. Transport of Nutrients: - water particles in the biochemical break-down of what we eat.

4. Body Temperature Regulation: - water has a large heat capacity which helps limit changes in body temperature in a warm or a cold environment. Water allows the body to release heat when ambient temperature is higher than body temperature. The body begins to sweat, and the evaporation of water from the skin surface very efficiently cools the body.

5. Lubrication: - water is an effective lubricant around joints. It also acts as a shock absorber for eyes, brain, spinal cord and even for the foetus through amniotic fluid.

6. Elimination of Waste Products: Water is excreted from the body in the form of urine. Water is used in urine as a solute and transporter of waste products, such as toxins and unwanted ions.

As a result of water's ubiquitous presence in the body, it is evident that a highly sophisticated transportation system must exist to deliver water to every tissue and cell in the human body, (1) (2). This is exemplified by urine concentration in the kidney (3), formation of tears in nasolacimal ducts (4), and secretion of saliva from salivary glands (5). The transcellular transportation of water is typically as a result of osmotic stimuli often owing to the transportation of salts (6).

1.1.1 Methods of Solute Transportation

There are two main methods by which transmembrane proteins are able to transport solutes across plasma membranes: active transport and passive transport. Active transport is the movement of an ion/molecule across a lipid bilayer against the concentration gradient, with the aid of energy from the system. However, passive transport (facilitated diffusion) is the spontaneous transport of an ion/molecule across a lipid bilayer down the concentration gradient without the aid of energy from the system. Figure 1.1 shows the classification of these transmembrane proteins based and their transportation method and selectivity.

1.1.1.1 Active Transport

Active transport can occur by two different methods, primary active transport and secondary active transport both of which are performed by specific transmembrane

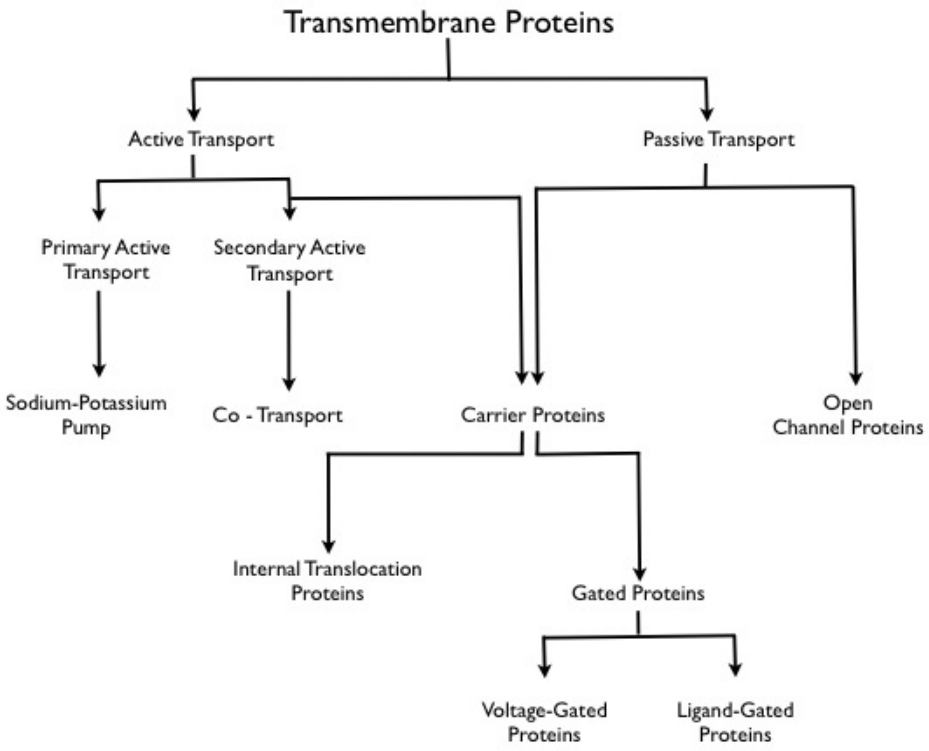

Figure 1.1: Transmembrane Protein Classification - The figure shows the classification of the different types of transmembrane proteins and their functionality

proteins.

Primary Active Transport or Direct Transport, directly uses Adenosine Triphosphate (ATP) to transport molecules across the membrane. This is usually performed by transmembrane ATPases, with the most characterised being the sodium potassium pump.

Secondary active transport, unlike primary active transport, does not require the direct coupling of ATP. It relies on the electrochemical potential difference caused by a primary active transport system. These secondary active transport proteins can again be divided into two subcategories, antiport and symport. Antiport proteins, have different molecules attached on opposite sides of the membrane. When both are attached, this activates a conformational change allowing for the simultaneous transportation of molecules across the membrane in opposite directions. In contrast, symport proteins transport two molecules but from the same side of the membrane in the same direction.

1.1.1.2 Passive Transport / Facilitated Diffusion

There are two main classes of proteins, which undergo facilitated diffusion, channel proteins, and carrier proteins. Channel proteins, are intrinsic proteins which span the lipid bilayer. They can actively select for a specific molecule by having amino acid sequences which ensure that only certain types of molecule can enter the channel, however, some can be ambivalent to the structure of the molecule, and only differentiate by size. Carrier proteins on the other hand are very selective and can be further characterised. There are two main forms of carrier proteins; intrinsic gated proteins and extrinsic proteins. On binding of the molecule of interest gated proteins change their conformation and transport the molecule/ion across the membrane down the concentration gradient, whereas the extrinsic proteins transport a molecule/ion across the lipid bilayer by internal translocation. Internal translocation is an active transport mechanism, and does require energy from the system, as it is always against the concentration gradient. Gated proteins can be further characterised into Voltage-Gated and Ligand Gated proteins. Voltage-Gated ion proteins are activated by changes in electrical potential differences near the channel. They are predominantly found in neurones, however, are

common in other cells. Their structure comprises of several subunits with a central pore through which ions can travel down their electrochemical gradient. Ligand-Gated transport proteins open and close in response to the binding of a chemical messenger/ligand, independent of the ion they are transporting, and they are usually very selective to one or more ions (Na^+, K^+, Ca^{2+}, or Cl^-). Unsurprisingly transport by channel proteins is much faster than that of carrier proteins.

1.1.2 Transcellular Transportation of Water

As already discussed transcellular water flow, like any transcellular movement, is dependent on the permeability of the plasma membrane. There are three main methods by which water can move, passive co-transport, osmosis, and aquaporin transportation. Many people would think that simple diffusion should be documented in this section, however, diffusion is the process by which molecules intermingle in space, as a result of their kinetic energy. If molecules of water were to diffuse they would come in contact with the barrier and rebound away. Although, if the barrier was removed the brownian motion of the molecules would encourage the two solutions to mix until water was evenly distributed. Therefore, water cannot move across plasma membranes via diffusion, which is why this method will not be discussed any further in this section.

There is a lot of controversy around true co-transportation of water, as many believe the flow is osmotic due to an increase in osmolarity. However, molecular dynamic simulations performed by Choe *et al* (7) showed that a significant number of water molecules cross the plasma membrane through the sugar-binding site in the presence and absence of galactose for a sodium dependent galactose co-transporter vSGLT. They identified that 70-80 molecules of water accompany galactose as it moves from the binding site into the intracellular space. During this, the majority of water molecules are unable to diffuse around the galactose, resulting in water being pushed into the intracellular space and replaced by extracellular water. This supported the notion that co-transporters acted as both passive water channels and active water pumps with the transported substrate acting as a piston to rectify the motion of water (7). These finding have been further substantiated by Santacroce *et al* and their investigations

into wild type and mutagenised amino acids co-transporters and their permeability to water.

Osmosis is the diffusion of water through a semipermeable membrane from an area of low solute concentration to an area of high solute concentration, until the concentration on both sides is equal or more scientifically put the system reaches equilibrium. Osmosis does also not require the addition of energy, in the form of ATP.

1.2 Aquaporins

For many years it was assumed that all biological membrane's permeability allowed for the osmotic motion of water down its concentration gradient, making the mere notion of a family of water channel proteins to be absurd. However, biophysical studies in eurythrocytic kidney tubules between 1960 and 1990, revealed that some membranes were more permeable to water than others. This gave rise to proposals suggesting that water movement may be through pore-like structures. This consequently led to experimental investigations resulting in the identification of the first water channel, aquaporin 1 (AQP1), in 1992 by Preston and Agre, (8), for which Agre, jointly, won the 2003 Nobel prize in chemistry. AQP1 was found to have little similarity to other known proteins except for the Major Integral Protein (MIP) of lens fibre, which was consequently named AQP0. This lead to a flurry of research trying to identify more AQPs in animals, yeast, bacteria and plants, with so far, 13 AQPs being identified in humans.

1.2.1 Aquaporin Structure

High resolution X-ray crystal structures have been determined for several mammalian AQPs. Each 30kDa AQP monomer comprises six tilted transmembrane helices and two half-helices that extend into the inner and outer leaflets of the lipid bilayer. Four AQP monomers coordinate and interact to form tetramers in the plasma membrane, see Figure 1.2.

Structural data, coupled with mutagenesis, and molecular dynamics simulations have identified two highly conserved asparagine-proline-alanine motifs (NPA motif)

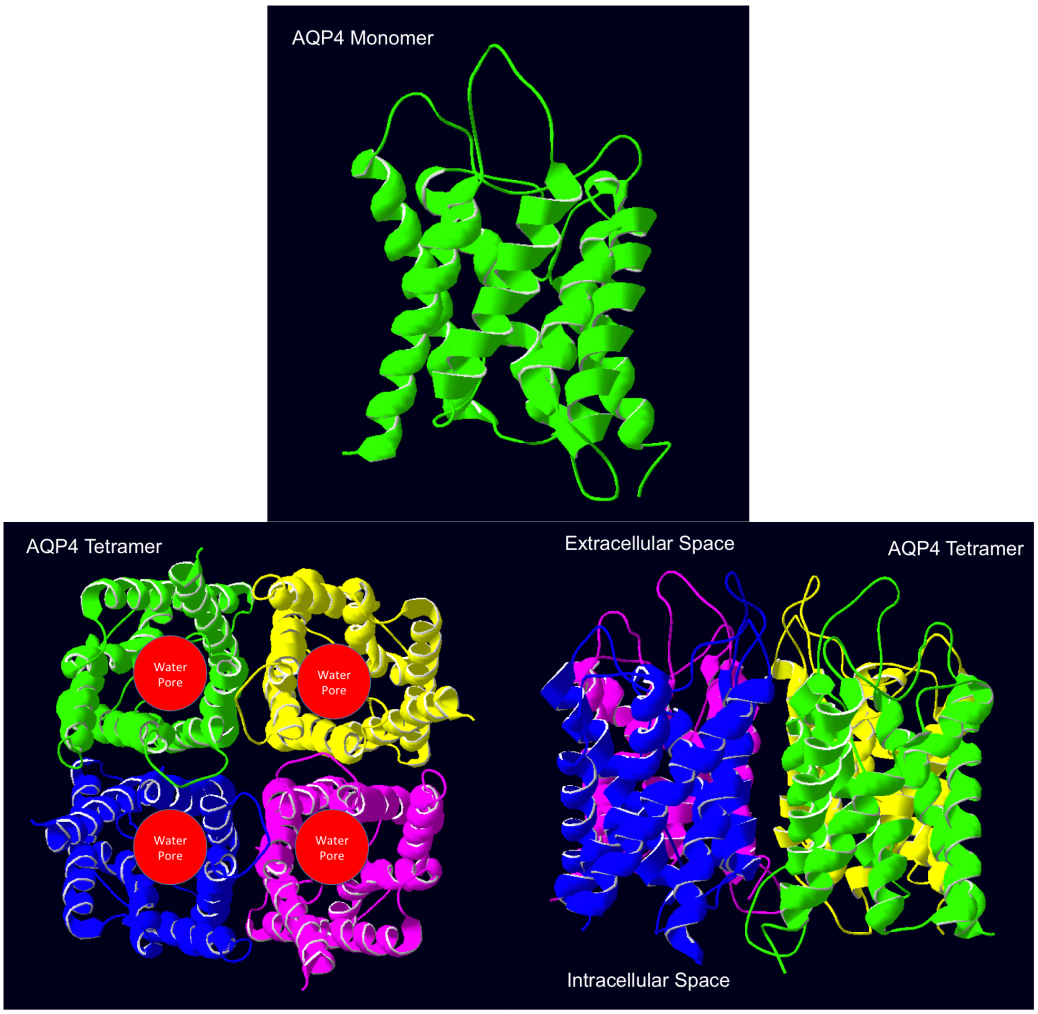

Figure 1.2: Aquaporin 4 Monomeric and Tetrameric Structure - Monomeric and Tetrameric Structure of AQP4 with each colour representing one of the monomers (9), and the red circles representing the location of the water pores.

4.1, at the entrance and exit of each narrow pore, to be crucial for water transport and selectivity (10), (11). These motifs form hydrogen bonds with water molecules in the pore, whilst also maintaining steric blocking of the passage towards other large molecules. The single file orientation through the protein, and the coordinated rotation of hydrogen ions towards the exterior of the pore, prevents the conduction of protons (hydrogen ions) via the Grotthuss mechanism (12). In 2000, Verkmann and Mitra (13), found that plasma membranes expressing AQPs had an ∼5 to ∼50-fold higher osmotic water permeability than membranes without. Some AQPs have been identified to transport glycerol, and are subsequently named aquaglyceroporins. Aquaglyceroporins have a less constricted pore (3.4$\mathring{A}$), and more hydrophobic residues lining that pore, compared with that of water-selective AQPs (2.8$\mathring{A}$) (14).

1.2.2 Characterisation of Different Aquaporins and Their Functionality

Over the past 40 years aquaporins have been identified throughout the human body, in a number of different tissues. Each tissue is specific to its function and therefore needs to be permeable to a variety of different molecules. So far, 13 AQPs have been characterised along with the molecules they transport, as shown in table 1.1 and figure 1.3, however, this does not mean that more can not be discovered, in the future. Many AQPs have been extensively researched owing to the molecules they transport and the tissues they are expressed in. This section will discuss the impact of those specific areas of research, identifying similarities and differences between the 13 AQPs.

1.2.2.1 Aquaporin 1

Agre *et al* (37), identified the first water channel protein, which was initially named CHIP28 (channel like integral protein). The discovery was made in pursuit to identify the Rh blood group antigens. One of the Rh antigens was isolated from the radiolabeled red blood cell membranes hydroxylapatite chromatography and was found to be approximately 32kDa (38). The protein did not stain well with Coomassie Blue, however when silver reagent was used, another protein of 28kDa was detected. Initially it was thought that the protein was a fragment of the 32kDa protein, however, further characterisation identified that an antibody for the 28kDa protein, did not bind to

Aquaporin	Location in the Body	Molecules Transported
0	Lens Fibre Tissue	Water
1	Erythrocytes, Renal Tubules, Retinal Pigment Epithelium, Heart, Lung, Skeletal Muscle, Kidney, Pancreas, Brains, Placenta, and Liver	Water and NH_3
2	Renal Collecting Duct	Water
3	Epithelial Cells of Collecting Ducts, Epithelial Cells of Airways, Keratinocytes, and Immature Dendritic Cells	Glycerol and Water
4	Brain, Heart, Kidney, Lung, Trachea	Water, CO_2, and NH_3
5	Mouth, Tear-ducts, and in Pulmonary Secretion Tissue	Water and NH_3
6	Loop of Henle	Anions and Water
7	Adipose Cells	Water, Glycerol, and Urea
8	Pancreas, and Colon	Water
9	Peripheral Leukocytes, Liver, Lung, and Spleen	Water, Glycerol, Urea, and also permeable to other solutes
10	Duodenum, and the Epithelial cells at the tips of villi in the Jejunum	Water, Glycerol, and Urea
11	Intracellular in Proximal Tubules	Water
12	Pancreas	Water

Table 1.1: Localisation of all Characterised AQPs in the Human Body, (15), (16),(17), (18), (19), (20), (21), (22), (23), (24), (25), (26), (27), (28), (29), (30), (31), (32), (33), (34), (35).

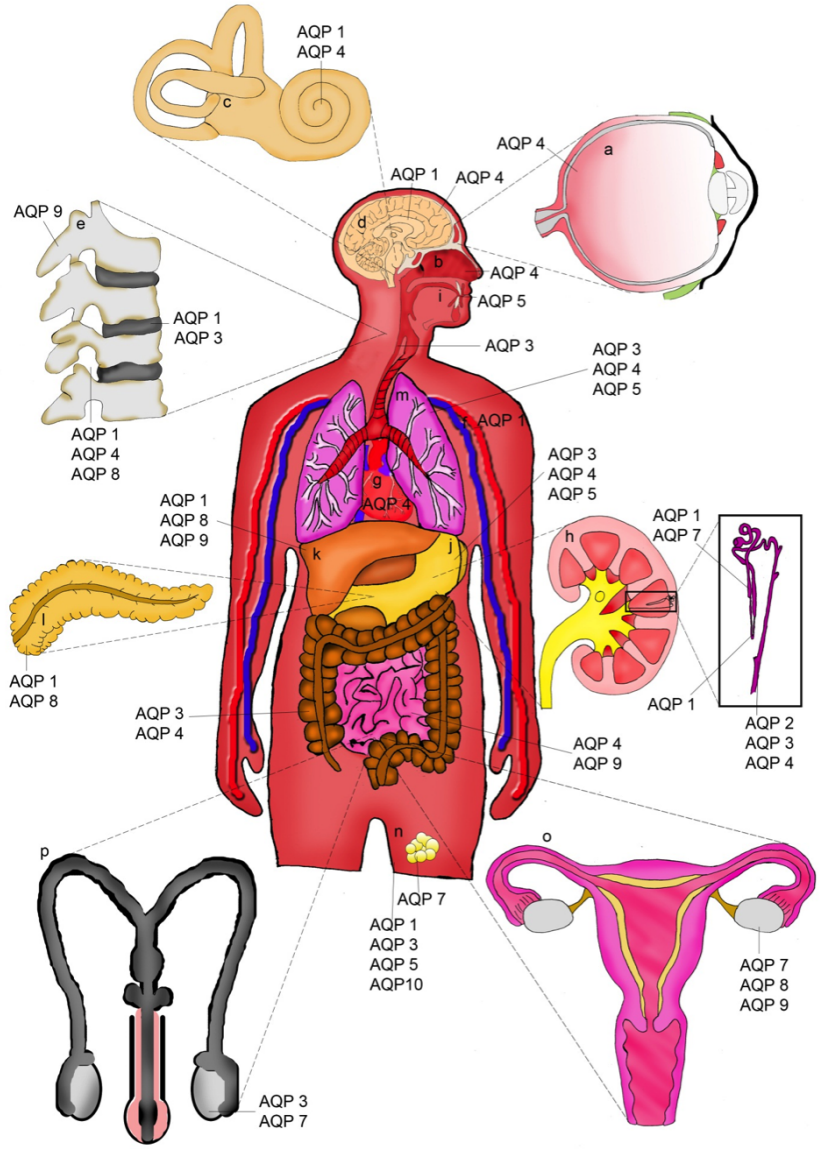

Figure 1.3: AQP expression in humans - a)Retina-AQP4 b)Olfactory epithelium-AQP4 c)Inner ear-AQP 4, 1 d)Astrocytes-AQP4. Choroid plexus-AQP1 e)Spinal cord-AQP 1, 4, 8. Nucleus pulposus-AQP 1, 3. Osteoclasts-AQP9 f)Blood endothelium-AQP1 g)Heart-AQP4 h)Kidney-AQP 1, 2, 3, 4, 7 i)Salivary glands-AQP5 j)Intestinal tract-AQP 3, 4, 5, 9 k)Liver-AQP 1, 8, 9 l)Pancreas-AQP 1, 8 m)Lungs-AQP 3, 4, 5 n)Adipocytes-AQP7. Skin-AQP 1, 3, 5, 10 o)Ovaries-AQP 7, 8, 9. p)Sperm Cells-AQP 3, 7, (36).

the 32kDa protein. Denker *et al* (39), was the first to name the protein CHIP28 as it resembled the physical properties of an integral membrane channel protein.

1.2.2.2 Aquaporin 2

The discovery of AQP 1 sparked the idea that there may be more AQPs in the human body regulating water permeability. Further investigation resulted in the isolation of the full-length cDNA and subsequent functional assay in oocytes. Four months later the confirmation of its immunohistochemical localisation with newly generated antibodies was established, (40). This newly identified channel protein demonstrated 42% amino acid homology with AQP1 (CHIP28). This protein was exclusively localised to the apical and subapical regions of the principal cells and intracellular vesicles of the renal collecting ducts, (41). This newly identified water channel protein was named AQP2 and is the only AQP known to always be regulated by vasopressin(42), (43). Vasopressin is a neurohypophysial hormone, found in most mammals, with its main function to retain water in the body and constrict blood vessels. Vasopressin type 2 receptors found in the basolateral membrane of the renal collecting duct, bind vasopressin after its release is triggered by the increase in serum osmolarity and a reduction in the circulating blood volume, (44), (45), (46). The binding of vasopressin to its receptor causes a transformation of the G Protein-Coupled Receptor (GPCR) to release the coupled adenylate cyclase. Adenylate cyclase catalyses the conversion of ATP to cAMP. cAMP then causes activation of PKA which leads to the phosphorylation of AQP 2 at Serine^{256}, (47), (48). At least three of the four monomers in the AQP2 tetramer must be phosphorylated at Ser^{256} for successful cell surface localisation, indicating the importance of phosphorylation at this site (49). This phosphorylation event is required for AQP2 to be translocated, along the microtubules from intracellular storage vesicles to the apical membrane see figure 1.4, (50), (51).

Owing to technological advancement, large scale proteomic analysis has led to remarkable progress in the field of phosphorylation site identification. Hoffert *et al* (52), identified 714 phosphorylation sites on 223 unique phosphoproteins in isolated rat inner medullary collecting duct segments, and found that for the first time three new serine phosphorylation sites had been discovered at serine 261, 264, and 269 in addition to

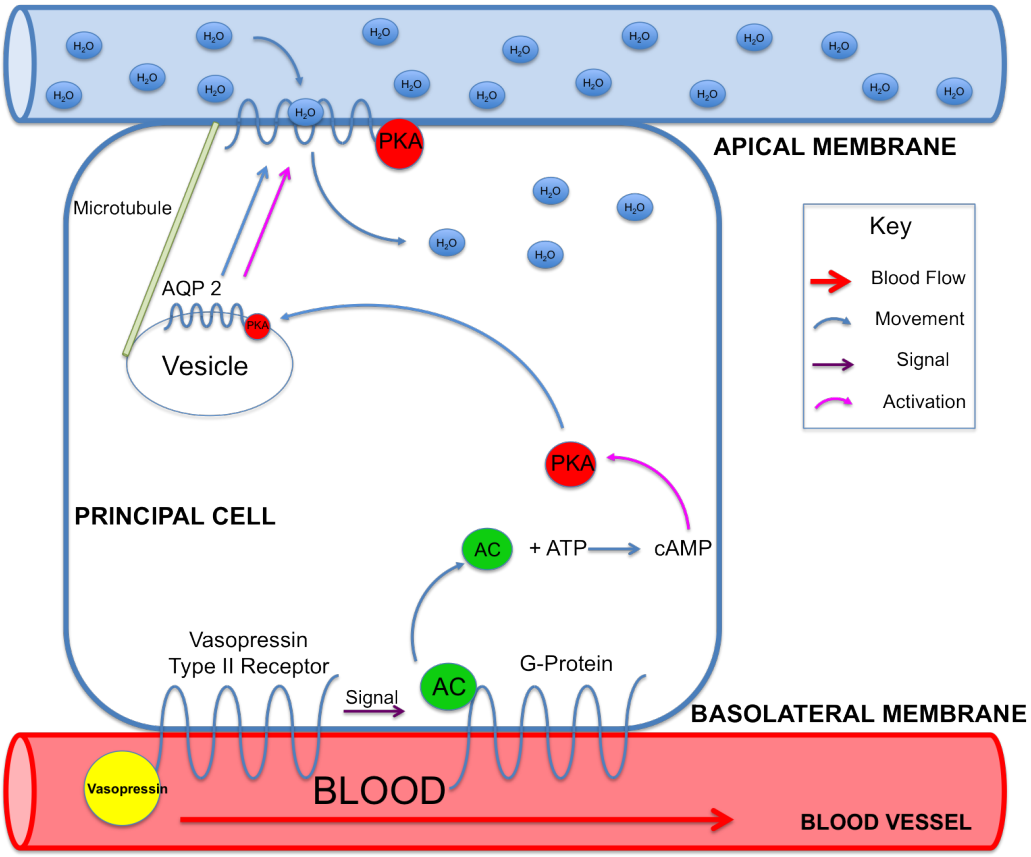

Figure 1.4: Vasopressin Signalling Cascade, Activation, and Translocation of AQP2 - Schematic representation of the vasopressin signalling cascade to facilitate the readsorption of water from the renal collecting duct into the blood stream. Vasopressin in the blood binds to the vasopressin type II receptor, which signals to the neighbouring GPCR. GPCR then undegoes a conformational change releasing Adenylate Cyclase (AC in green circle). Adenylate Cyclase, with the use of ATP, produces cAMP which then, activates PKA. PKA phosphorylates AQP2 in intracellular vesiclas at the S^{256} phosphorylation site. This phosphorylation then activates the translocation of AQP2 along the microtubules and inserts the protein into the apical membrane. AQP2 then facilitates the transport of water from the renal collecting duct into the principal cells down the concentration gradient.

known serine 256 in the c-terminus of AQP2. Subsequent studies have shown that vasopressin increases phosphorylation at Ser^{264} and that this phosphorylation event also translocated AQP2 to the plasma membrane (53). Alternatively vasopressin was found to decrease the phosphorylation of Ser^{261} and the localisation of phosphorylated Ser^{261} AQP2 differed from that of phosphorylated Ser^{256} AQP2, (54). However, another report by Lu *et al* (55) showed no effect of Ser^{261} phosphorylation on AQP2 translocation. Quantitative phosphorylation analysis identified that Ser^{256} phosphorylated AQP2 is more constitutively expressed and not responsive to vasopressin, and that Ser^{269} expression in the apical membrane increases in response to vasopressin, (56). This suggests that Ser^{269} phosphorylation is essential for membrane retention, (57). However, phosphorylation of Ser^{264} and Ser^{269} depends on the phosphorylation of Ser^{256} for AQP2 translocation to the apical plasma membrane, and retention once in situ, (58). In contrast, Ser^{256} phosphorylation is not dependent on any other phosphorylation event, indicating that Ser^{256} is the most important phosphorylation site of AQP2,(41).

1.2.2.3 Aquaporin 4

AQP4 has been identified to be heavily expressed in astrocytes and throughout the central nervous system (CNS), with an increased expression at brain-fluid interfaces such as the blood brain barrier and ependymal-CSF barriers. Unlike AQP1 and AQP2, AQP4 further assembles into supramolecular arrays of particles, which are maintained by inter-tetrameric N-terminal interactions involving specific residues (59). AQP4's monomeric structure is illustrated in figure 1.2 and the complete primary amino acid sequence illustrated in figure 4.1.

Manley *et al* found that mice with water intoxication, ischaemic stroke, cytotoxic brain oedema and bacterial meningitis had brain swelling, however, AQP4 null mice improved outcome and reduced brain water accumulation compared with that of wild-type (60) (61). In contrast Vasogenic oedema, involves the movement of water into the brain via a leaky blood brain barrier, which then exits through the AQP4-rich glia limitans, which line the ventricles and the surface of the brain. AGP4 knock-out mice demonstrated a worse clinical outcome and greater brain water retention in models of vasogenic oedema including, intraperenchymal fluid infusion, cotical-freeze injury,

brain tumour and brain abscess, (62) (63).

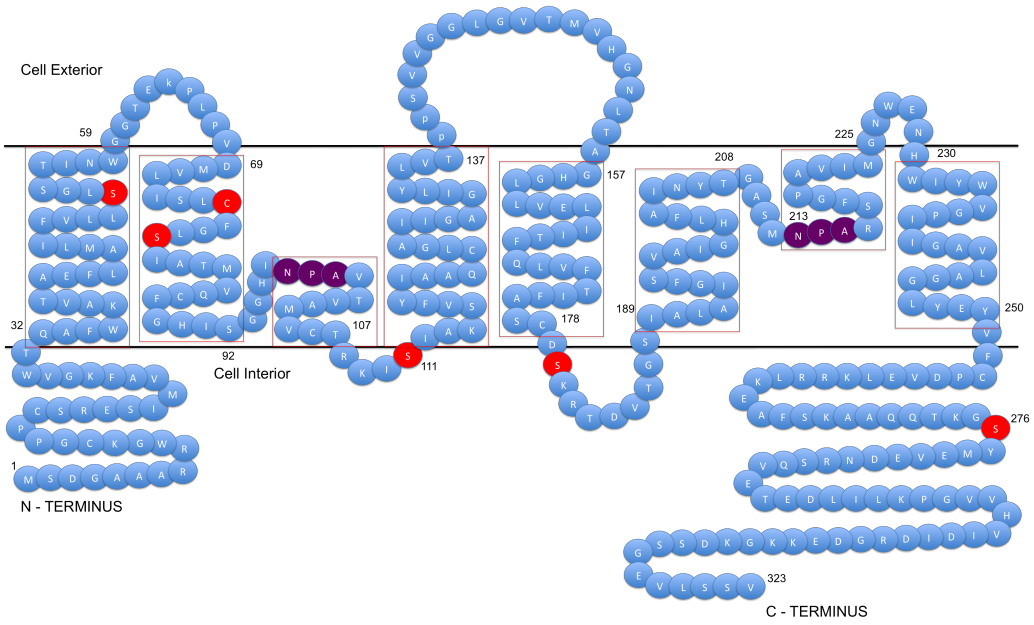

Figure 1.5: Primary Amino Acid Structure of AQP4 - Schematic representation of the primary amino acid structure of AQP4. Purple amino acids mark the NPA motifs and the red boxes indicate the assumed helical structures, (64).

AQP4 has also been identified to play a role in the inner ear, olfactory receptor neurons, and the retina, as AQP4 null mice showed impaired vision (65), hearing (66), and olfacation (67). AQP4 deficient brains also have a reduced seizure threshold and a prolonged seizure duration (68). Although AQP4 has been identified as playing an important part in many of these disorders, exactly how it does so has not been understood. This gives excellent opportunity for further research in this area.

1.2.2.4 Aquaglyceroporins

AQP3, AQP7 and AQP9 have all be identified as aquaglyceroporins. This means that they have been found to transport both water and glycerol. Studies have even suggested that AQP9 can transport other small polar solutes, such as sugars, amino acids, and ammonia (69), (70), (71). AQP3 has been identified as playing a key role in skin

hydration and fat metabolism. Ma *et al* in 2002 (72), established that AQP3-facilitated glycerol transport in the skin is an important determinant of epidermal and stratum corneum (the outermost layer of the skin) hydration. They did this by using knockout mice which demonstrated reduced hydration of the statum corneum, and skin elasticity. This, they found to be as a result of their being a reduced amount of glycerol, which acts as a 'humectant' or a water-retaining osmolyte (Hara *et al.*, 2002, (73)). Hara and Verkaman in 2003 (74) , then found that if you systematically normalised glycerol content in the stratum corneum and epidermis then the skin hydration defect was corrected. AQP7 on the other hand has been identified as having a role in obesity, as it is expressed in the plasma membrane of adipocytes. AQP7-null mice demonstrated an increase in fat mass and adipocyte hypertrophy (the accumulation of glycerol and triglycerides) as they age (75), (76). Hara - Chikuma *et al* and Hibuse *et al* also suggest that altering AQP7 expression and/or function in adipocyte, could change fat mass. Maeda *et al* (77) suggested that AQP9 was a key regulator of hepatic glycerol uptake and a key metabolic regulator in diabetes and obesity. Although many of these studies have demonstrated the role of AQPs, it hasn't fully explained the regulation of these processes and how the AQPs are involved.

1.2.3 Cell Volume Regulation

Cell volume regulation (CVR) is a necessary mechanistic component of AQP mediated transcellular water flow 1.6. It comprises of regulatory volume decrease (RVD), usually in response to hypotonicity-induced cell swelling, and regulatory volume increase (RVI), usually in response to hypertonicity-induced cell shrinkage. The molecular mechanisms underlying these responses are not yet fully understood, but it is unlikely that there is a single common mechamism. The signalling pathways associated with CVR appear to be cell-type dependent. Nonetheless, the end results of these varied pathways are the same: RVD relies on lowering intracellular osmolality by removal of potassium chloride and taurine (a sulfonic acid with roles in cardiovascular and muscular function) from the cell whereas RVI is achieved by increasing intracellular osmolality via import of sodium to the cell.

1.2.3.1 Regulatory volume decrease

In RVD, the activation of K^+ channels allows efflux of K^+ from the cell and subsequent water loss by osmosis either through AQPs or directly through the lipid bilayer. This can be both $[Ca^{2+}]_i$ dependent (e.g in human cervical cancer cells) or $[Ca^{2+}]_i$ independent (e.g. Ehrlich ascites tumour cells). In most cell types an intact actin cytoskeleton is necessary for hypotonicity-induced K^+ efflux. However, in trigeminal ganglion neurons, cytochalasin D (an actin polymerisation inhibitor) treatment stimulated swelling activation of a K^+ current demonstrating that in these cells, an intact actin network is not only unneccessary for RVD, but appears to be inhibitory. In some cells, protein kinase C (PKC) activation has also been shown to induce an outward K^+ current via the same channels that are activated in RVD. Movement of K^+ out of the cell is favoured by the concentration gradient but to maintain the electrostatic membrane potential, volume-regulated anion channel(s) (VRAC) simultaneously move anions (mainly Cl^- during RVD) out of the cell, probably activated by tyrosine kinases. It is also thought that four K^+-Cl^- cotransporters (KCCs), known to be activated by cell swelling, may be involved.

1.2.3.2 Regulatory volume increase (RVI)

In RVI, the main effect involves the activation of Na^+-H^+ exchangers and Na^+-K^+-$2Cl^-$ cotransporters (NKCCs) causing influx of Na^+ to the cell and subsequent volume increase by osmotic movement of water. The Na^+-H^+ exchange pump NHE1 is known to be activated by cell shrinkage, which may be mediated by binding of calmodulin to the C-terminus. The cotransporter NKCC1 is known to be activated by cell shrinkage, potentially through lysine-deficient protein kinase 1 (WNK1) and proline/alanine-rich protein kinase (SPAK) signalling. Amiloride-sensitive non-selective cation channels (NSCCs) could also play a role.

1.2.4 The Regulatory Role of Aquaporin

Any rapid change in cell volume is thought to be mediated by water movement through AQPs, although it is possible that cell membrane water permeability is not the rate-limiting factor in CVR. However, the role of AQPs in volume regulation may go further than simply acting as a passive mechanism by which membrane water permeability is

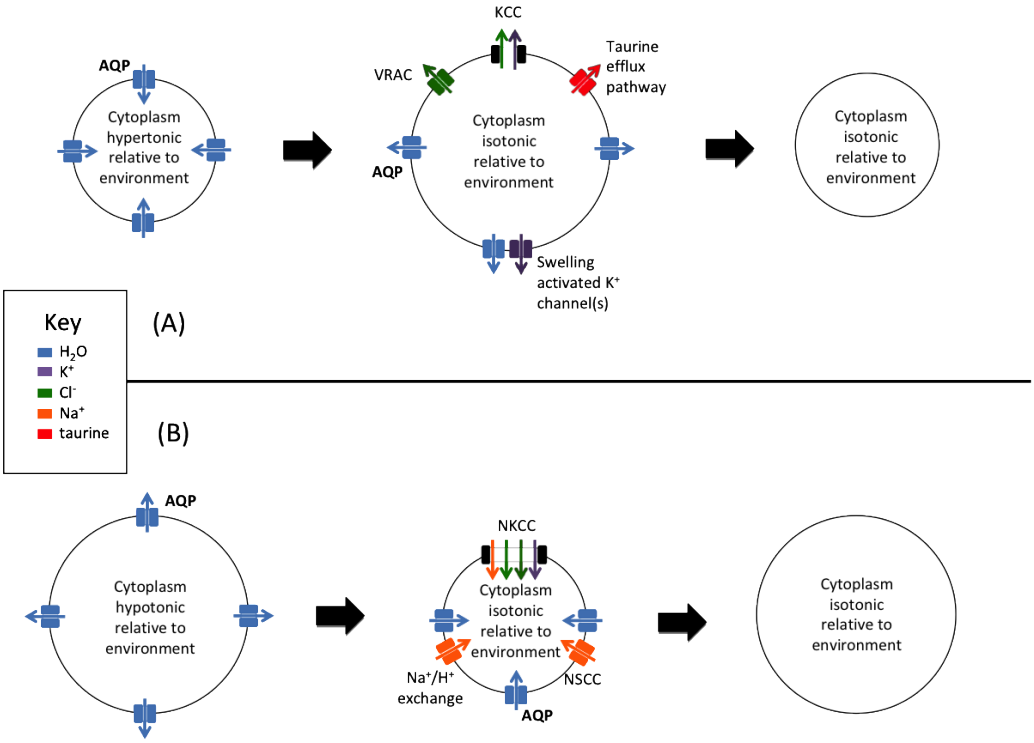

Figure 1.6: Solute transport pathways mediating (A) regulatory volume decrease and (B) regulatory volume increase - Water movement by osmosis may be through aquaporins or directly through the cell membrane depending on the cellular AQP isoforms and expression levels. KCC: potassium chlorine co-transporter. NKCC: sodium potassium chlorine co-transporter. VRAC: volume regulated anion channel. NSCC: non-selective cation channel, (36).

increased. For example, the stretch-activated transient receptor potential vanilloid type 4 (TRPV4) channel is a Ca^{2+}-biased NSCC that is activated by cell swelling and has been implicated in osmosensing. In some cell types TRPV4 has been shown to provide a Ca^{2+} signal that is correlated with activation of the K^+ and Cl^- channels responsible for the decrease in cellular osmolality associated with RVD. In human and murine salivary gland cells, TRPV4 has a functional interaction with AQP5: in AQP5 knockout cells, the hypotonicity-induced calcium influx through TRPV4 was attenuated and subsequent RVD was abolished. Hypotonicity also increased cell surface expression of both TRPV4 and AQP5 and increased their co-localisation.

Upon entry into the female reproductive tract, sperm encounter a decrease in extracellular osmolality. This hypotonic stress is thought to be the signal that activates sperm motility. However, the hypotonic stress also causes cell swelling which, if left uncorrected by RVD, leads to impaired fertilisation caused by excessive bending of the sperm tail inside the uterus. The sperm of AQP3 -/- mice do not undergo their normal RVD process and the mice display reduced fertility. If AQP3 were simply acting passively as a water pore, RVD would not be abolished but rather the timescale on which the cell reaches osmotic equilibrium would be increased. In order to explain these observations AQP3, either alone or as part of a macromolecular complex, might be involved in the signalling pathway that activates RVD in sperm.

Renal cortical collecting duct cells (RCCDs) which do not endogenously express AQP2, when exposed to a hypotonic extracellular solution swell in proportion to the change in extracellular osmolality but do not have an RVD. However, when they are transfected with AQP2, these cells show an RVD of approximately 40%. This shrinkage is mediated by Ca^{2+} influx through TRPV4, which activates Ca^{2+}-dependent Ca^{2+} release from intracellular stores and Ca^{2+}-dependent K^+ and Cl^- channels. In cells expressing AQP2, hypotonic stress causes translocation of TRPV4 to the plasma membrane. This translocation is absent in AQP2-negative cells. There does not appear to be any co-localisation between endogenous TRPV4 and overexpressed AQP2 in this system, either before or after hypotonic shock, indicating a functional rather than physical interaction. These observations imply that AQP2 (and therefore possibly other members of the AQP family) forms part of a sensory and signalling pathway that results in

TRPV4 translocation, possibly via sensing of extracellular osmolality.

Taken together, these examples support the idea of a signalling or sensory role for AQPs in RVD mechanisms. We have been unable to find any evidence of AQPs playing similar roles in RVI. However, given that a variety of AQPs could be involved in the RVD mechanism and that RVI and RVD are closely related osmoadaption mechanisms, it would not be surprising to discover a link between RVI and AQPs that goes beyond a passive water conduction mechanism.

1.3 Cerebral Oedema

A cerebral oedema is a relative increase in the water content of the brain and this may be either in the intracellular, extracellular, or both compartments. This causes swelling in the brain, and pressure to build within the skull, damaging brain tissue. This disorder is thought to be governed by the specific control of water by aquaporins, however, as this review may suggest, this hypothesis is as yet unconfirmed, allowing for areas of further investigation. There are two other causes of brain swelling, vascular congestion and hydrocephalus, however, neither of these are due to oedema, although, are often diagnostically confused.

A cerebral brain oedema can be classified into four different classes of brain oedema, vasogenic, cytotoxic, osmotic and interstitial; classified based on causality.

1.3.1 Vasogenic Oedema

A vasogenic oedema occurs owing to a breakdown of the tight endothelial junctions which make up the blood-brain barrier (BBB). The disintegration of the BBB allows intravascular proteins and fluid to penetrate into the parenchymal extracellular space. Once plasma constituents cross the BBB, the oedema spreads, which can be a rapid and extensive process. As water enters the white matter, it moves extracellulary along fibre tracts and can also affect gray matter. This type of oedema may results from trauma, tumours, focal inflammation, late stages of cerebral ischemia, and hypertensive encephalopathy. Subtypes of vasogenic oedema are: hydrostatic cerebral oedema, cerebral oedema from a brain cancer, and high altitude cerebral oedema.

1.3.1.1 Hydrostatic

The term hydrostatic cerebral oedema was first introduced by Ishii et al (78) in 1985. He found that hydrostatic cerebral oedema, resulted from unfavourable hydrostatic pressure gradients between blood vessels and brain tissue. This gradient increased hydrostatic pressure causing tissue damage resulting in the biphasic opening of the BBB. This type of oedema is a typical problem during certain brain surgery procedures, such as craniectomies and is heavily researched.

1.3.1.2 Brain Cancer/Tumour

Cancerous glial cells (glioma) of the brain, can increase secretion of vascular endothelial growth factor (VEGF), which weakens the junctions of the BBB, which inturn causes the formation of a cerebral oedema

1.3.1.3 High Altitude Cerebral Oedema

High altitude cerebral oedema (HACE) is a severe form of altitude sickness, and almost always begins with acute mountain sickness (AMS). HACE is the result of swelling in the brain which is frequently fatal, however there are many hypothesese of its true physiological cause.

In 1975 Houston and Dickinson proposed that the hypoxia caused by the high altitude might impair cell membrane ion-channel active transport of sodium by decreasing the supply of ATP, thereby leading to cell swelling (79). However, in 1995 Severinghous *et al*, stated that HACE occurs at level of tissue oxygenation compatible with relatively normal cerebral functioning, whereas, in experimental hypoxia, ATP depletion occurs long after all neuronal activity has been lost (80). Previously in 1975 Lassen and Harper, hypothesised that the elevated capillary pressure due to hypoxic vasodilation and high cerebral blood flow (CBF) caused hydrostatic capillary leak. This theory is however, problematic as to the normally unique impermeability of brain capillaries. These theories are consistent with present thinking in that the main contributor is hypoxia, and that the end result is a combination of peripheral responses, which reach the brain and influence BBB permeability, cerebral oedem and cerebral blood volume causing increased intracranial pressure.

1.3.2 Osmotic Oedema

An osmotic brain oedema is caused by osmotic imbalances between blood and tissue. The speed at which these osmotic imbalances develop is of particular importance as concentration or dilution of osmolarity within the brain can only be compensated if osmolar gradients develop slowly. In a clinical setting the syndrome of inappropriate secretion of anti-diuretic hormone generates an osmotic imbalance known as serum hyposmolarity, which in turn causes an osmotic brain oedema. This is, however, not the only way in which an osmotic oedema can manifest. If cerebral tissue is in a hyperosmolar state, often formed post cerebral ischemia, an osmotic oedema can also manifest. Under such conditions, reperfusion with isotonic fluids may cause an additional water flux into the reperfused tissue (81), and (82).

1.3.3 Interstitial Oedema

An interstitial oedema occurs when the ventricle cavities containing cerebrospinal fluid (CSF) become obstructed preventing absorption into the bloodstream. This causes fluid to build up inside the ventricle and puts pressure on adjacent brain tissue, which is known as obstructive hydrocephalus. This results in trans-ependymal flow of CSF, causing CSF to penetrate the brain and spread to the extracellular spaces and the white matter. Interstitial cerebral oedema differs from vasogenic oedema as CSF contains almost no protein.

1.3.4 Cytotoxic Oedema

A cytotoxic brain oedema is different from the oedemas previously discussed, as the BBB remains intact. The oedema forms owing to disruption in cellular metabolism, impairing the function of sodium and potassium active transport pumps in the glial cell (astrocyte) membrane. This results in cellular retention of sodium and water. This mechanism has been investigated thoroughly however, without any true conclusions. The cytotoxicity can evolve from a number of different causes, Reye's Syndrome, severe hypothermia, early ischemia, encephalopathy, early stoke, hypoxia, cardiac arrest and pseudotumor cerebri. Nearly all of theses disorders involve reducing the amount of oxygen available to cells, essentially causing a localised hypoxic episode.

Nagelhus *et el* in 1999 (83), identified AQP4 as being present in the end feet of astrocytes. Physiologically AQP4 is thought to work with inward rectifying potassium channel Kir4.1, co localising with AQP4 in astrocytes. This clears both channel proteins of water, during high neuronal activity, from the extracellular compartment to neighbouring astrocytes and furthermore to the astrocytic syncytium. This hypothesis has however been challenged, owing to the fact that dissociation of AQP4 from Kir4.1 expression can occur, and that AQP4 is a bidirectional water channel protein (84). The most significant finding relating to oedema development is that AQP4 localisation in astrocytic end feet is dystrophin regulated as dystrophin-null mice showed delayed brain oedema development indicating a reduction in AQP4 expression in astroglial end feet but unaltered total AQP4 protein (85).

Although these discoveries seem to contradict each other, there is a common concensus that decreased AQP4 expression counteracts progression of brain oedema as AQP4 null mice showed significantly reduced brain oedema and decreased mortality after water intoxication, as well as following the middle cerebral artery ligation, while the BBB remained intact (60). Furthermore astrocytic AQP4 have been specifically identified to be involved in traumatic cytotoxic brain oedema. Marmoarou *et al*, Doppenberg *et al*, and Amorini *et al*, demonstrated that IV radioactive labeled sodium ions increased after traumatic brain injury, which was cleared intracellularly as tissue microdialysis fluid did not show an increase in sodium (86) (87) (88).

While AQP4 is able to drive cytotoxic brain oedema we still lack a full understanding of the role of AQP4 under pathological conditions. Moreover, the functions of AQP 1, 5, and 9 also located in astrocytes (Arima et al., 2003 (89); Badaut et al., 2001 (90), 2002 (91), 2003 (92), ; Yamamoto et al., 2002(93), are unknown, and the interaction of AQP's located in close neighbourhood to astrocytes (e.g. ependyma, neurons, blood vessels) structures, as well as the significance of tetrameric assembling of both AQP4 splice variants to orthogonal array of particles (Rash et al., 1998 (94)), and their further agglomeration, require further research (82).

This thesis, will endeavour to fully understand the role of AQPs (with particular focus on AQP 4) and their involvement in forming cytotoxic brain oedemas.

1.3.4.1 Stroke

A stroke is the second leading cause of death worldwide, responsible for 4.4 million (9%) of the total 50.5 million deaths each year, and in 2010 the 4th largest cause of death in the UK causing almost 50,000 deaths (95). According to the national stroke association there are 152,000 strokes in the UK every year; which is more than one every 5 minutes (95). There are approximately 1.1 million stroke survivors living in the UK, and as a result this is the leading cause of adult disability, as more than half of UK stroke victims are dependent on others following a stroke (96). A stroke is said to account for 7% of fatalities in men and 10% of fatalities in women (95).

Stroke is one of the most common causes of cytotoxic brain oedema, which is one of the two main causes of death for stroke victims. A stroke is classified as rapid loss of brain function due to a disruption to the blood supplying the brain. This can be as a result of ischaemia, caused by a blockage, or a haemorrhage. An ischaemia means there is a lack of blood flow in the brain, which is commonly caused by either a thrombosis or an arterial embolism. Ischaemia can be treated in hospital with thrombolysis, which is the break down of a clot by pharmacological methods. A haemorrhage is a loss of blood from the vascular system into the body cavity or space. It is a serious medical condition in the brain and requires neurosurgery (97).

Considering that 85% of stroke victims present with ischaemic strokes, having a greater understanding of the physiology of a cytotoxic cerebral oedema and the involvement of AQPs (with particular focus on AQP 4), will help to guide research in the field, allowing for specific drug design (98). This is a very important point to make, as only £22 a year is spent on medical research for every stroke patient, compared to £295 a year per cancer patient, so focused research is essential (99). It is also possible that this treatment will become useful for all the other forms of oedema, if not as a cure but as a method for reducing onset of the disorder decreasing the chance of mortality.

1.3.4.2 Hypoxia

Hypoxia is obviously another way by which cytotoxic cerebral oedemas can present themselves. The physiology involving oedemas has already been discussed in section

1.3.1.3 HACE, however, there are many different ways by which hypoxia can manifest. For an oedema to form the pathological condition will be referred to as tissue hypoxia/regional hypoxia, however the whole body can become hypoxic which is known as generalised hypoxia. Hypoxia can also present and be a serious consequence of preterm birth in the neonate. This is because lungs are one of the last organs to form, meaning in preterm babies they aren't fully developed, meaning less oxygen is inhaled and absorbed by the blood, causing an hypoxic state.

There are three other forms of hypoxia, anaemic hypoxia, historic hypoxia and ischaemic hypoxia. Anaemic hypoxia is whereby the arterial pressure of oxygen is normal but total oxygen content of blood is reduced owing to the diminished ability for haemoglobin to carry oxygen. Historic hypoxia is whereby the blood containing and supplying the cells with oxygen is normal however, the cells ability to use the oxygen effectively is diminished, owing to disabled oxidative phosphorylation enzyme. Ischaemic hypoxia, is when there is decreased blood flow supplying tissues or cells.

1.3.4.3 Ischaemia Reperfusion Injury

Ischaemia reperfusion injury, although is not related to oedemas, indicates furthermore the importance of understanding oedema formations. Ischaemic periods for tissue, cells, or stroke, can be rectified using thrombolysis, this however, can be problematic, as the tissue/cells can then undergo reperfusion injury. Reperfusion injury is the damage caused to tissue, when blood supply returns to tissue following periods of ischaemia. This is as a result of inflammation and oxidative damage through the induction of oxidative stress. The brain is made up of tissue known as aerobic tissue, which has been classified as being part of tissues undergoing the ischaemic cascade after seconds to minutes of ischaemia.

1. Ischaemic episode in the brain (100).

2. Brain tissue deprived of glucose and oxygen, and acidic by-products accumulate. A loss of nutrients and decrease in pH causes the Electron Transport Chain (ETC) to stop, in the mitochondria resulting in a rapid decline in ATP concentration (101), (102), (103), (104).

3. ATP loss causes disruption of active transport ion pumps like Na^+-K^+-ATPase, Ca^{2+}-H^+ATPase, reversal of Na^+-Ca^{2+} transporter resulting in an increase in intracellular Na^+, Ca^{2+}, Cl^- concentration and efflux of K^+, (105), (106).

4. The redistribution of ions across the plasma membrane causes neuronal depolarisation, leading to excess release of neurotransmitters in general, and glutamate in particular cause neuronal excitotoxicity, (107).

5. Glutamate causes an excessive increase in Ca^{2+} concentration into nerve cells through over-activation of their receptors which then triggers a variety of processes that can lead to necrosis and apoptosis, (108), (109). These processes include Ca^{2+} overload of mitochondria, oxygen free radical formation and activation of caspases-9,3,8,BAD, BAX and Calpains resulting in oxidative stress and apotosis respectively, (110), (111).

6. Ca^{2+} dependent activation of Neuronal Nitric Oxide Synthase (nNOS), causes an increase in NO production and the formation of toxic peroxynitrite ($ONOO^-$) which contributes to oxidative stress and excitotoxicty, (112), (113), (114).

7. Upregulation of a variety of enzyme systems such as lipases, proteases, phosphotases, kinases and endonucleases activate various inflammatory molecules like cytokines and interleukins (ILs) such as TNF-α, NF-κB that results in neuroinflammation, (115), (116), (117).

8. Excessive influx of Na^+, Ca^{2+} and efflux of K^+ and recruitment of inflammatory mediators like leukocytes and adhesion molecules, it causes fluid accumulation at the injury site resulting in oedema formation, (118), (119), (120), (121).
endenumerate

   All these damaging factors lead to irreversible final events in cerebral ischaemic stroke.

As this introduction demonstrates, there is not a full understanding around the physiological mechanisms, which evolve a cytotoxic oedema, however the research

already done around aquaporins involvement seems to warrant further investigation.

/sectionAims This PhD thesis will investigate all AQPs for their potential role, function and mechanism for tranporting water across plasma membranes. Investigation into the involvement of AQPs in the formation of cytotoxic brain oedema, and their role in transporting molecules involved in hypoxia formation will also be performed.

To start this thesis will characterise all aquaporins for their expression localisation in cells before and after exposing them to different extracellular tonicities. This will enable us to determine which aquaporins may possibly be involved in the transportation of water across the atrocytic membrane. This is because research indicates that these aquaporins don't always reside in the cell membrane but are activated via transduction cascades, coordinating their expression to different locations. Following this I will investigate these AQPs further to understand their translocation mechanisms. In understanding the mechanisms which enable the oedema to form I may be able to understand how to stop the mechanisms. The goal of this PhD thesis is to try prevent the transportation of water and formation of a cytotoxic oedema, whilst also invstigating AQPs role in transportation of other small molecules potentially involved in the formation of hypoxic oedemas or HACE. This will be done by performing sensitive nitrate/nitrite studies using and modifying techniques and perfected by Martin Feelisch's lab.

2

Materials & methods

2.1 Materials

Below is a list of all inhibitors, antibodies, and kits puchased, and who they were purchased from, during the course of this thesis:

- W7 Calmodulin Antagonist (N-(6-aminohexyl)-5-chloronaphthalene-1-sulphonamide, $K_d \sim$ 1 μM from Sigma.
- Myr-PKC 19-27 and hypericin ($K_d \sim$ 100nM) from Fisher Scientific (Loughborough, UK).
- Myr-PKA 14-22 from Merck Chemicals (Nottingham, UK)
- CPA (cyclopiazonic acid, inhibits sacro/endoplasmic reticulum Ca^{2+}-ATPase with nanomolar affinity) from Tocris Bioscience (Bristol, UK).
- Fluorodish^{TM}dishes were from WPI, Ltd (Stevenage, UK)
- Primary polyclonal mouse anti-AQP4 (ab125049) from Abcam
- Primary polyclonal rabbit anti-AQP4 (ab85904) from Abcam
- Secondary donkey anti-rabbit IgG-HRP (sc-2313) from Santa Cruz Biotech (Dallas, Texas, USA)
- Gateway^{TM} vectors were from Invitrogen (Paisley, UK)
- TransFast^{TM} transfection reagents from Promega (Southampton, UK)

- PowerPrep^{TM} HP plasmid purification systems (Maxiprep and Miniprep) from OriGene (Rockville, USA)
- Protease inhibitor from Calbiochem, subsidiary of Merck Millipore (Billerica, USA)
- Co-Immunoprecipitation beads, from Merck Millipore (Billerica, USA)
- Unless specified all other chemicals were ordered from Sigma, Fisher, Promega or Invitrogen.

2.2 Expression Constructs

AQPs were fused with carboxyl-terminal GFP (Green Fluorescent Protein) using the Invitrogen Gateway^{TM}cloning system according to the manufacturers instructions. Sequence-verified AQP cDNAs were a kind gift of Dr. Kristina Hedfalk (Goteborg University). For directional cloning of blunt-ended PCR products into an entry vector using the Gateway^{TM} system, four bases (GGGG) were added to the 5'-end of the forward primer followed by the 25-bp attB1 attachment sequence (underlined). This was followed by five bases (bold- face type) to introduce a Kozak sequence upstream and to keep the sequence in frame with the AQP coding sequence. Finally, 18–25 base pairs (bp) of the AQP sequence were added to create the aminoterminal forward primers, 5'-GGGG ACA AGT TTG TAC AAA AAA GCA GGC T**CC ACC** ATG-AQP(1825 bp)-3'. For the reverse primer, four bases (GGGG) were added to the 5'-end followed by the 25-bp attB2 attachment sequence (underlined), and then one base (bold-face type) was added to keep the sequence in frame with the AQP coding sequence. Finally, 18–25 bp of the AQP sequence without the stop codon were added to create the carboxyl-terminal forward primers 5'-GGG GAC CAC TTT GTA CAA GAA AGC TGG GT**C** AQP(18–25 bp)-3'. DNA polymerase from Thermococcus *kodakaraensis* (KOD) polymerase was used in PCR amplification of the AQP cDNA. Samples were heated to 94°C for 2min, followed by 30 cycles of 94°C for 30s, 55°C for 30s, and 68°C for 3min, and then 68°C for 7min. Purified PCR products were subcloned into the pDONR221^{TM} entry vector (Invitrogen) using the attB1 and attB2 sites in a reaction with Gateway^{TM} BP Clonase^{TM}enzyme

Reagents	DNA Sample	Water Control
Template	1μL	1μL
Forward Primer	2.5μL	xxxxx
Reverse Primer	2.5μL	xxxxx
10x buffer	5μL	5μL
dNTPs (2mM)	5μL	5μL
Deionised, Sterile Water	33μL	38μL
PFU Polymerase	1μL	1μL

Table 2.1: PCR Reagents

mix (Invitrogen). pDONR221^{TM} vectors containing the required sequences were recombined with the pcDNA-DEST47 Gateway^{TM} vector using the attL and attR reaction with Gateway^{TM} LR Clonase^{TM} enzyme mix (Invitrogen). This created expression vectors with the cycle 3 mutant of the GFP gene at the carboxyl terminus of the AQP gene of interest, which was expressed subsequently as fusion proteins. All mutant constructs were amplified using the well established, modified QuikChange procedure (Stratagene), as described previously. All plasmids were handled and purified using standard molecular biological procedures.

2.3 Mutagenesis

2.3.1 PCR Mutagenesis Protocol

Vector pcDNA - Dest 47 is 7780bp long

Extension Time = 18 minutes

The reagents detailed in table 2.1 were mixed together in two separate eppendorf tubes, labelled DNA sample and water control, and stored in ice.

The eppendorf vials were then added to a PCR machine and run though a typical PCR protocol with an extension time of 18 minutes, owing to the 7780bp of the pcDNA-Dest 47 vectors length.

Following the PCR, a sample was removed (5μL) and stored in a separate labelled eppendorf tube. The remaining PCR mix was digested with Dpn1 (1μ) for 1 hour at 37°C. Following that incubation, another sample (5μL) was removed and added to another separately labelled eppendorf tube. These two samples were then run through a DNA agarose gel.

2.3.1.1 DNA Gel Electrophoresis

5x TBE buffer (50mL) was added to deionised water (dH_2O, 450mL) to make a TBE dilution. Agarose powder (1.5g) was added to the TBE dilution (150mL) in a 250mL conical flask. The solution was stirred and heated in a microwave until all the solid had dissolved. Ethidium bromide (1.5μL) was then added, cautiously and in a fume hood, to the hot agarose solution. The solution was stirred gently and poured into the gel cast and left to cool and solidify. Once the gel had set, the remaining TBE dilution was poured into the cast until the gel was completely covered. The comb was removed from the gel, and a ladder, pre, and post Dpn1 samples were added to their own wells. A voltage of 150V was then applied to the solution for 1 hour, and the gel visualised under UV light. For the digest to have worked a band present in the pre Dpn1 sample had to have vanished in the post Dpn1 sample column, confirming the digestion of the methylated template DNA, leaving just the amplified construct. If however this hadn't have happened then the PCR would need to have been repeated, and the primers checked/sequenced.

2.3.1.2 Transformations

XL10 gold cells (20μL) were added to cold eppendorf tubes, along with DNA (3μg, 2μL). The cells were then forced to endure shock treatment, 30 seconds in a water bath at 42°C followed by immediate removal and placement in ice for 5 minutes. LB broth (1mL) was then added to each eppendorf and put, securely, in a shaking incubator for 1 hour. Using aseptic techniques, the cell solution, was plated onto ampicillin resistant agar plates and left for 15 hours to culture at 37°C in an incubator. A control of water was run alongside this protocol as well as a template control, allowing for comparison against the DNA plate. If all plates had

had colonies something would have gone wrong meaning the entire process would have needed to be repeated depending on which control had colonies present. An ampicillin plate was used as the DNA construct made has an ampicillin resistant gene present.

Next, three isolated colonies were picked using a sterile pipette tip and scraped into a vial of LB broth (5mL) containing ampicillin (5μL). This vial was then incubated in a shaker at 37°C for 1 hour. The LB solution was then poured into sterile conical flasks, 500mL, along with LB broth (150ml) and ampicillin (50μL). The conical flasks were then secured in the shaking incubator and left for 15hours at 37°C. Post incubation the, now cloudy, LB broth was aliquoted into labelled falcon tubes and spun in a centrifuge at 1000rpm, until a pellet formed. Once the pellet had formed the solution was removed and the pellet purified using a miniprep and then maxiprep kit.

2.3.1.3 Miniprep and Maxiprep Protocol

Miniprep

(a) Equilibration Buffer (2mL) was added to the column, and the solution allowed to drain by gravity flow/low spin.

(b) 10 to 15 mL of an overnight culture was pelleted and all medium thoroughly removed.

(c) Cell Suspension Buffer (0.4mL), containing RNase A, was added to the pellet until the cells were suspend in a homogeneous solution.

(d) Cell Lysis Solution (0.4mL) was then added and the ependorf tube inverted 5 times, and left at RT for exactly 5 mins.

(e) Neutralisation Buffer (0.4mL) was added to the eppendorf tube and inverted until the solution was homogeneous. The solution was then centrifuged at 12,000 x g at RT for 10 mins.

(f) The supernatant was pipetted onto the equilibrated column allowing the solution to drain by gravity flow. The flow-through was discarded.

(g) The column was then washed twice with Wash Buffer (2 x 2mL) and the solution allowed to drain from the column by gravity flow/low spin. The wash was discarded after each flow-through.

(h) The DNA was eluted by adding Elution Buffer (0.9mL) to the column, which was allowed to drain by gravity flow/low spin.

(i) Isopropanol (0.63mL) was then added to the eluate. and the mixture centrifuged at 12,000 x g at 4°C for 30 min. The supernatant was then carefully discarded and the pellet washed with ethanol (1mL at 70%) and centrifuged at 12,000 x g at 4°C for 5min. The ethanol wash was carefully and fully removed and the pellet dried in air for 10 min.

(j) The pelleted DNA was dissolved in TE Buffer (50μL).

Maxiprep

(a) Equilibration Buffer (30mL) was added to the column, and the solution allowed to drain by gravity flow.

(b) 100mL of an overnight culture was pelleted and all medium thoroughly removed.

(c) Cell Suspension Buffer (10mL), containing RNase A, was added to the pellet until the cells were suspend in a homogeneous solution.

(d) Cell Lysis Solution (10mL) was then added and the ependorf tube inverted 5 times, and left at RT for exactly 5 mins.

(e) Neutralisation Buffer (10mL) was added to the eppendorf tube and inverted until the solution was homogeneous. The solution was then centrifuged at 15,000 x g at RT for 10 mins.

(f) The supernatant was pipetted onto the equilibrated column allowing the solution to drain by gravity flow. The flow-through was discarded.

(g) The column was then washed twice with Wash Buffer (60mL) and the solution allowed to drain from the column by gravity flow. The wash was discarded after each flow-through.

(h) The DNA was eluted by adding Elution Buffer (15mL) to the column, which was allowed to drain by gravity flow.

(i) Isopropanol (10.5mL) was then added to the eluate. and the mixture centrifuged at 15,000 x g at 4°C for 30 min. The supernatant was then carefully discarded and the pellet washed with ethanol (5mL at 70%) and centrifuged at 15,000 x g at 4°C for 5min. The ethanol wash was carefully and fully removed and the pellet dried in air for 10 min.

(j) The pelleted DNA was dissolved in TE Buffer (500μL).

2.4 Cell Culture and Transfection

Human Embryonic Kidney (HEK)293 cells were cultured routinely in DMEM supplemented with 10% (v/v) foetal bovine serum (FCS) in humidified 5% (v/v) CO_2 in air at 37°C. Cells were seeded into 30mm Fluorodish^{TM} dishes and transfected after 24h at 50% confluency using the TransFast^{TM} transfection protocol with 3μg of DNA per dish. Cortices were dissected from neonatal 25-day-old Wistar rats and placed in cold HEPES-buffered saline. Following mechanical digestion in modified glial medium (DMEM/F12 culture medium with 10% fetal bovine serum, 1% glutamine, and 10 μg/ml gentamicin), the tissue was digested chemically in 1x trypsin and DNase for 25min at 37°C. The tissue was then washed twice with glial medium and dissociated into a cell suspension by trituration three times sequentially through a 5ml pipette followed by a fire-polished Pasteur pipette. Suspended cells were diluted in 10ml of glial medium, and passed through a 40μM strainer. Following centrifugation (500 X g for 5min), the supernatant was removed, and the pellet was suspended in glial medium (10mL). Cells were seeded at 2 X 10^6 cells/T75 cm^2 flask in glial medium (15mL) and incubated at 37°C in 5% CO_2, changing the medium every 2 days until confluency was achieved (∼6–7 days). Astrocytes were purified by shaking at 350rpm for 6h at 37°C to separate oligodendrocytes from astrocytes; the glial medium and oligodendrocytes were replaced with fresh medium and shaken for 18h and then again for a further 24h changing the medium every 6h. Cells were reseeded at 3

X 10^5 cells/T75 cm^2 flask. Identification of primary astrocytes was confirmed by immunocytochemistry.

2.4.1 HEK293 Transfection protocol

Nuclease free water (400μL) was added to a vial of TransFast^{TM} lyphilised powder. This was then vortex mixed for a couple of seconds. DNA (3μg, 2μL) was added to the TransFast^{TM} solution (18μL) in a universal tube (50ml). The solution was gently mixed with a pipette and left at room temperature (RT) for 15 mins. The DNA/TransFast^{TM} mix (20μL) was added to the HEK293 cells in DMEM full media (2mL). The confocal dish was then, gently placed in an incubator (37°C) for 1 hour. After an hour the media was aspirated away very carefully so as not to dislodge the HEK293 cells, and replaced with fresh DMEM full media (2mL). The cells are then returned to the incubator for 48 hours. This protocol for transfection is slightly different from most protocols as most require a media to be used without FCS, however, TransFast^{TM} has been specifically designed to be used in the presence of FCS.

2.4.2 Immortalysed Astrocytes Transfection Protocol

Although this was tried and tested using TransFast^{TM} the expression was very poor, making it difficult to get clear confocal imaging of the translocation response to changing extracellular tonicity. Following further research and discussion with biological supplies companies, Mirus Bio LLC made a variety of transfection regents for particularly difficult to transfect cell lines. The reagent found to be successful, 70-80% transfection expression, was TransIt^{TM} 2020. The following protocol was applied. A Fluorodish^{TM} of 50% confluent astrocytes containing DMEM full media (2mL) had the DMEM aspirated away. Then DMEM Full Media (2.5mL) was added to the Fluorodish^{TM} along with a transfection mix of TransIT^{TM} 2020 (7.5μL), DNA (3-4μg, 2.5μL) and DMEM (250μL) FCS-free and dye-free, which had previously been left at RT for 30mins. The TransIT^{TM} 2020 reagents unlike TransFast^{TM} was not toxic to the cells, so the transfection

and media mix did not have to be replaced, meaning it could be placed in the incubator at 37°C for 48 hours.

2.5 Confocal Microscopy

AQP-GFP fusion proteins were visualized in live cells enclosed in a full environmental chamber by confocal laser scanning microscopy. Confocal images were acquired with a Leica SP5 laser scanning microscope and a Zeiss Axiovert 200m inverted microscope with a 63x (1.4 numerical aperture) oil immersion objective for immunocytochemical analysis or a Zeiss Axiovert 200m upright microscope with a 20x (1.0 numerical aperture) water dipping objective for live cell analysis. The nucleus and the plasma membrane were sometimes stained with DAPI and always 5μg/ml FM4-64 (Molecular Probes), respectively. Images were acquired using an argon laser (excitation, 488nm; emission, band pass, 505–530nm) for GFP, UV excitation and a band pass 385–470nm emission filter for DAPI, and a He-Ne laser (excitation, 543nm; emission filter, long pass, 650nm) for FM4-64. 48h post-transfection, cells in Fluorodishes^{TM} were incubated with or without 50μM Myr-PKC, 50μM Myr-PKA, 50μM hypericin, 10μM 1-oleoyl-2-acetyl-sn-glycerol, 5μM PMA, 10mM caffeine, 10μM CPA (30 min), 10mM TRPC1 antagonist SKF96365 or 100μM W7 for 1h at 37°C and 5% CO^2. For inhibitor and activator experiments, the concentrations used were derived from the literature and were a minimum of 10x K_d (where known) to ensure 90%, theoretical fractional occupancy of the target protein. Where no effect was seen, the dose was increased: for example, 1,000x K_d achieves 99.9% fractional occupancy. The volume of inhibitor (in water) added to the cells was 1% (v/v) to ensure a minimum effect on osmolality. Cells were visualized in control medium (DMEM) that has an inorganic salt concentration of 120mM, a glucose concentration of 25mM, and an osmolality in the range 322–374 mosM/kg H_2O. Hypotonic medium has an osmolality in the range 107–125mosM/kg H_2O through dilution of DMEM by a factor of thrre with water. Protein localization was measured using a line profile (pixel density) traced on each transfected cell.

2.6 Determination of Subcellular Localisation, Image J Analysis and Matlab

A minimum of 3 line profiles were measured and distributed at regular intervals covering the plasma membrane and the cytosol but avoiding the nucleus of a minimum of three different, isolated cells from at least three independent experiments. The fluorescence intensity over this distance was measured, and the difference between the peak and the plateau of fluorescence was divided by the maximum fluorescence along the line scan to calculate the percentage of fluorescence at the membrane. This was termed the relative membrane expression (RME). Identification of the plasma membrane was achieved by staining with FM4-64 and overlaying the GFP images. Nuclei were identified through DAPI staining. The overlay of the GFP image either with the brightfield image or the red fluorescence emitted by FM4-64 clearly indicated integration of GFP-tagged AQP at the plasma membrane as well as in the cytoplasm of HEK293 cells. Once the overlaying had been identified visually, this laser was turned off and just the GFP imaged as this prolonged the half-life of the fluorescence, enabling longer experimentation time, with clearer images. The profiling was performed using a software programe called Image J. This is a public domain, java-based image processing programme developed by the National Institute of Health.

2.6.1 Image J Macros Script

Specific user friendly macros were created to aid a users to perform profile analysis. The following code is additional comuptational coding and is not a standard functionality of the native software:

```
macro "Membrane Expression" {
// 24/03/2012
// Last edited: 16/04/2012
// Confocal data analysis macro, to be used with
// "Membrane1.m" Matlab program.
```

```
// Gets profile data from a set of selected ROIs and saves to file,
// followed by particle anaylsis to calculate cell x-sectional areas.

open(""); //prompt user to select image

ID = getImageID; // get image details for switching between images
name = getTitle; // and file i/o.

CellNo = getNumber("How many cells in the image would you like to
    analyse?",1);

k = 1; //counter for plot profile file naming

for (l=0; l<CellNo; l++)
{
   for (i=0; i<3; i++) //If more (or less!) than 3 ROIs per image are
       desired, change the 3 in this line to the desired number
   {
      setTool("line");

      if (i == 0)
      { waitForUser("Begin on a new cell and select the line ROI to be
          analysed"); //prompt user to set ROI}
      else
      { waitForUser("Select the line ROI to be analysed"); //prompt user
          to set ROI}

      selectImage(ID);
      // generates and saves the plot profile data
      A = getProfile; //get the profile data along the current ROI
      B = newArray(A.length);

      for (j=0; j<A.length; j++)
```

```
      { B[j] = j+1; //This variable counts the number of datapoints in
          the line profile. Count from 1 not 0 to make Matlab
          compatibility simple! }
      f = File.open("/Users/meaningless_s/Desktop/Final Thesis/PhD
          Images/"+name+"_"+(k)+".txt"); // open text file to write to.

      k++; //increment k ready to open the next file

      for (j=0; j<A.length; j++)
      { print(f, B[j]+" \t"+d2s(A[j],10)+"\n"); //print datapoint number
          plus line profile data to the open file }
      File.close(f);
   }
}

// particle analysis
selectImage(ID);
run("Duplicate...", "title=duplicate"); // keep a copy of the raw image
    open
run("Make Binary"); // binary conversion required for particle analysis
ID2 = getImageID; //Get the ID of the binary image
setForegroundColor(1, 1, 1); //change the brush colour to black ready
    for the user to draw on the binary image if necessary
waitForUser("Does the binary look OK? If yes, click OK now.\nIf not, use
    the paintbrush tool to fix it, then click OK"); //prompt user to
    check the binary
selectImage(ID2); //make sure the correct image is selected
setTool("rectangle");
setBackgroundColor(255,255,255);
waitForUser("Are there cells in the image that are not being analysed?\n
    If so, highlight them and press backspace, then click OK.\n If not,
    just click OK."); //prompt user to check the binary
run("Make Binary");
```

```
run("Analyze Particles...", "size=50-infinity circularity=0.00-1.00
    show=Outlines display clear include"); //particle analysis (gets
    cell outlines and areas)
selectImage(ID2); //make sure the correct image is selected
close;          //get rid of binary image

saveAs("Results", "/Users/meaningless_s/Desktop/Final Thesis/PhD
    Images/"+name+"_"+"areas.txt");}

 }
```

This code saves a file from which analysis can be performed to calculate the RME and determine the statistical significance in the variance. Analysis was also performed on the surface area data, determining the percentage change in size, and its statistical significance. This analysis was performed by a software programme called Matlab using the following code.

2.6.2 Matlab Script for Membrane Profile Analysis

```
function [] = Membrane(N_Number, N1, N2, ImageTitle1, ImageTitle2,
    ImageTitle3, ImageTitle4, ImageTitle5, ImageTitle6)

%MEMBRANE 1 PROFILE ANALYSIS
% 16/04/2012
% This program is a second attempt at performing the analysis of line
% profiles from confocal imaging of cells expressing GFP-tagged AQP4. The
% original program(s) (ProfileStats.m, ProfileSingle.m) looks for the
% highest fluorescence values and take those to be the mombrane region.
% This program will implements a more rigorous approach to
% finding the membrane regions which will not break when analysing images
% which show low (i.e. comparable to cytosol) membrane expression levels.
%
```

```
fprintf('\n n = 1\n\n');
RME1 = zeros(1,N1);   %pre-allocate memory for these vectors
RME2 = zeros(1,N1);
A1 = 0;
while (A1*A1) < N1    %calculate the number of tiles required in the
    first subplot window
   A1 = A1 + 1;
end
A2 = 0;
while (A2*A2) < N2    %calculate the number of tiles required in the
    second subplot window
   A2 = A2 + 1;
end
fprintf('Starting First Image....\n\n');
for i = 1:N1
buffer = strcat(ImageTitle1,'_',num2str(i),'.txt'); %Need to do this bit
    to include the iteration number as part of the imput file name
Input = importdata(buffer);
InputData = Input(:,2);
Threshold = mean(InputData);
ThresholdExceeded = find(InputData > Threshold);
MemLeftStart = ThresholdExceeded(1);
MemLeftEnd = MemLeftStart + 9;     %Take membrane region to be 10 pixels
    across
MemRightEnd = ThresholdExceeded(end);
MemRightStart = MemRightEnd - 9;
MembraneAverage = mean([max(InputData(MemLeftStart:MemLeftEnd))
    max(InputData(MemRightStart:MemRightEnd))]);
CytosolAverage = mean(InputData(MemLeftEnd+1:MemRightStart-1));
RME1(i) = ((MembraneAverage - CytosolAverage) / MembraneAverage)*100;
fprintf(' \n Cytosol Average: %f \n Membrane Average: %f \n RME: %f
    \n\n',CytosolAverage, MembraneAverage, RME1(i));
subplot(A1,A1,i);
```

```
        plot(1:length(InputData),InputData);
        set(gcf,'Color',[1,1,1]);
        set(gca, 'Fontsize', 16);
        hold on;
        plot([0 length(InputData)], [CytosolAverage CytosolAverage],
            'red');
        plot([0 length(InputData)], [MembraneAverage MembraneAverage],
            'green');
        plot([0 length(InputData)], [Threshold Threshold], 'black');
        xlabel({'Distance Across the Yellow Line';'(No. Pixels)'},
            'Fontsize', 16);
        ylabel({'Fluorescence Intensity'; '(Arbitrary Units)'},
            'Fontsize', 16);
        hold off;
        set(gca,'ylim',[0 max(InputData)+50],'xlim',[0 length(InputData)]);
end
set(gcf,'NextPlot','add');
axes;
h = title(ImageTitle1,'FontSize', 16); %This block puts the title at the
    top centre of the subplot figure window
set(gca,'Visible','off');
%set(h,'Visible','on');
if N1 > 1  %no point doing this bit if N = 1!
    TotalRME1 = sum (RME1) /N1; %average over all N measurements
    StdErr1 = std(RME1)/sqrt(N1); %calculate the standard error. This is
        the sample standard deviation with Bessel's correction, over the
        root of the sample size
   fprintf('Average RME: %f  %f \n \n', TotalRME1, StdErr1);
end
%%%%%%%%%%%%%%%%%%%%%%
fprintf('Starting Second Image....\n\n');
figure;
for i = 1:N2
```

```
buffer = strcat(ImageTitle2,'_',num2str(i),'.txt'); %Need to do this bit
    to include the iteration number as part of the imput file name
Input = importdata(buffer);
InputData = Input(:,2);
Threshold = mean(InputData);
ThresholdExceeded = find(InputData > Threshold);
MemLeftStart = ThresholdExceeded(1);
MemLeftEnd = MemLeftStart + 9;     %Take membrane region to be 10 pixels
    across
MemRightEnd = ThresholdExceeded(end);
MemRightStart = MemRightEnd - 9;
MembraneAverage = mean([max(InputData(MemLeftStart:MemLeftEnd))
    max(InputData(MemRightStart:MemRightEnd))]);
CytosolAverage = mean(InputData(MemLeftEnd+1:MemRightStart-1));
RME2(i) = ((MembraneAverage - CytosolAverage) / MembraneAverage)*100;
fprintf(' \n Cytosol Average: %f \n Membrane Average: %f \n RME: %f
    \n\n',CytosolAverage, MembraneAverage, RME2(i));
subplot(A2,A2,i);
      plot(1:length(InputData),InputData);
      set(gcf,'Color',[1,1,1]);
      set(gca, 'Fontsize', 16);
      hold on;
      plot([0 length(InputData)], [CytosolAverage CytosolAverage],
          'red');
      plot([0 length(InputData)], [MembraneAverage MembraneAverage],
          'green');
      plot([0 length(InputData)], [Threshold Threshold], 'black');
      xlabel({'Distance Across the Yellow Line';'(No. Pixels)'},
          'Fontsize', 12);
      ylabel({'Fluorescence Intensity'; '(Arbitrary Units)'},
          'Fontsize', 12);
      hold off;
      set(gca,'ylim',[0 max(InputData)+50],'xlim',[0 length(InputData)]);
```

```
end
set(gcf,'NextPlot','add');
axes;
h = title(ImageTitle2,'FontSize', 16); %This block puts the title at the
    top centre of the subplot figure window
set(gca,'Visible','off');
%set(h,'Visible','on');
if N2 > 1  %no point doing this bit if N = 1!
    TotalRME2 = sum (RME2) /N2; %average over all N measurements
    StdErr2 = std(RME2)/sqrt(N2); %calculate the standard error. This is
        the sample standard deviation with Bessel's correction, over the
        root of the sample size
   fprintf('Average RME: %f  %f \n \n', TotalRME2, StdErr2);
end
%%%%%%%%%%%%%%%%%%%%%%%%%%%%%%%%%%%%%%%%
% Statistics for the two samples
[h1,p1] = ttest2(RME1,RME2,0.01,'both','unequal');
if h1 == 0 %if the null hypothesis is not rejected at the 99% level, try
    95%
   [h2,p2] = ttest2(RME1,RME2,0.05,'both','unequal');
   if h2 == 1
       fprintf('The null hypothesis was rejected at the 95%% level. p =
           %f \n \n',p2);
   elseif h2 == 0
       fprintf('The null hypothesis could not be rejected at the 95%%
           level. p = %f \n \n',p2);
   end
elseif h1 == 1
    fprintf('The null hypothesis was rejected at the 99%% level. p = %f
        \n \n',p1);
end
%%%%%%%%%%%%%%%
if N_Number > 1
```

```
fprintf('\n\n n = 2 \n\n');
figure;
RME3 = zeros(1,N1);   %pre-allocate memory for these vectors
RME4 = zeros(1,N1);
fprintf('Starting First Image....\n\n');
for i = 1:N1
   buffer = strcat(ImageTitle3,'_',num2str(i),'.txt'); %Need to do
       this bit to include the iteration number as part of the imput
       file name
   Input = importdata(buffer);
   InputData = Input(:,2);
   Threshold = mean(InputData);
   ThresholdExceeded = find(InputData > Threshold);
   MemLeftStart = ThresholdExceeded(1);
   MemLeftEnd = MemLeftStart + 9;     %Take membrane region to be 10
       pixels across
   MemRightEnd = ThresholdExceeded(end);
   MemRightStart = MemRightEnd - 9;
   MembraneAverage = mean([max(InputData(MemLeftStart:MemLeftEnd))
       max(InputData(MemRightStart:MemRightEnd))]);
   CytosolAverage = mean(InputData(MemLeftEnd+1:MemRightStart-1));
   RME3(i) = ((MembraneAverage - CytosolAverage) /
       MembraneAverage)*100;
   fprintf(' \n Cytosol Average: %f \n Membrane Average: %f \n RME:
       %f \n\n',CytosolAverage, MembraneAverage, RME3(i));
   subplot(A1,A1,i);
   plot(1:length(InputData),InputData);
   set(gcf,'Color',[1,1,1]);
   set(gca, 'Fontsize', 16);
   hold on;
   plot([0 length(InputData)], [CytosolAverage CytosolAverage],
       'red');
```

```
    plot([0 length(InputData)], [MembraneAverage MembraneAverage],
        'green');
    plot([0 length(InputData)], [Threshold Threshold], 'black');
    xlabel({'Distance Across the Yellow Line';'(No. Pixels)'},
        'Fontsize', 12);
    ylabel({'Fluorescence Intensity'; '(Arbitrary Units)'},
        'Fontsize', 12);
    hold off;
    set(gca,'ylim',[0 max(InputData)+50],'xlim',[0 length(InputData)]);
end
set(gcf,'NextPlot','add');
axes;
h = title(ImageTitle1,'FontSize', 16); %This block puts the title at
    the top centre of the subplot figure window
set(gca,'Visible','off');
%set(h,'Visible','on');
if N1 > 1  %no point doing this bit if N = 1!
    TotalRME3 = sum (RME3) /N1; %average over all N measurements
    StdErr3 = std(RME3)/sqrt(N1); %calculate the standard error. This
        is the sample standard deviation with Bessel's correction, over
        the root of the sample size
    fprintf('Average RME: %f  %f \n \n', TotalRME3, StdErr3);
end
%%%%%%%%%%%%%%%%%%%%%
fprintf('Starting Second Image....\n\n');
figure;
for i = 1:N2
    buffer = strcat(ImageTitle4,'_',num2str(i),'.txt'); %Need to do
        this bit to include the iteration number as part of the imput
        file name
    Input = importdata(buffer);
    InputData = Input(:,2);
    Threshold = mean(InputData);
```

```
    ThresholdExceeded = find(InputData > Threshold);
    MemLeftStart = ThresholdExceeded(1);
    MemLeftEnd = MemLeftStart + 9;     %Take membrane region to be 10
        pixels across
    MemRightEnd = ThresholdExceeded(end);
    MemRightStart = MemRightEnd - 9;
    MembraneAverage = mean([max(InputData(MemLeftStart:MemLeftEnd))
        max(InputData(MemRightStart:MemRightEnd))]);
    CytosolAverage = mean(InputData(MemLeftEnd+1:MemRightStart-1));
    RME4(i) = ((MembraneAverage - CytosolAverage) /
        MembraneAverage)*100;
    fprintf(' \n Cytosol Average: %f \n Membrane Average: %f \n RME:
        %f \n\n',CytosolAverage, MembraneAverage, RME4(i));
    subplot(A2,A2,i);
    plot(1:length(InputData),InputData);
    set(gcf,'Color',[1,1,1]);
    set(gca, 'Fontsize', 16);
    hold on;
    plot([0 length(InputData)], [CytosolAverage CytosolAverage],
        'red');
    plot([0 length(InputData)], [MembraneAverage MembraneAverage],
        'green');
    plot([0 length(InputData)], [Threshold Threshold], 'black');
    xlabel({'Distance Across the Yellow Line';'(No. Pixels)'},
        'Fontsize', 12);
    ylabel({'Fluorescence Intensity'; '(Arbitrary Units)'},
        'Fontsize', 12);
    hold off;
    set(gca,'ylim',[0 max(InputData)+50],'xlim',[0 length(InputData)]);
end
set(gcf,'NextPlot','add');
axes;
```

```
h = title(ImageTitle4,'FontSize', 16); %This block puts the title at
    the top centre of the subplot figure window
set(gca,'Visible','off');
%set(h,'Visible','on');
if N2 > 1  %no point doing this bit if N = 1!
   TotalRME4 = sum (RME4) /N2; %average over all N measurements
   StdErr4 = std(RME4)/sqrt(N2); %calculate the standard error. This
       is the sample standard deviation with Bessel's correction, over
       the root of the sample size
   fprintf('Average RME: %f  %f \n \n', TotalRME4, StdErr4);
end
%%%%%%%%%%%%%%%%%%%%%%%%%%%%%%%%%%%%%%%%%%%%%%%%
% Statistics for the two samples
[h1,p1] = ttest2(RME3,RME4,0.01,'both','unequal');
if h1 == 0 %if the null hypothesis is not rejected at the 99% level,
    try 95%
   [h2,p2] = ttest2(RME3,RME4,0.05,'both','unequal');
   if h2 == 1
      fprintf('The null hypothesis was rejected at the 95%% level. p =
          %f \n \n',p2);
   elseif h2 == 0
      fprintf('The null hypothesis could not be rejected at the 95%%
          level. p = %f \n \n',p2);
   end
elseif h1 == 1
   fprintf('The null hypothesis was rejected at the 99%% level. p =
       %f \n \n',p1);
end
%%% n = 2 stats
if N_Number == 2
   fprintf('\n\nCombined RME for n = 2\n\n')
    MeanRME1 = mean([RME1 RME3]);
   StdErrorRME1 = std([RME1 RME3])/sqrt(length([RME1 RME3]));
```

```
        MeanRME2 = mean([RME2 RME4]);
        StdErrorRME2 = std([RME2 RME4])/sqrt(length([RME2 RME4]));
        fprintf('Mean RME before treatment = %f
            %f\n\n',MeanRME1,StdErrorRME1);
        fprintf('Mean RME after treatment = %f
            %f\n\n',MeanRME2,StdErrorRME2);
        [h1,p1] = ttest2([RME1 RME3],[RME2 RME4],0.01,'both','unequal');
        if h1 == 0 %if the null hypothesis is not rejected at the 99%
            level, try 95%
           [h2,p2] = ttest2([RME1 RME3],[RME2 RME4],0.05,'both','unequal');
           if h2 == 1
              fprintf('The null hypothesis was rejected at the 95%% level.
                  p = %f \n \n',p2);
           elseif h2 == 0
              fprintf('The null hypothesis could not be rejected at the
                  95%% level. p = %f \n \n',p2);
           end
        elseif h1 == 1
           fprintf('The null hypothesis was rejected at the 99%% level. p =
               %f \n \n',p1);
        end
     end
  end
  if N_Number == 3
     figure;
     fprintf('\n\n n = 3 \n\n');
     RME5 = zeros(1,N1);   %pre-allocate memory for these vectors
     RME6 = zeros(1,N1);
     fprintf('Starting First Image....\n\n');
     for i = 1:N1
        buffer = strcat(ImageTitle5,'_',num2str(i),'.txt'); %Need to do
            this bit to include the iteration number as part of the imput
            file name
```

```
    Input = importdata(buffer);
    InputData = Input(:,2);
    Threshold = mean(InputData);
    ThresholdExceeded = find(InputData > Threshold);
    MemLeftStart = ThresholdExceeded(1);
    MemLeftEnd = MemLeftStart + 9;    %Take membrane region to be 10
        pixels across
    MemRightEnd = ThresholdExceeded(end);
    MemRightStart = MemRightEnd - 9;
    MembraneAverage = mean([max(InputData(MemLeftStart:MemLeftEnd))
        max(InputData(MemRightStart:MemRightEnd))]);
    CytosolAverage = mean(InputData(MemLeftEnd+1:MemRightStart-1));
    RME5(i) = ((MembraneAverage - CytosolAverage) /
        MembraneAverage)*100;
    fprintf(' \n Cytosol Average: %f \n Membrane Average: %f \n RME:
        %f \n\n',CytosolAverage, MembraneAverage, RME5(i));
    subplot(A1,A1,i);
    plot(1:length(InputData),InputData);
    set(gcf,'Color',[1,1,1]);
    set(gca, 'Fontsize', 16);
    hold on;
    plot([0 length(InputData)], [CytosolAverage CytosolAverage],
        'red');
    plot([0 length(InputData)], [MembraneAverage MembraneAverage],
        'green');
    plot([0 length(InputData)], [Threshold Threshold], 'black');
    xlabel({'Distance Across the Yellow Line';'(No. Pixels)'},
        'Fontsize', 12);
    ylabel({'Fluorescence Intensity'; '(Arbitrary Units)'},
        'Fontsize', 12);
    hold off;
    set(gca,'ylim',[0 max(InputData)+50],'xlim',[0 length(InputData)]);
end
```

```
set(gcf,'NextPlot','add');
axes;
h = title(ImageTitle1,'FontSize', 16); %This block puts the title at
    the top centre of the subplot figure window
set(gca,'Visible','off');
%set(h,'Visible','on');
if N1 > 1  %no point doing this bit if N = 1!
   TotalRME5 = sum (RME5) /N1; %average over all N measurements
   StdErr5 = std(RME5)/sqrt(N1); %calculate the standard error. This
       is the sample standard deviation with Bessel's correction, over
       the root of the sample size
   fprintf('Average RME: %f  %f \n \n', TotalRME5, StdErr5);
end
%%%%%%%%%%%%%%%%%%%%%
fprintf('Starting Second Image....\n\n');
figure;
for i = 1:N2
   buffer = strcat(ImageTitle6,'_',num2str(i),'.txt'); %Need to do
       this bit to include the iteration number as part of the imput
       file name
   Input = importdata(buffer);
   InputData = Input(:,2);
   Threshold = mean(InputData);
   ThresholdExceeded = find(InputData > Threshold);
   MemLeftStart = ThresholdExceeded(1);
   MemLeftEnd = MemLeftStart + 9;     %Take membrane region to be 10
       pixels across
   MemRightEnd = ThresholdExceeded(end);
   MemRightStart = MemRightEnd - 9;
   MembraneAverage = mean([max(InputData(MemLeftStart:MemLeftEnd))
       max(InputData(MemRightStart:MemRightEnd))]);
   CytosolAverage = mean(InputData(MemLeftEnd+1:MemRightStart-1));
```

```
    RME6(i) = ((MembraneAverage - CytosolAverage) /
        MembraneAverage)*100;
    fprintf(' \n Cytosol Average: %f \n Membrane Average: %f \n RME:
        %f \n\n',CytosolAverage, MembraneAverage, RME6(i));
    subplot(A2,A2,i);
    plot(1:length(InputData),InputData);
    set(gcf,'Color',[1,1,1]);
    set(gca, 'Fontsize', 16);
    hold on;
    plot([0 length(InputData)], [CytosolAverage CytosolAverage],
        'red');
    plot([0 length(InputData)], [MembraneAverage MembraneAverage],
        'green');
    plot([0 length(InputData)], [Threshold Threshold], 'black');
    xlabel({'Distance Across the Yellow Line';'(No. Pixels)'},
        'Fontsize', 12);
    ylabel({'Fluorescence Intensity'; '(Arbitrary Units)'},
        'Fontsize', 12);
    hold off;
    set(gca,'ylim',[0 max(InputData)+50],'xlim',[0 length(InputData)]);
end
set(gcf,'NextPlot','add');
axes;
h = title(ImageTitle4,'FontSize', 16); %This block puts the title at
    the top centre of the subplot figure window
set(gca,'Visible','off');
%set(h,'Visible','on');

if N2 > 1  %no point doing this bit if N = 1!
    TotalRME6 = sum (RME6) /N2; %average over all N measurements
    StdErr6 = std(RME6)/sqrt(N2); %calculate the standard error. This
        is the sample standard deviation with Bessel's correction, over
        the root of the sample size
```

```
        fprintf('Average RME: %f  %f \n \n', TotalRME6, StdErr6);
    end
    %%%%%%%%%%%%%%%%%%%%%%%%%%%%%%%%%%%%%%%%%%%%%%%%
    % Statistics for the two samples
    [h1,p1] = ttest2(RME5,RME6,0.01,'both','unequal');
    if h1 == 0 %if the null hypothesis is not rejected at the 99% level,
        try 95%
        [h2,p2] = ttest2(RME5,RME6,0.05,'both','unequal');
        if h2 == 1
            fprintf('The null hypothesis was rejected at the 95%% level. p =
                %f \n \n',p2);
        elseif h2 == 0
            fprintf('The null hypothesis could not be rejected at the 95%%
                level. p = %f \n \n',p2);
        end
    elseif h1 == 1
        fprintf('The null hypothesis was rejected at the 99%% level. p =
            %f \n \n',p1);
    end
end
end
```

2.6.3 Matlab Script for Cell Surface Area Analysis

```
function [] = Areas( N_Number, N1, N2, ImageTitle1, ImageTitle2,
    ImageTitle3, ImageTitle4, ImageTitle5, ImageTitle6)

% SURFACE AREA ANALYSIS
%  This function calculates the mean percentage change in size of cells,
    from isotonic to hypotonic solution. A Students T-test is then
    performed to determine the significance of the change from iosotonic
    to hypotonic extracellular environment.
```

```
Areas1 = importdata(strcat(ImageTitle1, '_areas.txt'));
Areas2 = importdata(strcat(ImageTitle2, '_areas.txt'));
fprintf('\n\nCell Cross-Sectional Areas\n\n');
for i = 1: min(length(Areas1.data(:,2)),length(Areas2.data(:,2)))
fprintf(strcat('Cell\f',num2str(i),'\f- area before: %f, area after: %f.
    Percentage change: %f \n\n'),Areas1.data(i,2),Areas2.data(i,2),
    ((100*Areas2.data(i,2)/Areas1.data(i,2))-100) );
end
if N_Number > 2
   Areas3 = importdata(strcat(ImageTitle3, '_areas.txt'));
   Areas4 = importdata(strcat(ImageTitle4, '_areas.txt'));
   fprintf('\n\nCell Cross-Sectional Areas\n\n');
   for i = 1: min(length(Areas3.data(:,2)),length(Areas4.data(:,2)))
      fprintf(strcat('Cell\f',num2str(i),'\f- area before: %f, area
          after: %f. Percentage change: %f
          \n\n'),Areas3.data(i,2),Areas4.data(i,2),
          ((100*Areas4.data(i,2)/Areas3.data(i,2))-100) );
   end
   if N_Number == 2
       mean1 = mean([((100*Areas4.data(i,2)/Areas3.data(i,2))-100)
           ((100*Areas2.data(i,2)/Areas1.data(i,2))-100)]);
       fprintf('Mean percentage change: %f \n\n',mean1);
   end
end
if N_Number > 2
   Areas5 = importdata(strcat(ImageTitle5, '_areas.txt'));
   Areas6 = importdata(strcat(ImageTitle6, '_areas.txt'));
   fprintf('\n\nCell Cross-Sectional Areas\n\n');
   for i = 1: min(length(Areas5.data(:,2)),length(Areas6.data(:,2)))
      fprintf(strcat('Cell\f',num2str(i),'\f- area before: %f, area
          after: %f. Percentage change: %f
          \n\n'),Areas5.data(i,2),Areas6.data(i,2),
          ((100*Areas6.data(i,2)/Areas5.data(i,2))-100));
```

```
    end
    mean2 = mean([((100*Areas4.data(i,2)/Areas3.data(i,2))-100)
        ((100*Areas2.data(i,2)/Areas1.data(i,2))-100)
        ((100*Areas6.data(i,2)/Areas5.data(i,2))-100)]);
    std_err = std([((100*Areas4.data(i,2)/Areas3.data(i,2))-100)
        ((100*Areas2.data(i,2)/Areas1.data(i,2))-100)
        ((100*Areas6.data(i,2)/Areas5.data(i,2))-100)]);
    std_err = std_err/sqrt(3);
    fprintf('Mean percentage change: %f  %f \n\n',mean2,std_err);
    fprintf('T-test against swelling of wild-type HEK cells...\n\n');
    [h,p] = ttest2([((100*Areas4.data(i,2)/Areas3.data(i,2))-100)
        ((100*Areas2.data(i,2)/Areas1.data(i,2))-100)
        ((100*Areas6.data(i,2)/Areas5.data(i,2))-100)], [1.4 6.5 13]);
    if p < 0.01
        fprintf('null hypothesis rejected at 99%% level');
    elseif p >= 0.01 && p < 0.05
        fprintf('null hypothesis rejected at 95%% level, but not at 99%%');
    end
    fprintf('p = %f \n\n', p);
end
end
```

2.7 Primary Astrocyte Immunocytochemistry

Endogenous AQP4 protein was visualized in isolated rat primary astrocytes.

Cells were grown on coverslips and exposed to glial medium or diluted glial medium, and then fixed by perfusing (optimized to ensure tonicity changes did not affect expression profile) with 4% (v/v) paraformaldehyde in phosphate-buffered saline for 15min at room temperature. These were washed twice with phosphate-buffered saline, and permeabilised using a blocking solution containing 0.25% (v/v) Triton X-100, 1% (v/v) goat serum and 1% (w/v) bovine serum albumin

in phosphate-buffered saline. Successive incubations with primary and secondary antibodies were carried out for 16h at 4°C and 1h at RT, respectively. Primary antibodies (1:500) were detected by species-specific FITC-conjugated secondary antibodies (1:1,000). Cells were washed in phosphate-buffered saline, and coverslips were mounted with Vectorshield (Vector Laboratories). The cells were visualized, and confocal images were acquired using confocal laser scanning microscopy as described below. Because perfused, fixed primary cells were used, the same live cell could not be compared under differing conditions; rather, cells from the same subcultured population were compared on different cover slips.

2.8 Co-Immunoprecipitation Protocol

2.8.1 Cell Lysis

6 well plates with living HEK293 cells, were placed on trays of ice. They were then washed gently with ice-cold PBS, and the wash repeated, removing PBS solution each time with an aspirator. Great care was taken with these steps, so as not to disturb the cells and dislodging them from the plate. Following the second wash all PBS was removed. The cells were then lysed using Triton lysis buffer:

(a) Add 250μL per p60 dish/500μL per p100 dish

(b) Scrape cells off the plate with a plastic scraper

(c) Place cells on ice in a pre-chilled eppendorf

The cell lysates were then incubated on ice for 30 minutes. Following incubation the lysates were centrifuged at 13,000 x g, at 4°C for 10 minutes. The supernatant from each tube was removed and placed in a newly labelled eppendorf.

Triton Lysis Buffer Protocol

(a) Tris (20mM, pH 7.4)

(b) NaCl (137mM)

(c) Glycerol (10%)

(d) Triton X-100 (0.5)

Sample Buffer

(a) SDS (10%)

(b) DTT (10mM)

(c) Glycerol (20%)

(d) Tris (0.1M, pH 6.8)

(e) Blue bromophenol (10%)

2.8.2 Preparation of Immunoprecipitation columns

Protein G Agarose (15μL) bead slurry was added to labelled spin columns and added to eppendorf tubes. Triton lysis buffer (1mL) was added to each column and inverted twice to wash the beads. The eppendorf tubes were then centrifuged at 100 x g, at 4°C for 1 minute. The liquid was removed carefully by an aspirator ensuring that just the beads were left. The wash process was then repeated another 2 times, and the required antibody added to each column (varied depending on product recommendations but in most cases it was 1μg).

2.8.3 Running of Immunoprecipitation Columns

Remove a sample of cell lysate (40μL) to run later on the gel alongside the IP sample. The remaining cell lysate was added to the IP column. The columns were then incubated for 3 hours at 4°C, whilst being continually shaken gently. The IP columns were then washed 3 times, as stated before in preparation of immunoprecipitation columns. 5 x sample buffer (20μL) and triton lysis buffer (10μL) was then added to each column, giving a gentle flick to mix. The samples were then incubated at 95°C for 5 mins. Following incubation the columns were centrifuged at 100 x g at 4°C for 1 minute. All the liquid was removed without

disturbing the beads. The solution was then loaded and run on a Tris-glycine gel, as indicated in the gel electrophoresis chapter.

2.8.4 Western Blot

2.8.4.1 Stock Solutions

Final Sample Buffer (FSB)

(a) 4% SDS

(b) 10% 2-mercaptoethanol

(c) 20% Glycerol

(d) 0.004% Bromophenol Blue

(e) 0.125M Tris HCl

RIPA Buffer

(a) 150mM Sodium Chloride (NaCl = 0.87g)

(b) 1% Np-40 or Triton x100

(c) 0.5% Sodium Deoxycholate

(d) 0.1% SDS (1mL of 10%)

(e) 50mM Tris pH8.0 (5mL of 1M)

(f) add to x2 Sample Buffer

Resolving Buffer 10%

(a) 3.3mL Protogel

(b) 2.5mL Tris-HCl (1.5M)

(c) 100μL SDS

(d) 3.96mL Deionised Water

Ammonium Persulphate Solution

(a) 0.1g in 1mL of water (10% W/V)

Stacking Gel 4%

(a) 1.3mL Protogel

(b) 2.5mL protogel stacking buffer

(c) 6.1mL Deionised Water

Transfer Buffer

(a) 20% Methanol

(b) 70% Deionised Water

(c) 10% 10x Tris Glycerol

Primary Antibody Concentrations

(a) Mouse 1:1000

(b) Mouse 1:250

(c) Rabbit 1:1000

(d) Rabbit 1:100

Secondary Antibody Concentrations

(a) Donkey Anti-Rabbit 1:5000 (in PBS-TWEEN made up to 5mL)

(b) Donkey Anti-Mouse 1:5000 (in PBS-TWEEN made up to 5mL

PBS (10mL) was added to a falcon tube along with 50μL PMSF.

Cells were washed with PBS/PMSF mix (1mL). The cells were spun and the supernatant removed. RIPA (1mL) and PMSF (10μL) was added to an eppendorf and the cells were resuspended in RIPA/PMSF mix (50μL). The cells were then agitated in a cold room for 30 mins. Whilst the cells are cooling the resolving buffer solution was prepared. After 30 mins the cells were removed from the cold room, centrifuged (10min, 13,000 revolutions), and the supernatant collected. Ammonium persulphate (100μL) was then added to stacking gel solution along with TEMD (10μL). The gel was left to set (approximately 10mins). Butanol was added to cassette after the stacking gel, to remove bubbles, and the butanol solution removed with the corner of a piece of filter paper. Whilst the gel was

drying samples were prepared by adding FSB (12μL) to the cell lysate (12μL). The solution was then heated at 95degC for 10 mins to denature. Load the solutions into the wells after removing the comb, add the running buffer (100mL in 900mL of water) and run the gel at 200V for approximately 45mins (Keep an eye on the cassette to make sure it doesn't get too hot, and check for bubbles which means the current has been sucessfully applied). After 45 mins the stacking gel was removed and running gel was added to transfer buffer for 15 mins. After 15 mins the membrane were rinsed with methanol foloowed by deionised water. The membranes and filters were then soaked in transfer buffer for 15mins. The membranes, filter and gel were then placed in a transfer stack, soaked in transfer buffer, and run at 100V for 1 hour. After an hour the membranes were blocked with milk (20%) in PBS-TWEEN for 1 hour at room temperature. The membranes were then washed (x3) with PBS-TWEEN by hand followed by 3 washed of 10mins each on a shacker. The membranes were then incubated overnight with the primary antibody (made up to 2mL in PBS-TWEEN), on a shaker at 4degC. The next day the mebranes were washed (3x) in PBS and then another 3 washes for 10 mins each with PBS-TWEEN. The membranes were than incubated to 1 hour at room temperature with the secondary antibody. After an hour the membranes were washed again in PBS (3x). The membranes were then washed with equal volumes (3mL) of Enhanced Chemiluminescence (ECL) for 60 seconds, and gently blotted dry. The membranes were then developed onto photo paper in a dark room.

2.9 Fluormetric modified Griess Assay for Nitrate and Nitrite Analysis

This methodology was adapted from the Nussler and Glanemann *et al* nature protocol (122), which was adapted from the Greiss reaction (123).

Using the previously described Cell Culture and Transfection Protocol above, culture 6 well plates, and treat the plates with PBS, Nitrite (NO_2, 20μM and 200μM), the cells were washed after the treatment, 3 times with PBS. Cells were

lysed with sterile H_2O (1mL) and dislodged from the plates and analysed using the following assay.

Lysate cell samples (150μL) were added to a black opaque well plate, along with DAN (75μL, 158μM) and HCl (75μL, 1.5M). The well plate was then incubated at 37° for 5 minutes, in the absence of light. NaOH (70μL, 2M) was then added and the solution analysed immediately in the Microtiter Fluorescence Photometer (Fluorstar Galaxy, BMG Labtech Instruments).

3

Characterisation of Aquaporins

To understand the mechanism of AQP trafficking a method of visualising the proteins was required. This was done by creating Green Fluorescent Protein (GFP) fusion AQP vectors. Fusion of the GFP to the C-terminus has already been shown not to interfere with AQP1 function and expression (124), we therefore made assumptions that this may be true and extend to all other AQP classifications. These fusion proteins were then transfected into HEK293 immortalised cell lines, and visualised using confocal microscopy.

The following table 1.1 indicates where within the body the different AQPs are located.

3.1 Expressin Profiles of GFP-tagged AQPs in HEK293 cells, using Confocal Microscopy

Most AQPs are generally thought to be constitutively expressed in the cell surface membranes, and data have been published which would support this theory (125), (126), (127), (128). However, there have been well studied exceptions to the rule, in the regulation of AQP2, by protein-kinase A (PKA) phosphorylation. This AQP is constitutively expressed in vesicles in the cytosol and is trafficked to the cell surface by the activation of vasopressin receptors on binding

of vasopressin(129), (130) to the active side of the receptor. This creates a conundrum as the constitutive cell surface expression model is not consistent with the phosphorylation-dependent cell-surface trafficking phenomena, established for AQP2. Conner *et al* (131), investigated this further with regards to the level of AQP1 membrane expression when cells were subjected to isotonic (1mL DMEM 1x) and hypotonic (3mL H_2O and 1mL DMEM 1x) extracellular environments. They found that membrane expression altered depending on the extracellular osmotic environment.

Replication of the Conner *et al* (131) experiments, were performed and then extended to all AQP (0-12) constructs, and their cellular localisation in isotonic and hypotonic environments recorded, to identify the expression profiles and how they alter, if at all, as a response to changing osmotic environments.

3.1.1 AQP1

AQP1 is a widely expressed protein, and has been extensively characterised in the basolateral and apical plasma membrane of the renal collecting duct in the kidneys. However, they have also been found in red blood cells, the descending limb of Henles loop, the descending portion of the vesa recta, vascular endothelium, gastrointestinal tract, sweat glands and lungs (Table 1.1).

Figure 3.1 demonstrates the results of the replication of Conner *et al* (131) experiement. The cellular expressions of AQP1, are shown in an isotonic extracellular environment (ai) and a hypotonic environment (bi), (aii) and (bii) demonstrates the Fluorescence Intensity Profile (FIP) across the cytosol and plasma membrane for images (ai) and (bi). When the cells were exhibited to a hypotonic extracellular environment the expression profile (bii) identified AQP1 to be mainly restricted to the cell membrane, nuclear membrane and small regions of vesicles within the cytosol. When this was compared with an isotonic extracellular solution, it was clear to see that the FIP (aii) identified no discrete expression

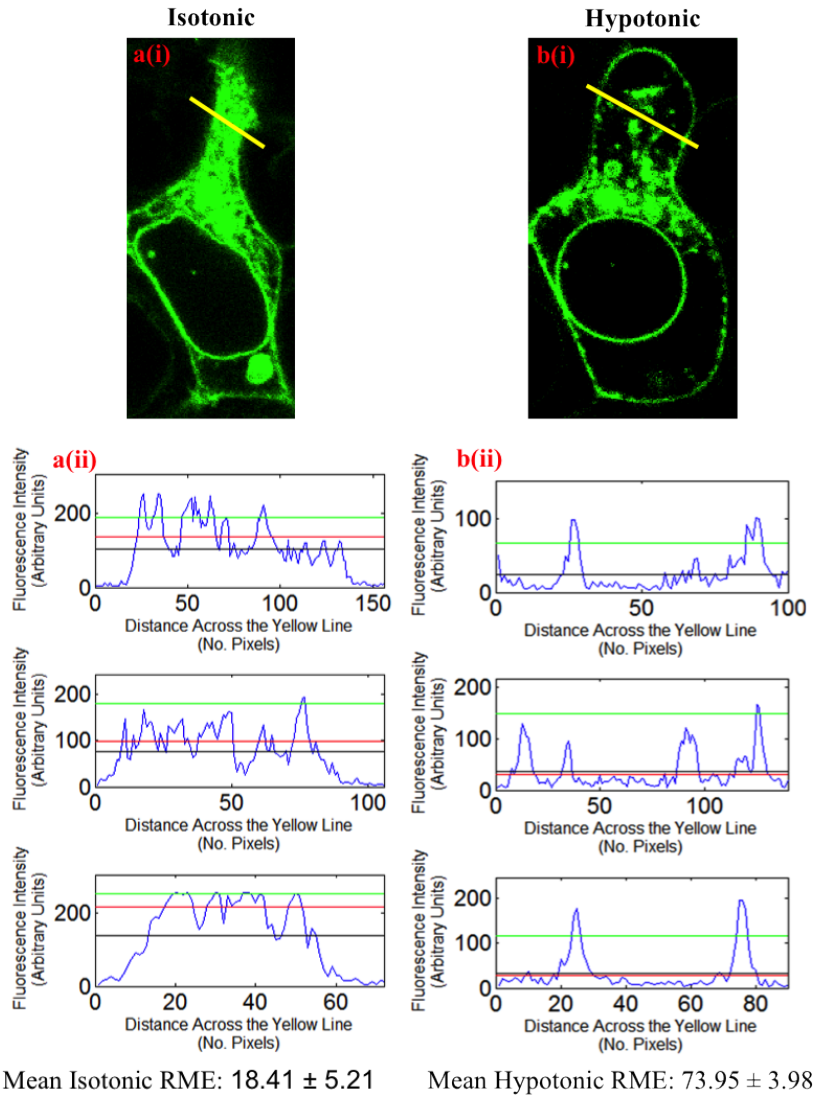

Figure 3.1: AQP1-GFP fusion proteins in HEK293 cells in isotonic (ai) and hypotonic (bi) extracellular environments, with FIP calculated across the yellow lines using ImageJ software. - The Fluorescence profiles (aii - isotonic) and (bii - hypotonic) indicate the fluorescence intensity across the yellow line (example shown in (ai) and (bi)). A minimum of three lines were drawn in three different positions, as shown in the representative image (ai) and (bi). The red line shows the average expression in the cytosol, the green line shows the average expression in the membrane, and the black line shows the threshold at which the fluorescnce profile is detected against the background noise.

profiles like (bii), instead it demonstrated a relatively even distribution of expression. This was also reflected in the realtive membrane expression (RME) values as they changed from 18.41 ± 5.21 in an isotonic environment to 73.95 ± 3.98 for a hypotonic extracellular environment. The RME is what the Conner lab group have termed and defined as the method for determining the subcellular localization. This is whereby a minimum of 3 line profiles were measured and distributed at regular intervals covering the plasma membrane and the cytosol but avoiding the nucleus of a minimum of three cells from at least three independent experiments. The fluorescence intensity over this distance was measured, and the difference between the peak and the plateau of fluorescence was divided by the maximum fluorescence along the line scan to calculate the percentage of fluorescence at the membrane. This was termed the relative membrane expression (RME) This rejected the null hypothesis that there was no change in cellular expression between a hypotonic and isotonic extracellular environment at a 99% level yielding a p-value of p=0.000001. Having successfully repeated the Conner and Conner et al experiment, the methodology was repeated for all 12 remaining AQP constructs, to establish their isotonic and hypertonic Fluorescence Intensity Profiles.

3.1.2 AQP0

AQP0 was far less characterised in published literature than AQP2, however, had been found to be expressed in Lens fibre gap junctions and renal collecting ducts (1.1). AQP0 contruct were transiently transfected into HEK cell lines, as was done with AQP1, and the living cells analysed by confocal microscopy. Figure 3.2 (ai) showed an even distribution expression profile across the cytosol and membrane and then when the extracellular tonicity was altered to be isotonic, the mean RME) changed from 24.83 ± 10.94 to 61.73 ± 14.66. This however, was not significant enough a change to reject the null hypothesis at a 95% level. This did identify a limitation to the technique, cells which did not transfect as well were difficult to analyse using the image analysis software, as it was difficult for the programme to significantly ditinguish the fluorescence profile of the AQPs with

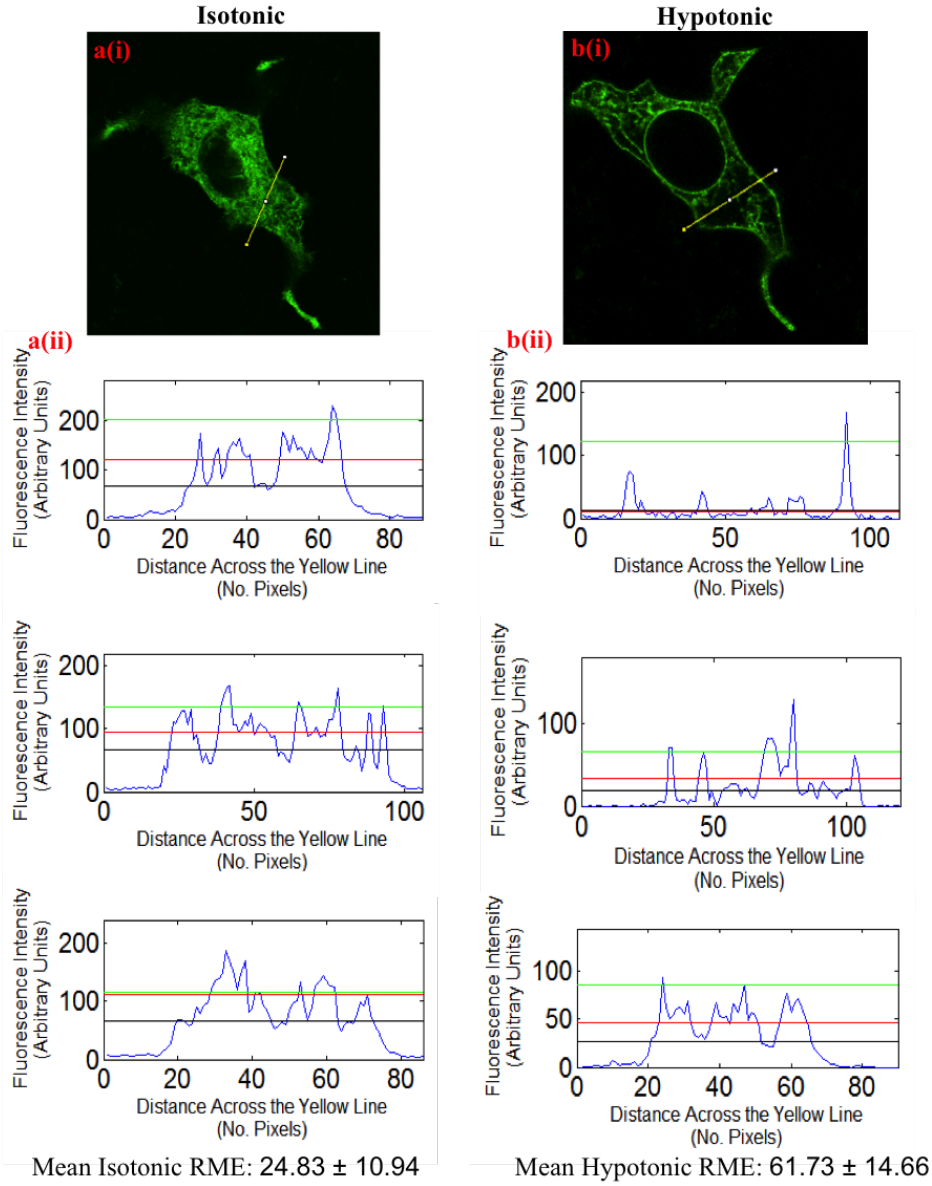

Figure 3.2: AQP0-GFP fusion proteins in HEK293 cells in isotonic (ai) and hypotonic (bi) extracellular environments, with FIP calculated across the yellow lines using ImageJ software. - The Fluorescence profiles (aii - isotonic) and (bii - hypotonic) indicate the fluorescence intensity across the yellow line (example shown in (ai) and (bi)). A minimum of three lines were drawn in three different positions, as shown in the representative image (ai) and (bi). A minimum of three lines were drawn in three different positions, as shown in the representative image (ai) and (bi). The red line shows the average expression in the cytosol, the green line shows the average expression in the membrane, and the black line shows the threshold at which the fluorescnce profile is detected against the background noise.

background fluorescence even when the contrast and brightness were altered, with standard scientific image adjustment protocols. This demonstrated quite clearly that the images or FIPs in their own right were insufficient to make decisions regarding cellular expression profile relocalisation as a response to a change in extracellular tonicity, and that both together were necessary to understand the regulation of AQPs, and that with further development of transfection reagents, these expression profiles could be improved.

3.1.3 AQP2

AQP2 is a heavily researched aquaporin owing to its expression in response to vasopressin regulation in the apical plasma membrane of the collecting ducts in the kidneys,(132), (130). This study found that Arginine-vasopressin (AVP) is released from the pituitary during dehydration, causing the need for more water to be absorbed from the filtrate. AVP then binds itself to the receptors in principal cells causing an increase in cAMP, which consequently activates protein kinase A (PKA), (133), (48). PKA is then required to activate three of the AQP2 polypeptide tetramers which consequently translocates the protein to the apical plasma membrane of the principal cell. Therefore, if we were to repeat Conner and Conner *et al* experiment we would have expected to have seen little to no change in the expression profile when the extracellular tonicity was altered. As we can see from figure 3.3, there was little to no change in the expression profile of AQP2 when the osmotic extracellular environment changed from an isotonic solution (mean isotonic RME = 10.98 ± 7.80) to, a hypotonic solution (mean hypotonic RME = 20.41 ± 3.07). This was a logical finding as there would have been no AVP available in the cellular medium broth to activate cAMP, to phosphorylate AQP2 and translocate it from an intracellular expression profile to a cellular membrane expression profile. This meant that the null hypothesis could not be rejected as there was no significant increase in REM between the two treatements.

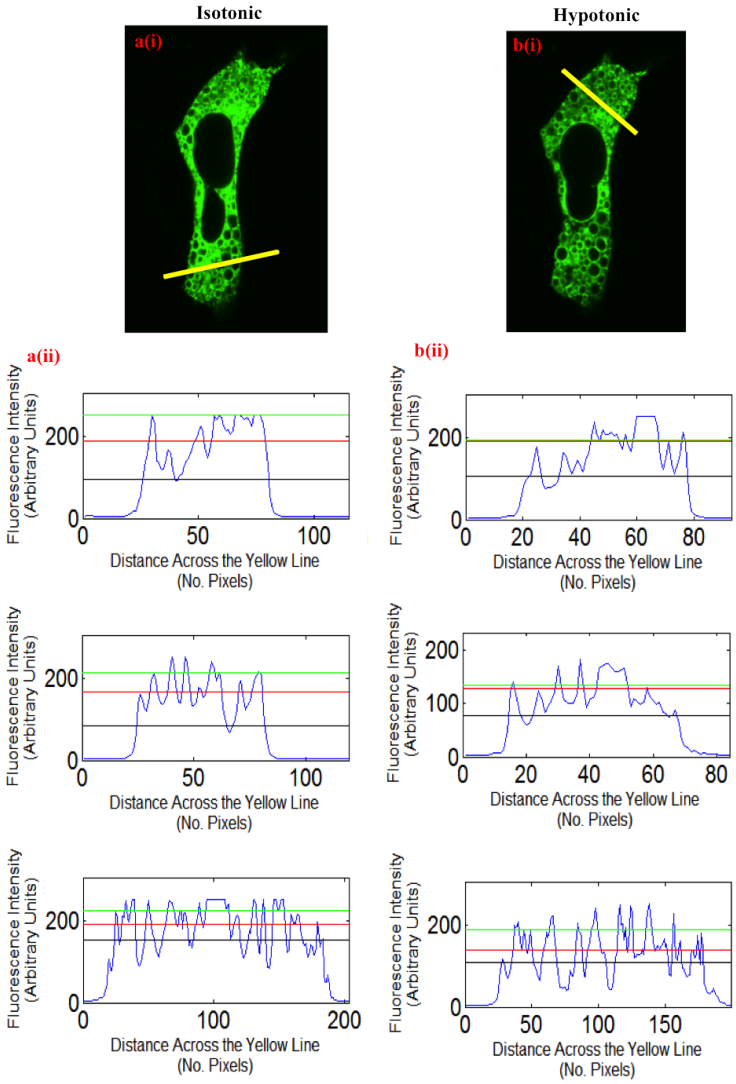

Figure 3.3: AQP2-GFP fusion proteins in HEK293 cells in isotonic (ai) and hypotonic (bi) extracellular environments, with FIP calculated across the yellow lines using ImageJ software. - The Fluorescence profiles (aii - isotonic) and (bii - hypotonic) indicate the fluorescence intensity across the yellow line (example shown in (ai) and (bi)). A minimum of three lines were drawn in three different positions, as shown in the representative image (ai) and (bi). A minimum of three lines were drawn in three different positions, as shown in the representative image (ai) and (bi). The red line shows the average expression in the cytosol, the green line shows the average expression in the membrane, and the black line shows the threshold at which the fluorescnce profile is detected against the background noise.

3.1.4 AQP3

AQP3 followed the same expression relocalisation profile (figure 3.4) as AQP1. This expression profile was to be expected as literature stated the AQPs were found in the basolateral membrane of the proximal collecting duct of the kidneys along with AQP1. However, a large difference between AQP1 and AQP3 is that AQP3 had been identified to be an aquaglyceroporin. This meant that AQP3 was not only selective for water but also for glycerol. There was also some discussion suggesting AQP3 may have been effective at transporting glycerol however this information was non-specific and unsubstantiated.

Figure 3.4 (ai) clearly demonstrated that AQP3 was constitutively expressed in the cytosol and membrane (mean isotonic RME = 41.91 $\pm$ 3.11) however when exhibited to a change in extracellular tonicity, the expression profile changed from (aii) to (bii) indentifying translocation of AQP3 from the cytosol to the plasma membrane (mean hypotonic RME = 73.43 $\pm$ 2.66). This change in RME yielded a p-value = 0.000001 rejecting the null hypothesis at the 99% level.

3.1.5 AQP4

AQP4 has been found in a variety of tissues including the heart, kidney, lung, trachea and brain, and is the most abundant water channel protein in the brain, with high levels of expression in the astrocytes forming part of the blood brain barrier **??**. Manley *et al* (60) (66) found that AQP4 knockout mice demonstrated protection against cytotoxic brain oedema. This suggested that it was the presence of AQP4 which was responsible for the formation of a brain oedema. However, it was also found that in stroke induced mice, the concentration of AQP4 did not significantly increase. This makes the investigation of a translocation phenomenon in AQP4 of particular interest as it could explain AQP4's role in the formation of an oedema, without change in protein concentration, simply expression profiling across the plasma membrane. Figure 3.5, showed AQP4 translocated to the cell membrane from a cytosoloic expression profile, in response to a change in

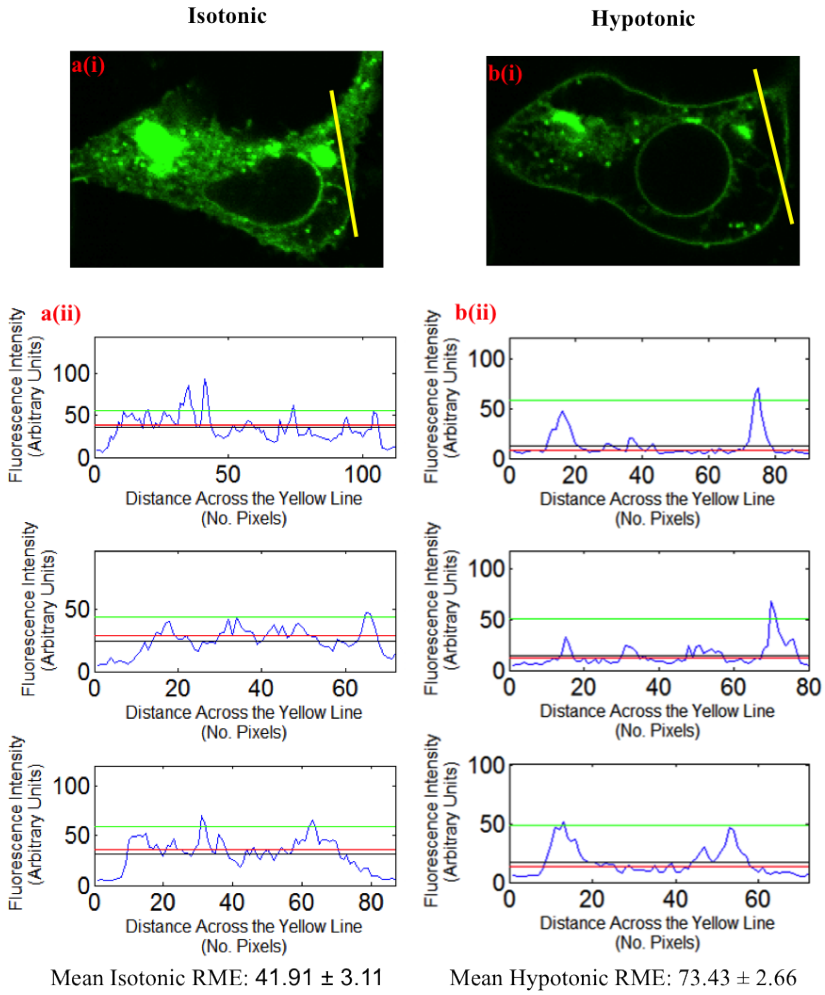

Figure 3.4: AQP3-GFP fusion proteins in HEK293 cells in isotonic (ai) and hypotonic (bi) extracellular environments, with FIP calculated across the yellow lines using ImageJ software. - The Fluorescence profiles (aii - isotonic) and (bii - hypotonic) indicate the fluorescence intensity across the yellow line (example shown in (ai) and (bi)). A minimum of three lines were drawn in three different positions, as shown in the representative image (ai) and (bi). A minimum of three lines were drawn in three different positions, as shown in the representative image (ai) and (bi). The red line shows the average expression in the cytosol, the green line shows the average expression in the membrane, and the black line shows the threshold at which the fluorescnce profile is detected against the background noise.

the extracellular tonicity from an isotonic to a hypotonic environment. It was clear to see from the Fluorescence Intensity Profiles (FIPs) (a(ii)) and (b(ii)) that the RME changed from RME = 28.77 ± 6.78 (isotonic) increasing to 78.84 ± 1.84 (hypotonic). This rejected the null hypothesis at a 99% level yielding a p=0.000050. This finding is of significance as it could explain, or give insight into the conflicting research findings when evaluating cytotoxic brain oedema formation.

3.1.6 AQP5

AQP5 as stated in the introduction, has been found to be located in the mouth, tear-ducts, and pulmonary secretion tissue, Table **??**. Regardless of this, it might still be expected that AQP5 would exibit the same physiological translocation process as AQP1 and AQP4, when the extracellular tonicity was altered.

It can be seen from figure 3.6 that AQP5 did not exhibit the same translocation process. In fact AQP5 seemed to have a very different isotonic FIP to AQPs 0-4 in an isotonic extracellular environment. It appeared that image (ai) had a heavy expression profile in the membrane on the cell, and as the extracellular environment was altered to be hypotonic, the membrane expression become slightly more intense suggesting that any cytosolically expressed protein also translocated to the cellular membrane. This was evident from the RME Values, the isotonic RME = 50.08± 8.38 and the hypotonic RME = 83.06 ± 2.05, which did not demonstrate a statistically significant change and the null hypothesis could not be rejected at a 95% level, P=0.51874. This however, did not mean it followed the same expression profile as AQP0may give some interesting insight into the role and function of cells in tissues in close proximity to AQP5.

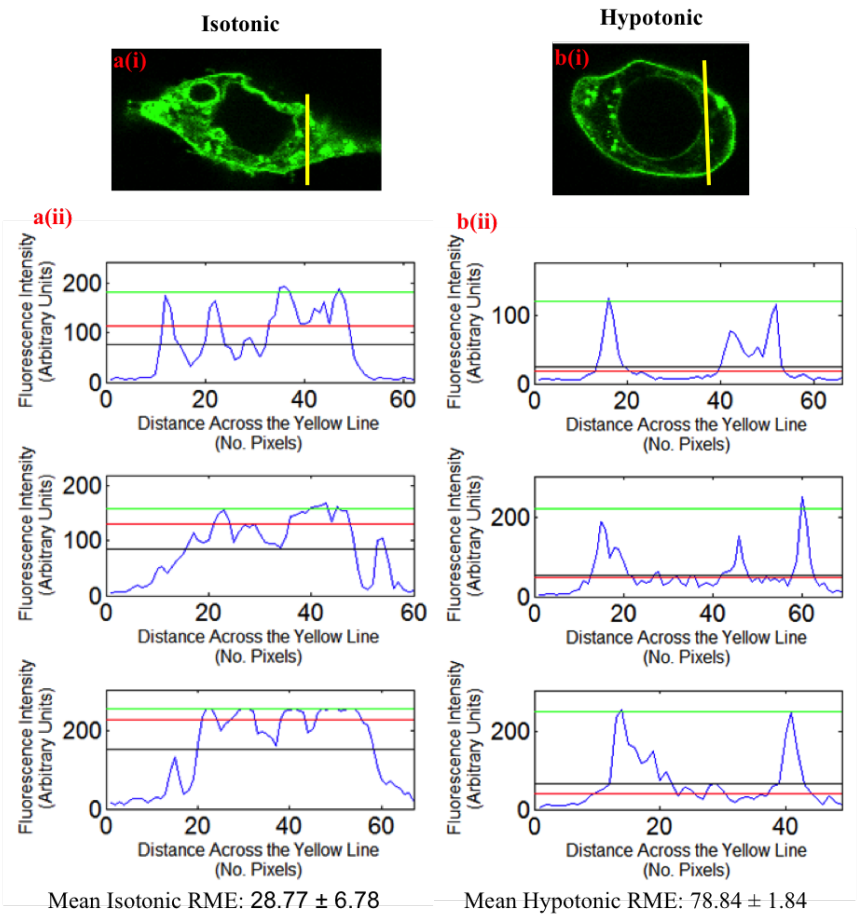

The null hypothesis was rejected at the 99% level. p = 0.000050

Figure 3.5: AQP4-GFP fusion proteins in HEK293 cells in isotonic (ai) and hypotonic (bi) extracellular environments, with FIP calculated across the yellow lines using ImageJ software. - The Fluorescence profiles (aii - isotonic) and (bii - hypotonic) indicate the fluorescence intensity across the yellow line (example shown in (ai) and (bi)). A minimum of three lines were drawn in three different positions, as shown in the representative image (ai) and (bi). A minimum of three lines were drawn in three different positions, as shown in the representative image (ai) and (bi). The red line shows the average expression in the cytosol, the green line shows the average expression in the membrane, and the black line shows the threshold at which the fluorescnce profile is detected against the background noise.

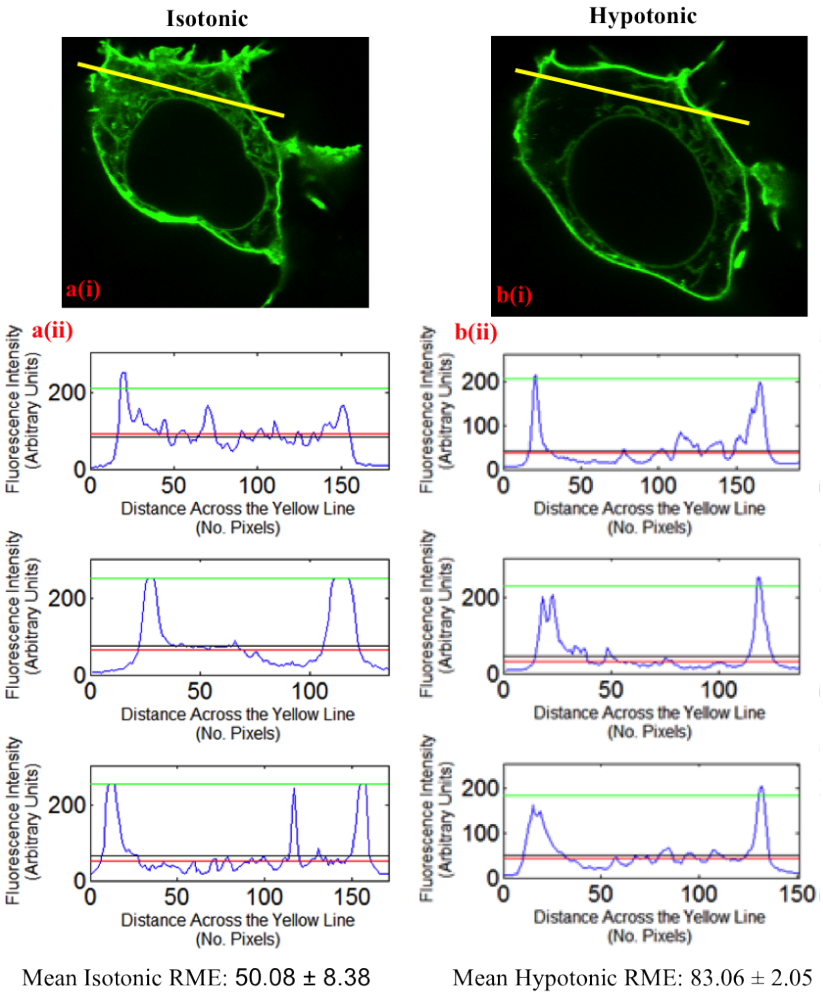

Figure 3.6: AQP5-GFP fusion proteins in HEK293 cells in isotonic (ai) and hypotonic (bi) extracellular environments, with FIP calculated across the yellow lines using ImageJ software. - The Fluorescence profiles (aii - isotonic) and (bii - hypotonic) indicate the fluorescence intensity across the yellow line (example shown in (ai) and (bi)). A minimum of three lines were drawn in three different positions, as shown in the representative image (ai) and (bi). A minimum of three lines were drawn in three different positions, as shown in the representative image (ai) and (bi). The red line shows the average expression in the cytosol, the green line shows the average expression in the membrane, and the black line shows the threshold at which the fluorescnce profile is detected against the background noise.

3.1.7 AQP6

AQP6 as stated in the introductions has been found to be located in the Loop of Henle, and also as a transporter of nitrates and nitrites, Table 1.1. This made it a very interesting aquaporin to investigate as understanding the transportation of nitrates and nitrites into specific tissues would enable us to better understand the effects of hypoxia or localised hypoxia, and potentially vasodilation better. It may also give insight as to why some tissues maintain a high level of nitrates and nitrites, even when the extracellular environments change (This is a comment based on as yet unpublished work by Prof Martin Feelisch, with whom I was previously working).

Unfortunately the transfection of AQP6-GFP into HEK293 proved exceptionally difficult even with a variety of modifications to the protocol, this resulted in little to no fluorescence so no image was captured.

3.1.8 AQP7

AQP7 has been found to be expressed in adipose cells and identified to be a class of aquaglyceroporin, Table 1.1. (134) identified that AQP7 facilitates efflux of glycerol from adipose tissue and that AQP7 deficiency leads to triglyceride accumulation in adipose tissue and adult onset diabetes. Understanding more the mechanism of activation for transportation, could help us better understand the onset of adult diabetes. Unfortunately AQP7-GFP expression proved exceptionally difficult to transfect even with a variety of modifications to the protocol. There was little to no fluorescence so no image was captured.

3.1.9 AQP8

Unfortunately AQP8-GFP expression proved exceptionally difficult to transfect even with a variety of modifications to the protocol. There was little to no fluo-

rescence so no image was captured.

3.1.10 AQP9

AQP9 was another aquaporin identified to be an aquaglyceroporin and involved in facilitating efflux of glycerol from adipose tissue, (134). Unfortunately AQP9-GFP expression proved exceptionally difficult to transfect even with a variety of modifications to the protocol. There was little to no fluorescence so no image was captured.

3.1.11 AQP10

Unfortunately AQP10-GFP expression proved exceptionally difficult to transfect even with a variety of modifications to the protocol. There was little to no fluorescence so no image was captured.

3.1.12 AQP11

Unfortunately AQP11-GFP expression proved exceptionally difficult to transfect even with a variety of modifications to the protocol. There was little to no fluorescence so no image was captured.

3.1.13 AQP12

AQP12-GFP expression proved exceptionally difficult to transfect, and the images where very poor. This meant that the image analysis software could not distinguish the fluorescence from the background sufficiently to form image analysis, to identify the specific localisation fo the AQP12-GFP expression. This can be seen in figure 3.7

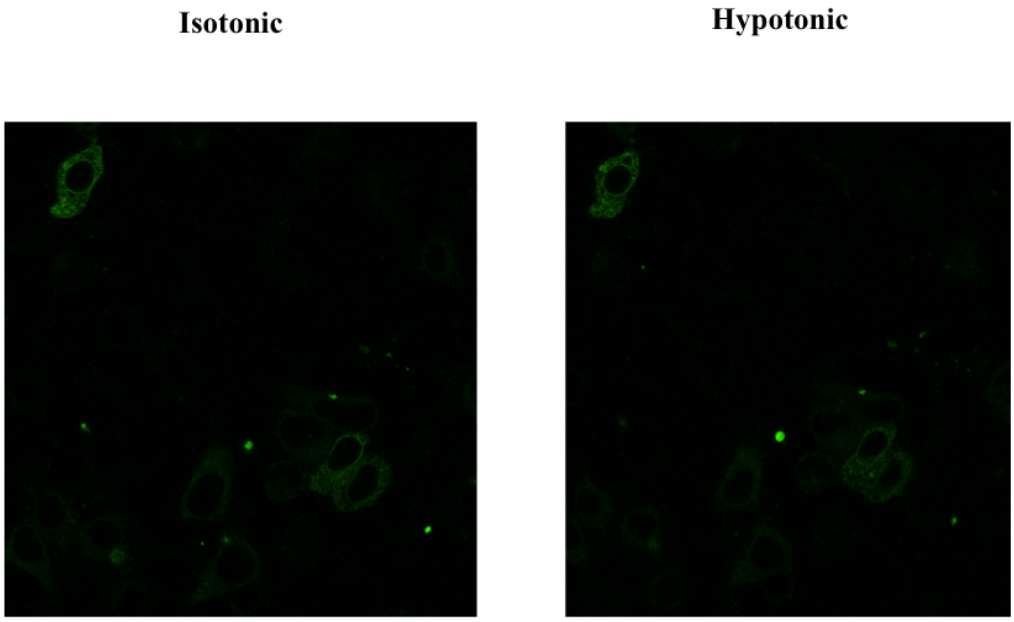

Figure 3.7: AQP12-GFP fusion proteins in HEK293 cells in isotonic (ai) and hypotonic (bi) extracellular environments. No FIP could be calculated as the software couldn't distringuish green pixels sufficiently from the background noise. -

As can be seen from the FIP analysis not all aquaporins are expressed in the same way. This can start to elucidate some information about the roles aquaporins have in those cells and tissues. AQP4 is of particular interest as this translocation phenomenon could provide important information about its activation and its involvement in the formation of a cytotoxic oedema, which could help to identify pathways for drugs to target to prevent this as a cause of death.

However, the expression profile translocating to the membrane upon changes in extracellular tonicity, does not indicate a functional response to the transportation of water across the cell membrane, as we would expect in a model of cytotoxic oedema.

As the images were analysed an odd phenomenon was identified. The cells that exhibited a translocation from cytosol expression to membrane expression profiles, following a change in extracellular tonicity from isotonic to hypotonic solutions, exhibited a form of cellular swelling 3.1, 3.2, 3.4, 3.5. However, those that did not observe this phenomenon did not appear to demonstrate any functional swelling 3.3. Therefore, a methodology was devised that would enable the surface area of the cell to be calculated based on the image, which would in turn quantify the functional swelling response to the translocation of AQPs from the cytosol to the cellular membrane, following a change in extracellular tonicity.

3.2 Functional Swelling Response as a Direct Result of Translocation to the Plasma Membrane

The methodology used to analyse the functional swelling was adapted from functions available in the the ImageJ software. Below is an example of how the macro detailed in the materials and methods, calculated the surface area of a cell. It starts by identifying images over a certain selected size, to eliminate fluorescence clusters in the image, see figure 3.8 (a). The macro then converts them into a

binary image. This means, whenever their is a pixel of fluorescence, the pixel is converted to black, if their is either no fluorescence or fluorescence below a certain threshold then a white pixel is recorded in the image, see figure 3.8 (b). The macro then runs analysis to find the edge of the black binary image and creates an outline, see figure 3.8 (c). The surface area of the outlined portion is then calculated.

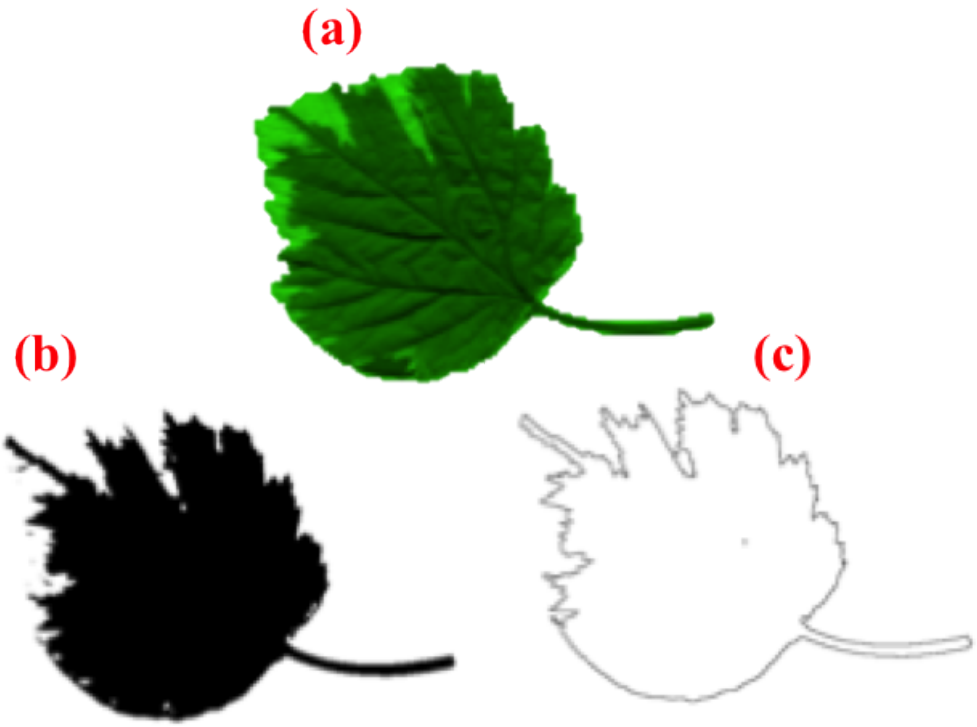

Figure 3.8: Outputs of the macro created to calculate the surface area of a leaf undergoing expression profiling and functional swelling analysis, using ImageJ - (a) is the Original image of a leaf, (b) the binary image, and (c) the outline of the original image

This methodology was applied to AQP4 to establish whether or not the functional swelling in an extracellular hypotonic solution was statistically significant in being different from the size of the cell in an isotonic extracellular environment. As we can see from figure 3.9 there is a statistically significant (p=0.0001) increase in

the cell surface area in a hypotonic environment (374.65mm^2) compared with that of an isotonic environment (523.92mm^2, total increase of 145.19%). This shows that the translocation of AQP4 from the cytosol, has a functional relationship with the cell volume. This phenomenon is also a fully reversible process when the solution is then changed back to an isotoni extracellular solution.

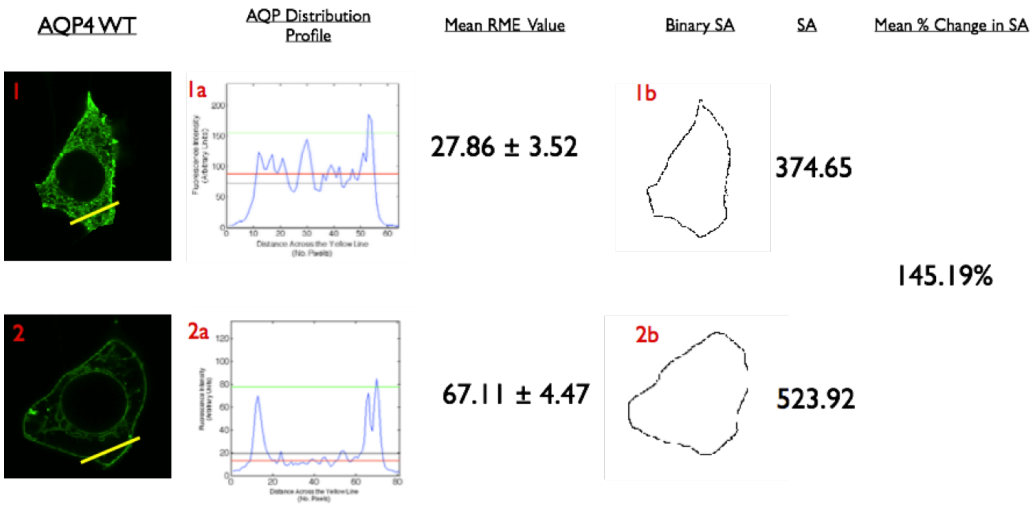

Figure 3.9: AQP4-GFP fusion proteins in HEK293 cells in isotonic (1) and hypotonic (2) extracellular environments, with FIP across the yellow lines and surface areas calculated using ImageJ and Matlab software. - The Fluorescence profiles (1a-isotonic) and (2b-hypotonic) indicate the fluorescence intensity across the yellow line (value shown in (Mean RME value column). A minimum of three lines were drawn in three different positions, as shown in the representative image (1) and (2).Oulines of the cells were generated (1b-Isotonic and 2b-Hypotonic) and the surface areas calculated (SA column) using matlab software. The mean percentage change for n=3 was calculated (mean % change column)

3.3 Aquaporin 4: Translocation and Inhibition

The next step forward was to use this new relationship to help define a mechanism for translocation from the cytosol to the cell membrane by exposing the cells to different metabolic cellular inhibitors. These included:

- Non-Specific Kinase Inhibitor - Hypericin (50μM), (135)
- PKC inhibitor - MryPKCi (50μM), (135)
- PKA inhibitor - MryPKAi (50μM), (135)
- Actin Inhibitor - Cytochalasin D
- Microtubule Formation - Demecolcine
- Calcium Free media

Using these matabolic inhibitors, it was possible to start to identify pathways by establishing which inhibitors retarded the normal translocation process. The above inhibitors were therefore used on WT AQP4 transiently transfected HEK293 cells.

3.3.1 Non-Specific Kinase Inhibitor - Hypericin

The first inhibitor used was a non-specific kinase inhibitor. Kinases are enzyme that transfer phosphate groups from high-energy donor molecules e.g. ATP, to substrates. They have been identified to be critical in cellular transport, metabolism, cell signalling, secretory processes, protein regulation, and many other cellular pathways, which is why they are of interest in the translocation phenomenon seen in AQP4, (136). In addition to this AQP2's translocation is regulated by PKA, and an initial assumption can be made that PKA may be involved in the translocation process of AQP4.

Hypericin, is the inhibitor utilised in this experiment, as it is a widley used non-specific kinase inhibitor. It would therefore be expected that the translocation of the AQP4-GFP tagged construct to the plasma membrane, from the cytosol,

when the the extracellular envionment changes from an isotonic to a hypotonic solution would be retarded, and that no statistically significant increase in the surface area of the cell is observed.

Figure 3.10 shows there is no significant increase in the surface area of the cell, and that there is a non-significant change in the RME value from 21.85 ±6.80 (isotonic) to 38.22 ±5.58 (hypotonic). This indicates that a kinase is essential in activating the translocation process for AQP4 to move from a cytosol expression profile to a plasma membrane expression profile. This is further confirmed by the very small increase in functional swell (103.5% ± 2.05%), which could not reject the null hypothesis at a 95% that there is no significant change in surface area of the cell when the extracellular tonicity changes from an isotonic solution to a hypotonic solution.

Further investigations into specific kinase inhibitors would enable the identification of which kinases are critical in the translocation mechanism.

3.3.2 PKC Inhibitor - MyrPKC

PKC is a well documented enzyme involved in controlling the function of other proteins via a phosphorylation process on amino acids serine and threonine. PKC in itself is regulated by signals such as increases in the concentration of diacylglycerol (DAG) or calcium ions, and as a result plays an important role in signal transduction cascades. This type of signalling cascade may be involved in the translocation of AQP4 from a cytosol expression profile to a plasma membrane expression profile, as it has already been established as an important regulator of AQP1 (131).

To investigate if PKC is involved in this phenomenon, the experiment with hypericin was adapted and the PKC inhibitor, MyrPKC, used in its place. If PKC was of significant importance in the translocation phenomenon, then after the

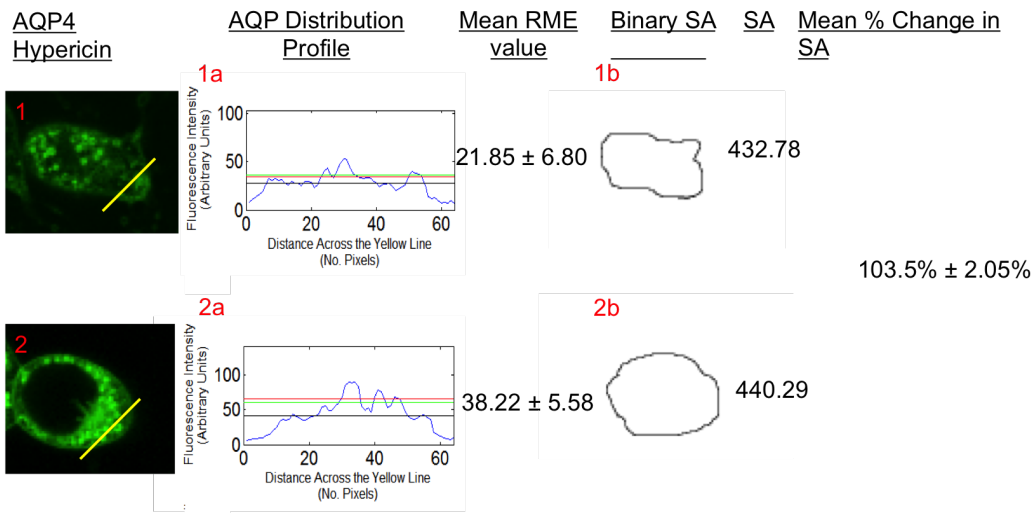

Figure 3.10: AQP4-GFP fusion proteins in HEK293 cells exhibited to non-specific kinase inhibitor, Hypericin, in isotonic (1) and hypotonic (2) extracellular environments, with FIP across the yellow lines and surface areas calculated using ImageJ and Matlab software. - The Fluorescence profiles (1a-isotonic) and (2b-hypotonic) indicate the fluorescence intensity across the yellow line (value shown in Mean RME value column). A minimum of three lines were drawn in three different positions, as shown in the representative image (1) and (2).Oulines of the cells were generated (1b-Isotonic and 2b-Hypotonic) and the surface areas calculated (SA column) using matlab software. The mean percentage change for n=3 was calculated (mean % change column)

addition of MyrPKC, the AQP4 would be unable to translocate from the cytosol to the plasma membrane, meaning the RME values would not significantly differ and the cell's surface area, would not significantly increase, as a result of a change in extracellular tonicity.

As can be seen from Figure 3.11 there is a translocation of the AQP4-GFP tagged construct from a predominantely cytosol expression profile in an isotonic extracellular envionvment to a plasma membrane FIP in a hypotonic extracellular environment. This is also mirrored in the mean RME values, which were found to have had a statistically significant change from 27.27 $\pm$ 4.73, to 55.28 $\pm$ 3.97 for isotonic and hypotonic environments, respectively, rejecting the null hypothesis at the 99% level ($p \leq 0.0001$). You can also see from (1b) and (2b) that the cells increased in surface area by an average of 141.86% $\pm$ 7.09%, also rejecting the null hypothesis at a 99% level.

This demonstrates that PKC, does not regulate the translocation phenomenon exhibited by AQP4-GFP tagged WT constucts, as is seen with AQP1. However, further research into other protein kinase inhibitors, may prove useful. For example Fushimi *et al* (47) and Katsura *et al* (48), identified PKA to be an important regulator of the translocation phenomenon found with AQP2, when it was activated by vasopressin.

3.3.3 PKA inhibitor - Myr PKA

Protein Kinase A is a very well documented cAMP activated kinase (137), and has already been identified as a regulator of AQP2's translocation from a cytosolic expression profile to a plama membrane expression. If AQP4's translocation were being regulated by PKA, then a PKA inhibitor would prevent PKA from activating AQP4 to translocate to the plasma membrane. It would therefore, in this experiment, be expected that there be no statistically significant change in the RME values or a functional swelling response, when comparing isotonic

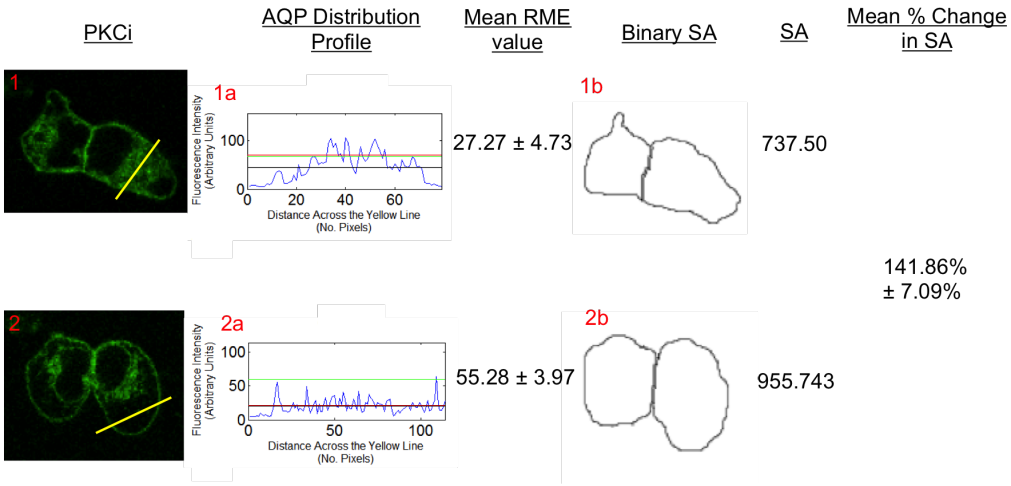

Figure 3.11: AQP4-GFP fusion proteins in HEK293 cells exhibited to PKCinhibitor MryPKCi in an isotonic (1) and hypotonic (2) extracellular environment, with FIP across the yellow lines and surface areas calculated using ImageJ and Matlab software. - The Fluorescence profiles (1a-isotonic) and (2b-hypotonic) indicate the fluorescence intensity across the yellow line (value shown in (Mean RME value column). A minimum of three lines were drawn in three different positions, as shown in the representative image (1) and (2).Oulines of the cells were generated (1b-Isotonic and 2b-Hypotonic) and the surface areas calculated (SA column) using matlab software. The mean percentage change for n=3 was calculated (mean % change column).

with hypotonic extracellular environments. The PKA inhibitor used for this experiement was, Myr-PKA.

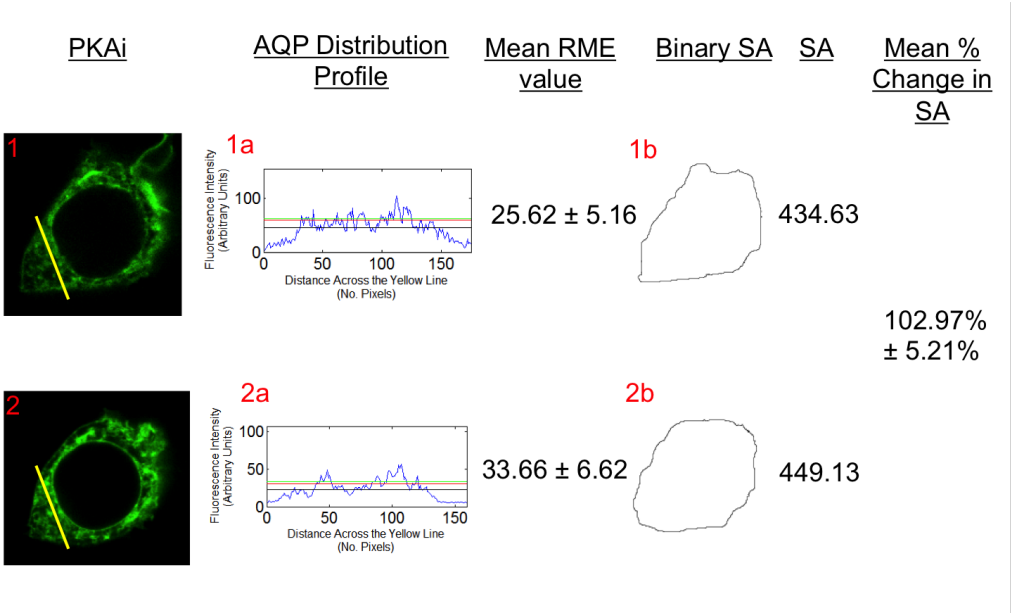

Figure 3.12: AQP4-GFP fusion proteins in HEK293 cells exhibited to Myr-PKA in an isotonic (1) and hypotonic (2) extracellular environment, with FIP across the yellow lines and surface areas calculated using ImageJ and Matlab software. - The Fluorescence profiles (1a-isotonic) and (2b-hypotonic) indicate the fluorescence intensity across the yellow line (value shown in (Mean RME value column). A minimum of three lines were drawn in three different positions, as shown in the representative image (1) and (2).Oulines of the cells were generated (1b-Isotonic and 2b-Hypotonic) and the surface areas calculated (SA column) using matlab software. The mean percentage change for n=3 was calculated (mean % change column)

As can be seen from figure 3.12 there was not a significant change in the RME of AQP4-GFP tagged HEK cell value for an isotonic solution (RME = 25.62 ± 5.16) compared with the RME value for a hypotonic solution (RME = 33.66 ± 6.62). This is not a significant change in RME, and therefore the null hypothesis could not be rejected at a 95% level (p=0.55). There was also no significant change in

the surface area of the cell 102.97% ± 5.21 % (p=0.54) as the extracellular solution changed from an isotonic to a hypotonic solution. This demonstrates that AQP4 is translocated by PKA in a similar way to AQP2, however, it is unlikely to be regulated by vasopressin, as this molecule was not available to the cell in this experiment.

3.3.4 Actin Inhibitor - Cytochalsin D

Actin is a multifunctional protein that forms microfilaments, one of 3 major components of the cytoskeleton. Owing to this, actin is known to be involved in more protein interactions than any other known protein. Aggregation of actin forms microfilaments, then microfilaments alongside micotubules combine to form the cytoskeleton. The cytoskeleton is the cellular scaffolding contained within the cells cytoplasm. The cytoskeleton plays an important role in both intracellular transport and cellular division. The intracellular transport is the movement of vesicles and organelles, such as those containing aquaporins, (136).

Cytochalsin D is a mycotoxin, which is an alkaloid. Cytochalasin D is cell permeable and a potent inhibitor of actin polymerisation, which disrupts the formation of microfilaments. Therefore, its use in this experiment would also inhibit actin and prevent the formation of microfilaments. This will ultimately disrupt the cytoskeleton, which is important in the role of vesicle transportation. This should therefore result in no significant difference in RME and cell surface area, when the extra cellular tonicity is changed from an isotonic solution to a hypotonic solution.

As can be seen from figure 3.13 there is no significant change in the translocation of the AQP4-GFP tagged construct from a cytosol expression profile to a plasma membrane expression profile, when the extracellular tonicity is changed from isotonic (RME = 26.07 ± 6.10) to a hypotonic (RME = 32.16 ± 4.48) environment, this does not reject the null hypothesis at a 95

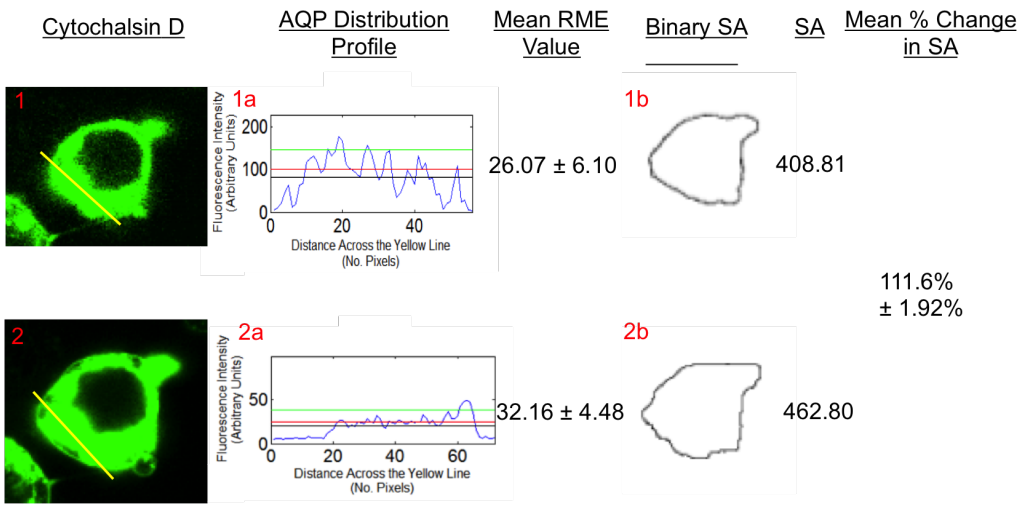

Figure 3.13: AQP4-GFP fusion proteins in HEK293 cells exhibited to Cytochalsin D in isotonic (1) and hypotonic (2) extracellular environments, with FIP across the yellow lines and surface areas calculated using ImageJ and Matlab software. - The Fluorescence profiles (1a-isotonic) and (2b-hypotonic) indicate the fluorescence intensity across the yellow line (value shown in (Mean RME value column). A minimum of three lines were drawn in three different positions, as shown in the representative image (1) and (2). Oulines of the cells were generated (1b-Isotonic and 2b-Hypotonic) and the surface areas calculated (SA column) using matlab software. The mean percentage change for n=3 was calculated (mean % change column)

3.3.5 Microtubule Inhibitor - Demecolcine

Demecolcin (also known as colcemid) is often used in chemotherapy. Demecolcine is a toxic molecule that depolymerises microtubules and limits microtubule formation and inactivates spindle formation, which in turn prevents cells from undergoing mitosis stopping metaphase. Preventing the formation of microtubules, results in a disruption in the formation of the cytoskeleton which prevents the translocation of vesicles from the cytoplasm to the plamsa membrane. We would therefore expect in this experiment that the translocation phenomenon would be prevented as we have seen in Cytochalsin D. There would not be a significant change in RME or cell surface area, as the vesicles containing the AQP4-GFP tagged construct, would not be able to translocate along the cytoskeleton from the cytoplasm to the membrane.

As can be seen from figure 3.14 there is a significant change in the translocation of the AQP4-GFP tagged construct from a cytosol expression profile to a plasma membrane expression profile, when the extracellular tonicity is changed from isotonic (RME = 42.25 $\pm$ 5.4) to a hypotonic (RME = 78.52 $\pm$ 2.62) environment. This does reject the null hypothesis at a 99% level (p=0.000075). The surface does also seem to alter as the mean percentage change in size is 126.57% $\pm$ 12.01%, which also rejected the null hypotheses at a 99% level.

This identifies that microfilaments are more involved in the translocation of AQP4 to the plasma membrane than microtubules are, as microtubules inhibitor did not appear to prevent the translocation. This is a little surprising as the cytoskeleton, would seemingly be sufficiently damaged to allow for any translocation. This could explain the slightly poor expression profiles observed in all demecolcine experiments.

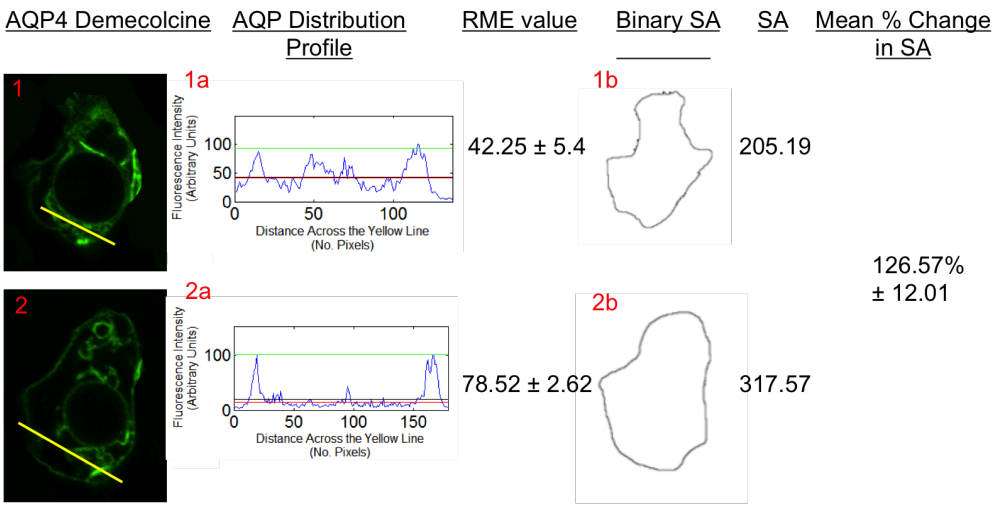

Figure 3.14: AQP4-GFP fusion proteins in HEK293 cells exhibited to Demecolcine in isotonic (1) and hypotonic (2) extracellular environments, with FIP across the yellow lines and surface areas calculated using ImageJ and Matlab software. - The Fluorescence profiles (1a-isotonic) and (2b-hypotonic) indicate the fluorescence intensity across the yellow line (value shown in (Mean RME value column). A minimum of three lines were drawn in three different positions, as shown in the representative image (1) and (2).Oulines of the cells were generated (1b-Isotonic and 2b-Hypotonic) and the surface areas calculated (SA column) using matlab software. The mean percentage change for n=3 was calculated (mean % change column)

3.3.6 Calcium-Free Extracellular Media

Conner *et al*, (131) found that a cytosolic elevation of calcium ions following hypotonic stimulus evokes, and is necessary for translocation of AQP1. We therefore wanted to see if this were true for AQP4, was calcium an integral part of the translocation pathway. We therefore decided to expose the cells to calcium free media for a period, before confocal microscopy, and use micropore filtered and deionised water to ensure a low calcium ion content (this is particularly difficult in the UK where there is a high amount of Calcium Carbonate in the ground and therefore water system). If calcium was an integral part of the translocation process we would expect there to be no significant change in RME or cell surface area, when the extracellular tonicity is changed from an isotonic to a hypotonic environment, in cells cultured in calcium-free media.

As can be seen from figure 3.15 there was no significant change in the translocation of the AQP4-GFP tagged construct from a cytosol expression profile to a plasma membrane expression profile, when the extracellular tonicity was changed from an isotonic (RME = 26.69 $\pm$ 6.03) to a hypotonic (RME = 34.91 $\pm$ 5.48) environment. This could not reject the null hypothesis at a 95% level (p=0.38). The surface also does not appear to alter as the mean percentage change in size is 121.87% $\pm$ 4.81%, which also did not reject the null hypotheses at a 99% level.

This indicates that a calcium ion influx into the cytosol is required for translocation as a response to a change in the tonicity of the extracellular environment, from an isotonic solution to a hypotonic solution. This is the same phenomenon observed by Conner *et al* (131) with AQP1.

3.4 Chapter conclusions and Next Step

It can be seen more clearly from Table 3.1 the different components that are and are not involved in the translocation process of AQP4-GFP tagged construct,

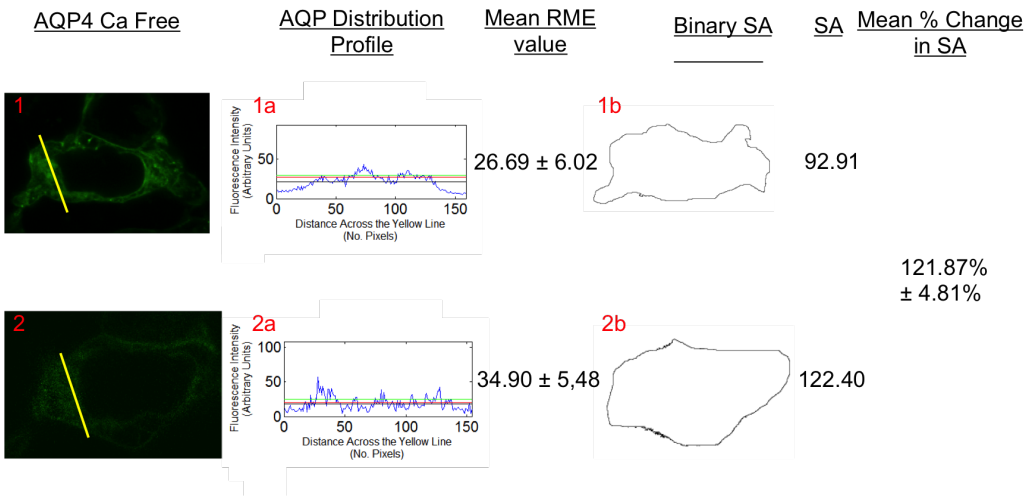

Figure 3.15: AQP4-GFP fusion proteins in HEK293 cells cultured in a Calcium-Free Media exhibited to an isotonic (1) and hypotonic (2) extracellular environment, with FIP across the yellow lines and surface areas calculated using ImageJ and Matlab software. - The Fluorescence profiles (1a-isotonic) and (2b-hypotonic) indicate the fluorescence intensity across the yellow line (value shown in (Mean RME value column). A minimum of three lines were drawn in three different positions, as shown in the representative image (1) and (2).Oulines of the cells were generated (1b-Isotonic and 2b-Hypotonic) and the surface areas calculated (SA column) using matlab software. The mean percentage changes for n=3 were also calculated and are displayed in the mean % change column

from the cytosol to the plasma membrane, when the extracellular tonicity is altered, and the functional swelling response caused by the influx of water across the plasma membrane into the cytosol. Using this a hypothesis for a mechanistic pathway can be formulated. Translocation and cell volume increase are inhibited by PKAi, Actin inhibitor, and extra and intracellular calcium depletion. Figure 3.16 identifies the proposed mechanism and the grey portions identify the most likely missing links in the mechanism. AQP4 is constitutively expressed in both the membrane and the cytosol, therefore, when the extracellular environment changes from an isotonic solution to a hypotonic solution, water passes into the cell via the AQP4 constitutively expressed at the plasma membrane. This in turn causes the cell to swell, and this swelling, activates stretch activated TRP channels. This is the same process as identified by Conner and Conner (131). Stretch activated TRP channels are a family of ion channel proteins, which are involved in the transportation of cations. Cations are positively charged ions such as calcium (Ca^{2+}). This mean that as the water molecules are transported across the constitutively expressed AQP4 proteins in the plasma membrane, pressure builds inside the cell, putting tension on the plasma membrane. This tension, causes the activation of the TRP channels, and they allow for the transportation of Ca^{2+} across the plasma membrane, into the cytosol.

At this stage in the mechanism the process becomes hypothesised. PKA acitvates the translocation of AQP4 in vesicles in the cytosol for insertion by transport along the microfillaments of the cytoskeleton. PKA, is well documented for its activation by cAMP, however, how does an influx of calcium activate the release of cAMP, needed to activate PKA? Inside the cell there are a class of signalling proteins called adenylyl cyclases, and it is these proteins that form the biochemical link between calcium influx and the actvation of the cAMP/PKA pathway, (138). It wasn't until recently that one of the 6 adenylyl cyclases (AC) was found to be expressed in both HEK293 cells and astrocytes (139), and that was AC3. Adenylyl cyclase 3 is activated by Calcium. When adenylyl cyclase is activated by calcium it then activates cAMP most likely via the platform of phosphodiesterases (PDE's). As the availability of cAMP increases, PKA is phosphorylated, and in-turn phosphorylates, AQP4, which initiates the translocation process along the

Inhibitor/ Control Medium	Isotonic	Hypotonic	Mean % SA	Translocation and Functional Swelling
Hypericin	21.85 ± 6.80	38.22 ± 5.58	103.5% ± 2.05%	**No**
PKCi	27.27 ± 4.73	55.28 ± 3.97	141% ± 2.05%	Yes
PKAi	25.62 ± 5.16	33.66 ± 6.62	102.97% ± 5.21%	**No**
Actin Inhibitor	26.07 ± 6.10	34.91 ± 5.48	121.87% ± 4.81%	**No**
Microtubule Formation Inhibitor	42.25 ± 5.4	78.52 ± 2.62	133.23% ± 8.89%	Yes
Calcium Free Media	26.69 ± 6.03	32.16 ± 4.48	111.6% ± 1.92%	**No**

Table 3.1: AQP4-GFP tagged Constructs, and their Translocation Response when Subjected to Different Inhibitors

microfilaments of the cytoskeleton, allowing for insertion of the cytosolically expressed AQP4 construct into the plasma membrane. This is better explained in the schematic representation in Firgure 3.16

Now that a mechanim has been established for the translocation and functional swelling phenomenon, it would be keen to probe this mechanism further, to enable better understanding around how PKA specifically activates AQP4, to hopefully identify and establish targets for the therapeutic intervention of a cytotoxic brain oedema.

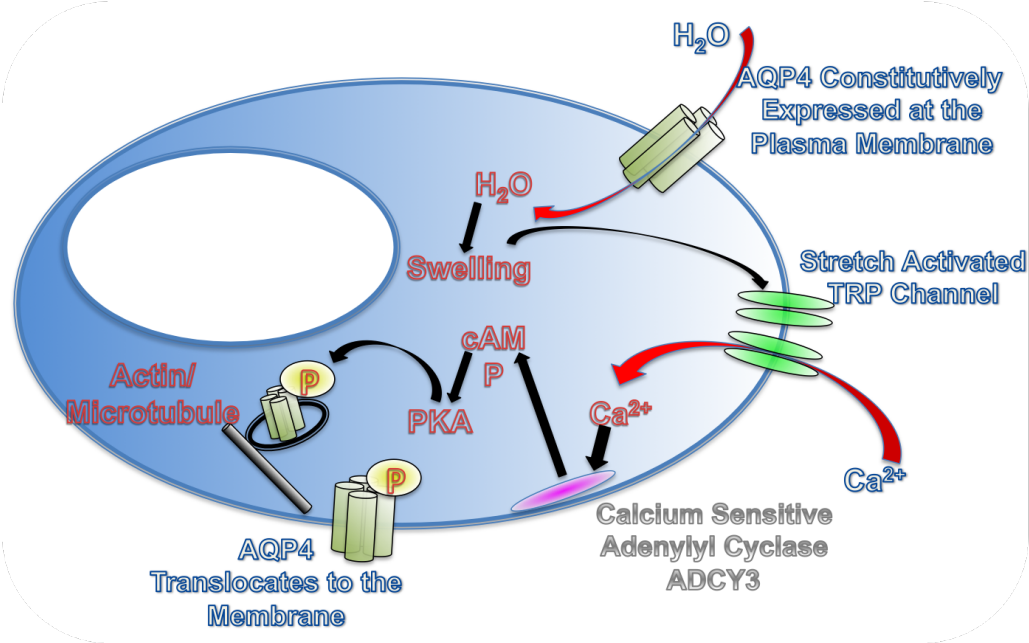

Figure 3.16: Schematic Representation of the AQP4 Translocation Activation Response to an Increase in Extracellular Hypotonicity - A model showing influx of water causes cell swelling that induces extracellular calcium entry leading to AQP4 translocation to the plasma membrane. This involved extracellular and intracellular calcium release, cytoskeletal filiamentation and activation of PKA.

4

Aquaporin 4: Mutagenesis to Elucidate Structure Function

4.1 Potential PKA Sites, their Position within the Monomer, and Site Directed Mutagenesis

PKA phosphorylates proteins that have the motif Arginine - Arginine - X - Serine exposed in their amino acid sequence. So to understand how PKA is interacting with AQP4, the nucleotide sequence and its amino acid sequence needed to be analysed to isolate sections with an Arg - Arg - X - Ser, sequence. Using the web-site swiss uniprot the full sequence for AQP4 (Acc No. P55087) was obtained. This nucleotide sequence was then run through a computer programme called NetPhosK. This computer programme, identifies phosphorylation sites within the P55087 sequence. The programme identified 5 PKA phosphorylation sites, S52, S111, S180, S188 and S276, and their position withinin the AQP4 sequence can be seen in figure 4.1. Forward and reverse primers were ordered to mutate these specific serines to an alanine (A) and an aspartic acid (D). The reason for this is that alanine is an innert amino acid and cannot be phosphorylated by PKA, and aspartic acid is said to approximate (mimic) phosphorylation. This technique is a well utilised methodology called phosphomimetics, and was first utilised in 1999

by Hiscott et al, (140).

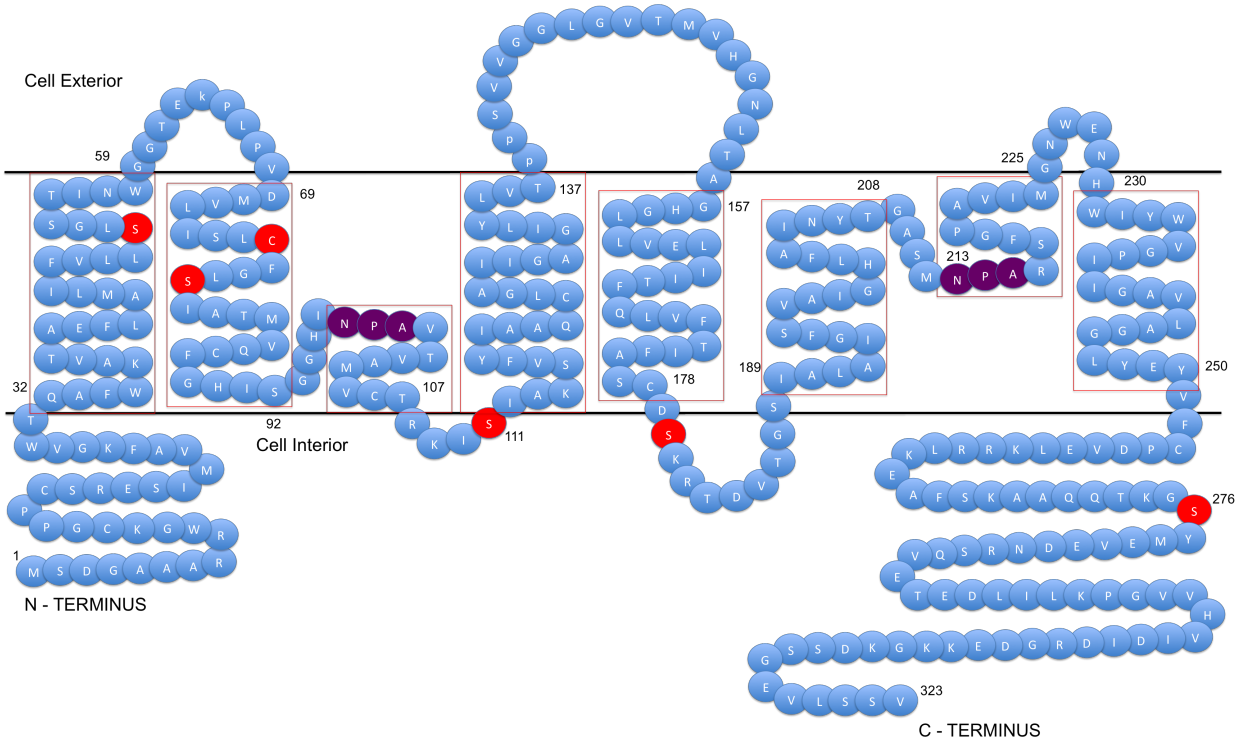

Figure 4.1: Primary Amino Acid Structure of AQP4 - Schematic representation of the primary amino acid structure of AQP4. The red coloured circles identify the PKA phosphorylation sites(64).

Site Directed Mutagenesis (SDM) is the process by which the amino acid sequence of AQP4 is altered, which is described in the materials and methods section of this thesis. The rest of this chapter will detail the results from the SDM analysis, exposing the mutated AQP4 constructs expressed in HEK293 to isotonic and hypotonic extracellular environments and reviewing the outcomes using confocal microscopy, as detailed in the previous chapter, and materials and methods.

4.1.1 S52 A and D

S52 was altered by SDM from a serine to alanine to form S52D, the AQP4 construct was then transfected into HEK293 cells. When cells were exposed to a change in extracellular tonicity, there was an expectation to see a strong constitutive expression of AQP4 in the plasma membrane, when compared with that AQP4 WT, as S52D is mimicking a phosphorylated serine. This would mean that all AQP4s should be activated and translocated to the plasma membrane. It would therefore result in a high RME value, and little to no change in surface area, however, the cell may look punctate. This is owing to the fact that water would have been transported across the plasma membrane into the cell by the increased constitutive expression of AQP4 at the plasma membrane.

Figure 4.2 shows that the RME value doesn't significantly alter when the tonicity of the extracelular envionment is increased (Isotonic RME = 17.62 ± 3.44, Hypotonic RME = 18.27 ± 3.88). However, it does seem to have a similar value to the isotonic RME value for AQP4 WT (Isotonic RME = 27.86). When the image was studied further the distribution of AQP4 expression appeared quite even. This was unexpected considering S52D was meant to mimic a phosphorylated serine and therefore have an activated AQP4 response. However, it seems that this mutation has in fact inhibited the translocation and functional swelling response to a change in the extracellular tonicity.

S52A mutants were created to see what functional response this would have on the translocation of AQP4. Alanine is a relatively inert amino acid, therefore it was likely they would block activation by PKA, which will in turn prevent the translocation and functional swelling response, upon an increase in extracellular tonicity. However, figure 4.3 shows there is a statistically significant change (p=0.000001, rejecting the null hypothesis at a 99% level) in the RME values from an isotonic (REM = 18.344 ± 4.06) to a hypotonic (RME = 59.341 ± 5.53) extracellular environment. There is also a function swelling response of 127.03% ± 5.99% which rejects the null hypothesis at a 95% level (p=0.046). This was

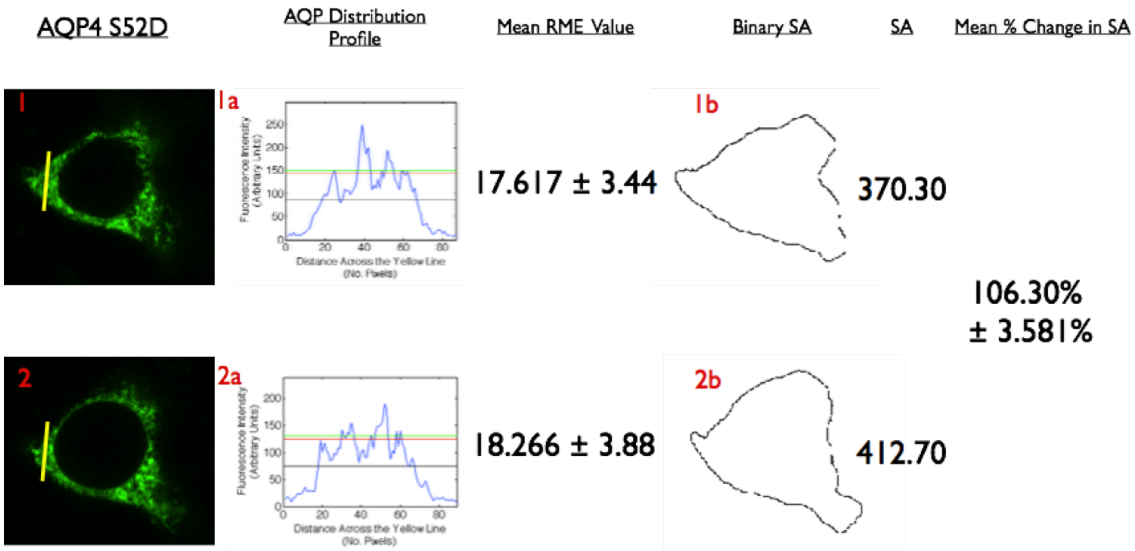

Figure 4.2: Regulation of hypotonicity-induced increase in cell volume by S52D mutated AQP4 translocation in HEK293 cell. - Representative images showing x-y surface area (SA) estimation of cell volume. The binary image and surface area are calculated from the z-stack plane at the maximum area. All measurements were taken at 48 h post-transfection. HEK293 cells transfected with S52D translocation-deficient mutant of AQP4-GFP. Control medium (1) and hypotonic medium (2) are DMEM with osmolalities of 322374 mosM/kg H_2O and 107125 mosM/kg H_2O (diluted with water), respectively. Distribution profiles along the line scans (in yellow on the image) are displayed graphically (1a and 2a) by each image indicating AQP distribution in control and hypotonic medium. The Binary Surface area (1b and 2b) demonstrates the swelling or lack thereof when the cells are exhibited to different tonicities. All images and analysis shown are a single representation contributing to the mean value quoted in the text and in Table 1.

also unexpected and poses more questions. If S52A is not inhibiting the translocation response, then it implies that it is not a PKA phosphorylation site. This when scrutinised further, is not wholly illogical, as the position of S52 in figure 4.1 is buried in the AQP4 structure, which would make it difficult for PKA to access and be able to phosphorylate the serine. However, mutation of that site to S52D mimicking a PKA activated serine, appears to inhibit the translocation phenomenom, which could be of significant interest as a potential drug target. For this to be of significant value, further investigations would be needed to fully understand how the phosphomimetics are causing this. This will be discussed further in section 4.2.

4.1.2 S111 A and D

As can be seen from Figure 4.1 S111, unlike S52, is clearly more accessible to PKA as it sits just on one of the turns on the intracellular side of the plasma membrane. It is therefore expected that S111A would prevent the translocation process and that S111D would translocate, or appear constitutively expressed at the plasma membrane.

Figure 4.4 shows that S111D had a translocation response with a functional swelling (rejected null hypothesis at a 95% level, $p = 0.039$) response to the change in tonicity, and S111A in figure 4.5 also showed a translocation and functional swelling reponse (rejected null hypothesis at a 95% level, $p = 0.039$) to a change in extracellular tonicity. Therefore the assumption canbe made that S111 is not invoved in this process, as none of the SDMs caused a functional change in translocation or swelling response to a change in the extracellular tonicity.

4.1.3 S276 A and D

Figure 4.1, show that S276 is a very, easily accessible serine to PKA, as it is part of the C-terminus in the cytosol. If this were therefore, a PKA phosphorylation

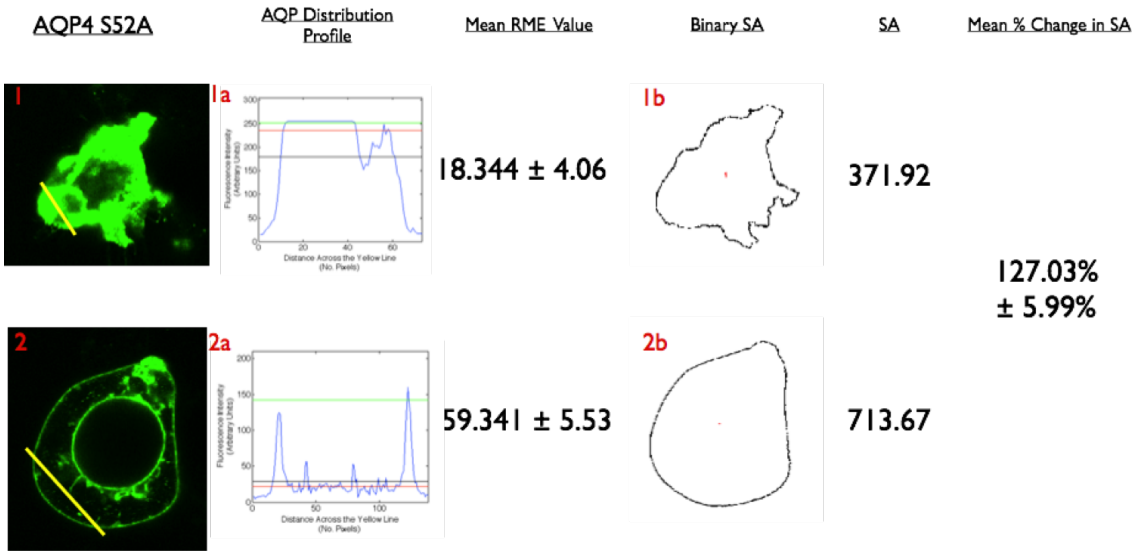

Figure 4.3: Regulation of hypotonicity-induced increase in cell volume by S52A mutated AQP4 translocation in HEK293 cell. - Representative images showing x-y surface area (SA) estimation of cell volume. The binary image and surface area are calculated from the z-stack plane at the maximum area. All measurements were taken at 48 h post-transfection. HEK293 cells transfected with S52A translocation-deficient mutant of AQP4-GFP. Control medium (1) and hypotonic medium (2) are DMEM with osmolalities of 322374 mosM/kg H_2O and 107125 mosM/kg H_2O (diluted with water), respectively. Distribution profiles along the line scans (in yellow on the image) are displayed graphically (1a and 2a) by each image indicating AQP distribution in control and hypotonic medium. The Binary Surface area (1b and 2b) demonstrates the swelling or lack thereof when the cells are exhibited to different tonicities. All images and analysis shown are a single representation contributing to the mean value quoted in the text and in Table 1.

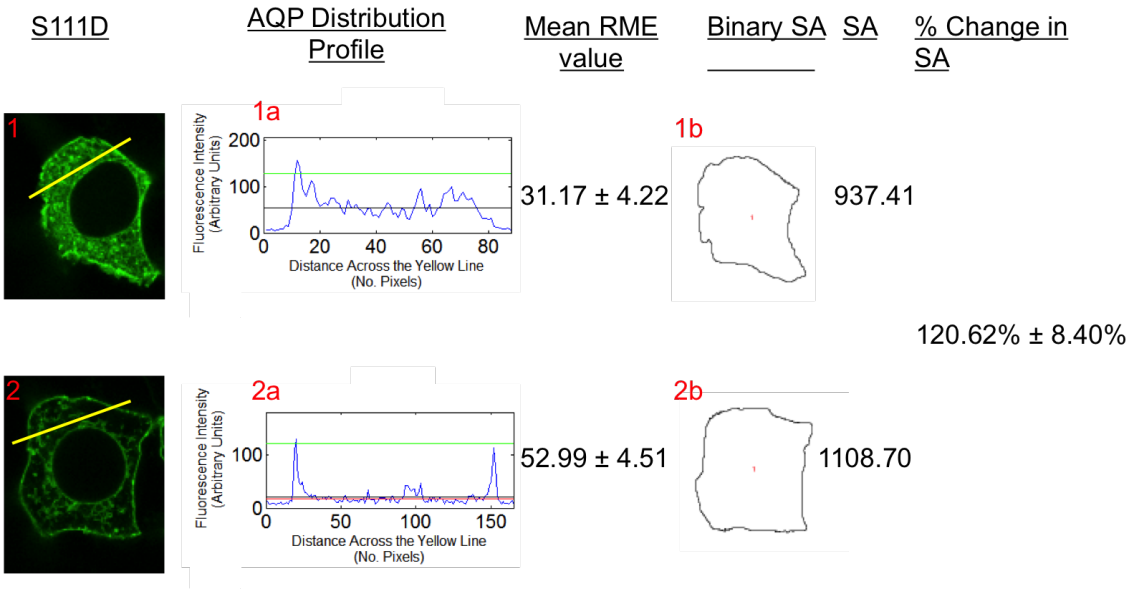

Figure 4.4: Regulation of hypotonicity-induced increase in cell volume by S111D mutated AQP4 translocation in HEK293 cell. - Representative images showing x-y surface area (SA) estimation of cell volume. The binary image and surface area are calculated from the z-stack plane at the maximum area. All measurements were taken at 48 h post-transfection. HEK293 cells transfected with S111D translocation-deficient mutant of AQP4-GFP. Control medium (1) and hypotonic medium (2) are DMEM with osmolalities of 322374 mosM/kg H_2O and 107125 mosM/kg H_2O (diluted with water), respectively. Distribution profiles along the line scans (in yellow on the image) are displayed graphically (1a and 2a) by each image indicating AQP distribution in control and hypotonic medium. The Binary Surface area (1b and 2b) demonstrates the swelling or lack thereof when the cells are exhibited to different tonicities. All images and analysis shown are a single representation contributing to the mean value quoted in the text and in Table 1.

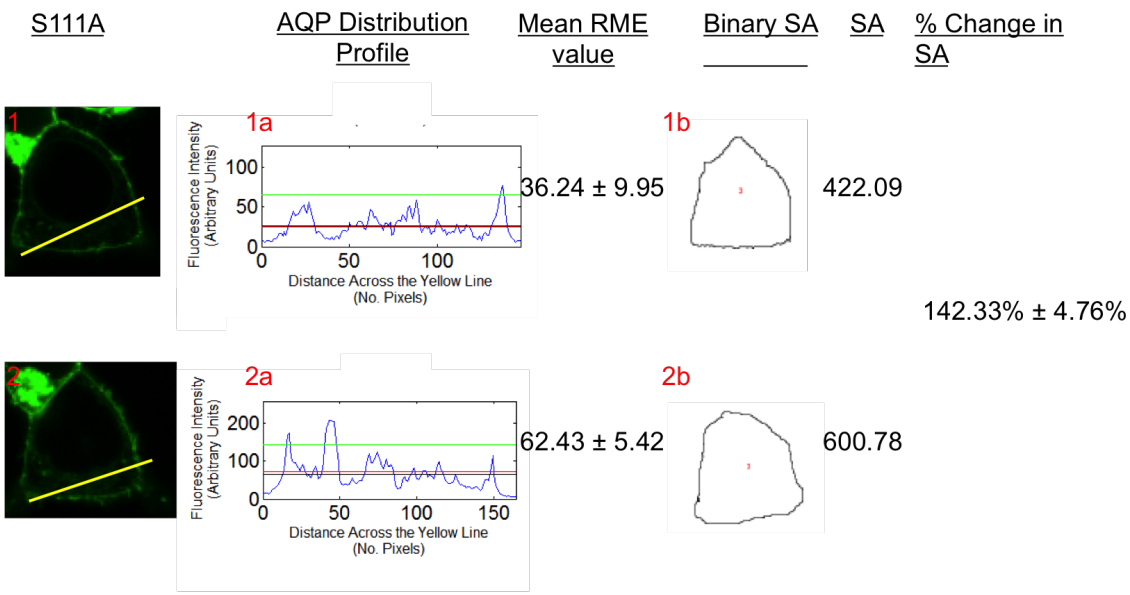

Figure 4.5: Regulation of hypotonicity-induced increase in cell volume by S111A mutated AQP4 translocation in HEK293 cell. - Representative images showing x-y surface area (SA) estimation of cell volume. The binary image and surface area are calculated from the z-stack plane at the maximum area. All measurements were taken at 48 h post-transfection. HEK293 cells transfected with S111A translocation-deficient mutant of AQP4-GFP. Control medium (1) and hypotonic medium (2) are DMEM with osmolalities of 322374 mosM/kg H_2O and 107125 mosM/kg H_2O (diluted with water), respectively. Distribution profiles along the line scans (in yellow on the image) are displayed graphically (1a and 2a) by each image indicating AQP distribution in control and hypotonic medium. The Binary Surface area (1b and 2b) demonstrates the swelling or lack thereof when the cells are exhibited to different tonicities. All images and analysis shown are a single representation contributing to the mean value quoted in the text and in Table 1.

site, S276A would be seen not to translocate and have a functional swelling response, and S276D to translocate or be constitutively expressed in the plasma membrane and either show a functional swelling response or appear punctate.

It is evident from figure 4.6, that S276A had no significant change (not rejecting the hypothesis at a 95% level, p = 0.96) in the mean RME values between an isotonic extracellular solution (RME = 36.608 ± 4.64) when compared with a hypotonic extracellular solution (RME = 36.970 ± 5.53). There was also no significant change in the cell surface area, (110.82% ± 3.85%, p=0.26).

Figure 4.7, shows that there is a significant change in the RME values for S276D, and there is a function swelling response. As the extracellular environment changes from an isotonic (RME = 25.723 ± 5.42) to a hypotonic (RME = 57.932 ±), the aquaporins translocate from the cytosol to the plasma membrane, allowing water to be transported into the cell, down the concentration gradient causing the cell to swell and increase in size by 34.18% ± 15.10% (p=0.043, rejects the null hypothesis at the 95% level).

This identifies S276 as a likely PKA phosphorylation site, for the activation of the translocation process of AQP4 from a vesicle expression profile in the cytosol to a predominantly plasma membrane expression profile. However, S276D was expected to be constitutively expressed in the plasma membrane, but instead observed to be in the same translocation response seen before. Therefore, it can only be assumed that there are either two or more phosphoylation sites of which S276 activation is essential but not exclusive, for the functional response owing to a change in the extracellular tonicity or a second process is required to complement PKA phosphorylation of S276D (possibly via calcium inhibition).

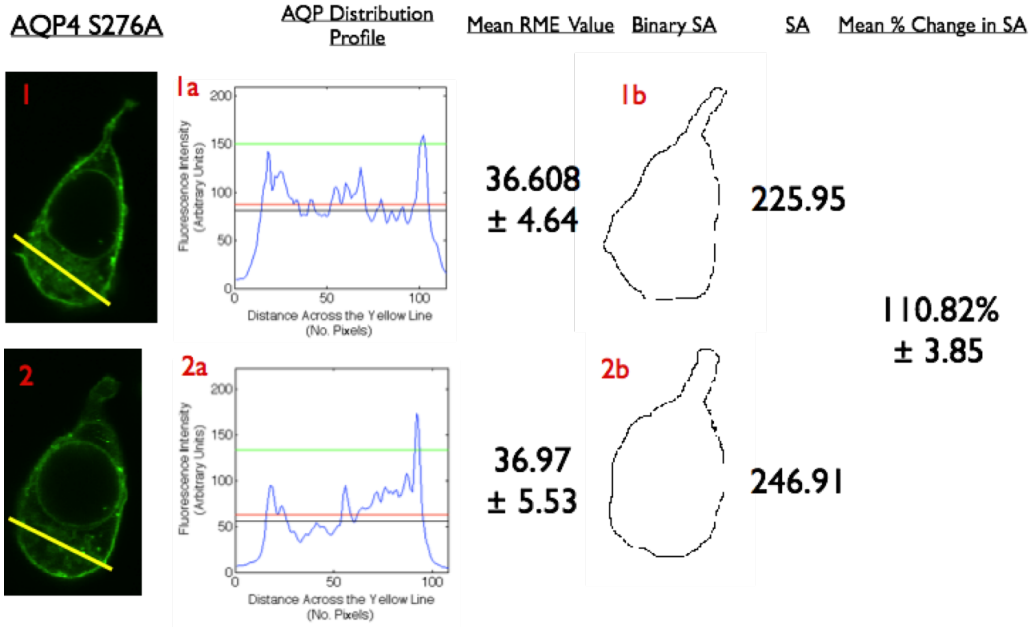

Figure 4.6: Regulation of hypotonicity-induced increase in cell volume by S276A mutated AQP4 translocation in HEK293 cell. - Representative images showing x-y surface area (SA) estimation of cell volume. The binary image and surface area are calculated from the z-stack plane at the maximum area. All measurements were taken at 48h post-transfection. HEK293 cells transfected with S276A translocation-deficient mutant of AQP4-GFP. Control medium (1) and hypotonic medium (2) are DMEM with osmolalities of 322374 mosM/kg H_2O and 107125 mosM/kg H_2O (diluted with water), respectively. Distribution profiles along the line scans (in yellow on the image) are displayed graphically (1a and 2a) by each image indicating AQP distribution in control and hypotonic medium. The Binary Surface area (1b and 2b) demonstrates the swelling or lack thereof when the cells are exhibited to different tonicities. All images and analyses shown are a single representation contributing to the mean value quoted in the text and in Table 1.

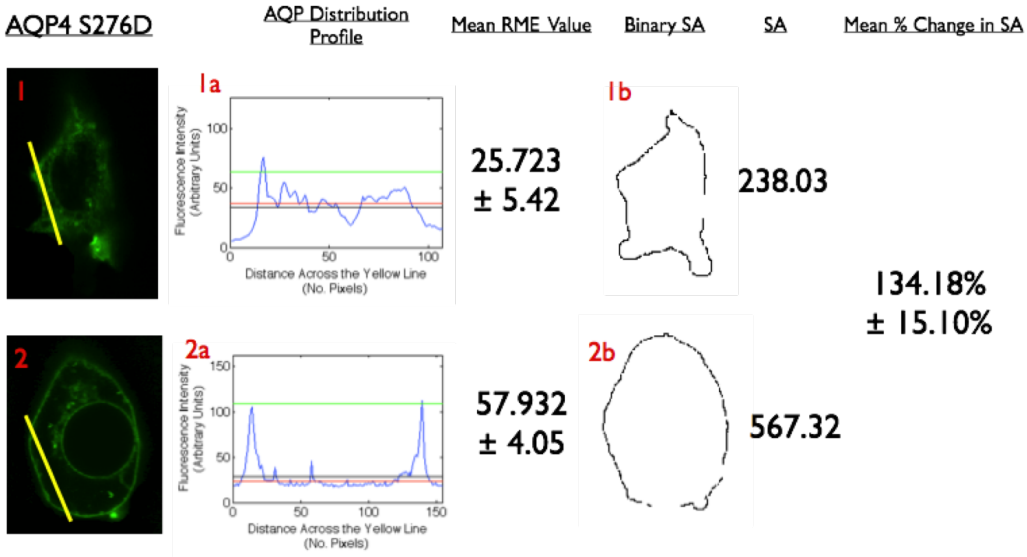

Figure 4.7: Regulation of hypotonicity-induced increase in cell volume by S276D mutated AQP4 translocation in HEK293 cell. - Representative images showing x-y surface area (SA) estimation of cell volume. The binary image and surface area are calculated from the z-stack plane at the maximum area. All measurements were taken at 48 h post-transfection. HEK293 cells transfected with S276D translocation-deficient mutant of AQP4-GFP. Control medium (1) and hypotonic medium (2) are DMEM with osmolalities of 322374 mosM/kg H2O and 107125 mosM/kg H2O (diluted with water), respectively. Distribution profiles along the line scans (in yellow on the image) are displayed graphically (1a and 2a) by each image indicating AQP distribution in control and hypotonic medium. The Binary Surface area (1b and 2b) demonstrates the swelling or lack thereof when the cells are exhibited to different tonicities. All images and analyses shown are a single representation contributing to the mean value quoted in the text and in Table 1.

4.2 Molecular Modelling Comparison Between S52A, S52D and S52L using VMD

Revisiting the data from S52, the molecular interactions of the WT with nearby amino acids, when compared with the molecular modelling analysis of S52A and S52D, would hopefully demonstrate what is changing on a molecular level which may be causing the inhibition of the translocation and functional swelling response, with the mutant S52D.

Using the programme SwissPdb Viewer (141) S52 and S52D were simulated. As you can see from figure 4.8 S52 is in close proximity to C76 and S80, however they do not appear to be interacting. When the S52 residue is mutated to S52D, there is hydrogen bonding between C76 and S80, and in all rotations of the S52D residue, hydrogen bonding and intramolecular forces are present between S80. These intramolecular forces, exist because of the highly polar functional groups on the aspartic acid residue and the serine of the S80 residue. However, this added interaction of S52 with S80 may not be the cause of the translocation inhibition, it could simply be that the size of S52D is causing some steric hindrance and preventing PKA from phosphorylating another site within AQP4 amino acid sequence. To establish which was the case, the S52L mutant was created. Leucine (L), is a similar size to aspartic acid, however, is a neutral molecule, and so shouldn't form the hydrogen bonds with S80, but will cause the same amount of steric hindrance to PKA. Therefore, if S52D is inhibiting translocation by steric hindrance to PKA, then S52L will inhibit the translocation and functional swelling response to a change in the extracellular tonicity. Alternatively, if the reason for S52D inhibiting the translocation response is as a result of the hydrogen bonds which are formed with S80, then the translocation and functional swelling response will occur with S52L.

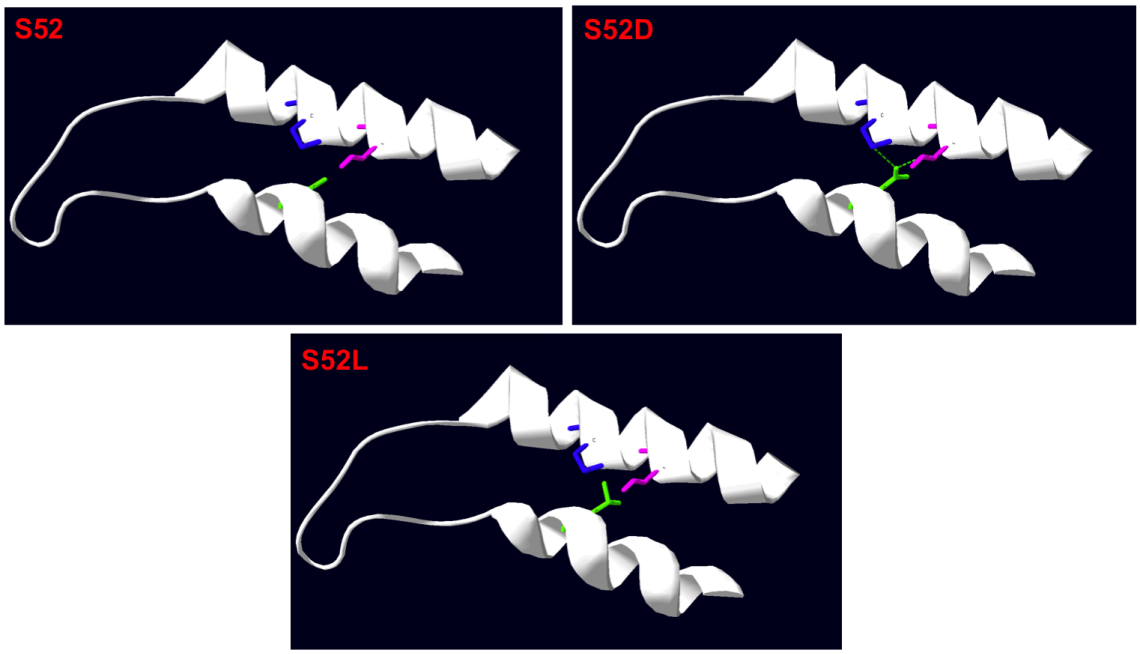

Figure 4.8: Swisspdb Viewer respresentation of the AQP4 amino acid sequance, with S52 residue mutated to S52D and S52L - Orientations of mutated residue sidechains were found using SwissPdb Viewer, and then a short (50ps) molecular dynamics simulation was run to relax the mutated residue into their lowest energetic states (Green = S52, Blue = C76, Pink = S80)

4.2.1 S52L

Figure 4.9, shows a significant change ($p = 0.000060$, rejecting the null hypothesis at a 99% level) in the expression profile of S52L AQP4 when the extracellular solution changed from an isotonic solution (RME = 43.998 ± 4.81) to a hypotonic solution (RME = 69.503 ±3.17). There was also a statistically significant increase in the cell surface area by 115.83% ± 4.25%, which rejects the null hypothesis by 95% ($p = 0.0317$). This implies that it is not the size of the aspartic acid residue that is inhibiting the function of AQP4 but the hydrogen bonds formed between S52 and S80.

Although this starts to answer some questions, it also asks others. Are the hydrogens bonds formed between S52D and S80, preventing PKA from activating S80 or are they altering the structure of the AQP4 protein, preventing its function? To try and understand this further, a mutate of S80 was created forming S80A and S80D, whilst leaving the S52 residue as wildtype.

4.2.2 S80A and D

Mutation of S80 to S80A and S80D whilst leaving the S52 residue as wildtype, should, according to the modeling, stimulate the same phenomonom as with mutation of S52 to S52A and S52D. This means with S80A we should observe structure funtion response to a change in extracellular tonicity, and the retardation of that response with S80D due to the hydrogen bonds formed with the S52 wildtype residue.

Figure 4.10 shows there was not a significant change ($p=0.85$, not rejecting null hyporthesis at a 95% level) in the translocation of the mutated S80D AQP4-GFP tagged protein from a cytosolic expression profile (RME=30.215 ±) to a membrane expression profile (RME=31.895 ±). There was also no significant increase ($p=0.48$, not rejecting null hypothesis at a 95%) in the cell surface area (107.93%

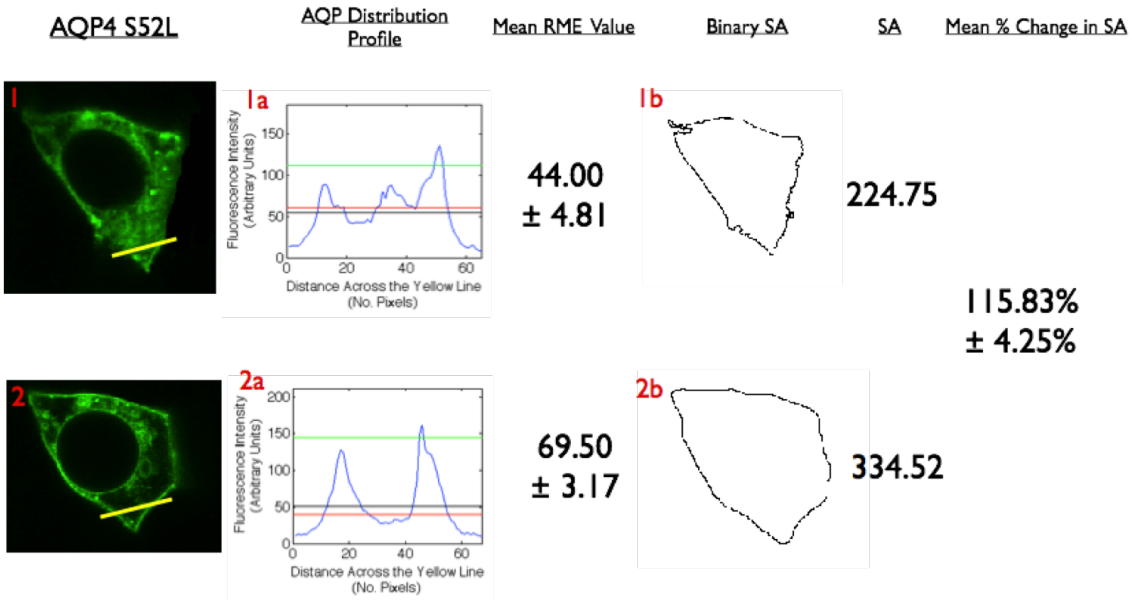

Figure 4.9: Regulation of hypotonicity-induced increase in cell volume by S52L mutated AQP4 translocation in HEK293 cell. - Representative images showing x-y surface area (SA) estimation of cell volume. The binary image and surface area are calculated from the z-stack plane at the maximum area. All measurements were taken at 48 h post-transfection. HEK293 cells transfected with S52L translocation-deficient mutant of AQP4-GFP. Control medium (1) and hypotonic medium (2) are DMEM with osmolalities of 322374 mosM/kg H_2O and 107125 mosM/kg H_2O (diluted with water), respectively. Distribution profiles along the line scans (in yellow on the image) are displayed graphically (1a and 2a) by each image indicating AQP distribution in control and hypotonic medium. The Binary Surface area (1b and 2b) demonstrates the swelling or lack thereof when the cells are exhibited to different tonicities. All images and analyses shown are a single representation contributing to the mean value quoted in the text and in Table 1.

±2.03).

Unfortunately mutagenesis to create the S80A mutant, proved extremely difficult, and over the course of a number of months yielded no funtioning AQP4 mutant. This meant it was not possible to quantify the effects of changing the extracellular environment. However, the retardation of the structure function response to an extracellular change in tonicity, indicates that the aspartic acid residue is forming hydrogen bonds with the wildtype S52 residue, and preventing its translocation. However, to better understand this, both residues were mutated at the same time, creating a double mutant. The S52D mutation would retard the translocation response, however, if it was indeed the hydrogen bonds between the aspartic acid residue and the S80 residue then a mutation of S80 to S80A, alanine an inert residue, would hopefully reinstate the structure function.

4.2.3 S52D/S80A

Mutagenesis as with the single S80A mutant proved very difficult to generate. However, analysis with a modelling programme, yielded some interesting suggestions. Figure 4.11 showed that with the S52D/S80A double mutant (image (B)), the hydrogen bonds (green hashed line) did not occur between the S52 and S80. However, the hashed green line was present with the single S52D mutant, seen in image (A). Therefore it was expected the structure function would be reinstated in comparison to the retardation affects on a single mutation of S52D or S80D.

4.3 Conclusion and Next Steps

Unfortunately due to the technical difficulty with the mutagenesis work, it was difficult for to establish a comprehensive picture of what is causing the retardation of the structure function response to the change in extracellular tonicity. However, due to the embedded location of S52 and S80 in the helical structure,

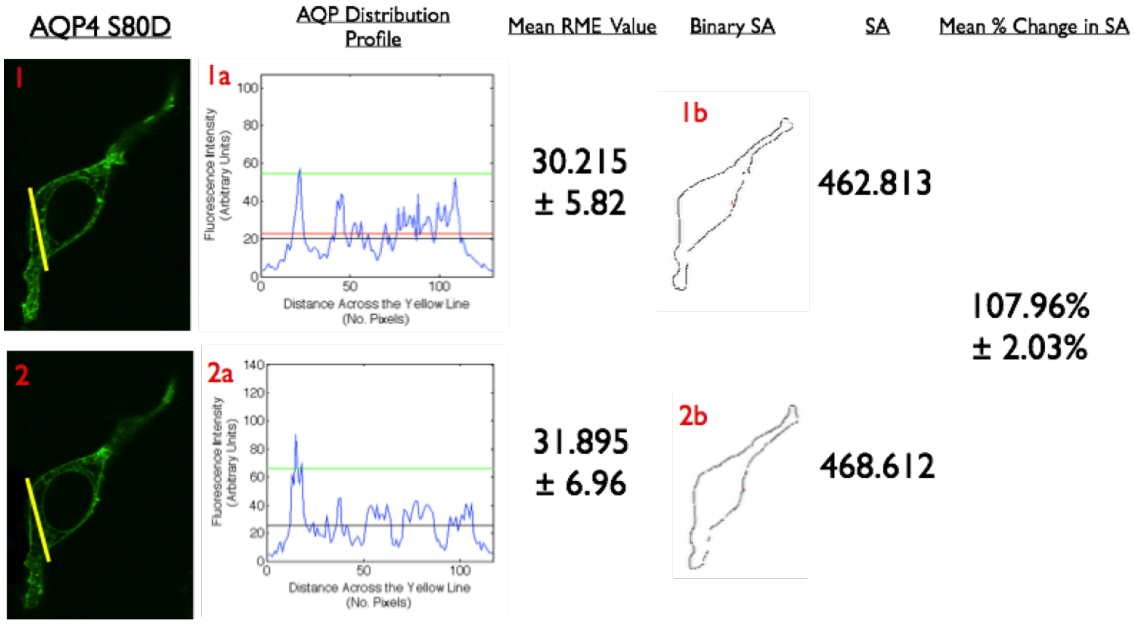

Figure 4.10: Regulation of hypotonicity-induced increase in cell volume by S80D mutated AQP4 translocation in HEK293 cell. - Representative images showing x-y surface area (SA) estimation of cell volume. The binary image and surface area are calculated from the z-stack plane at the maximum area. All measurements were taken at 48 h post-transfection. HEK293 cells transfected with S80D translocation-deficient mutant of AQP4-GFP. Control medium (1) and hypotonic medium (2) are DMEM with osmolalities of 322374 mosM/kg H_2O and 107125 mosM/kg H_2O (diluted with water), respectively. Distribution profiles along the line scans (in yellow on the image) are displayed graphically (1a and 2a) by each image indicating AQP distribution in control and hypotonic medium. The Binary Surface area (1b and 2b) demonstrates the swelling or lack thereof when the cells are exhibited to different tonicities. All images and analyses shown are a single representation contributing to the mean value quoted in the text and in Table 1.

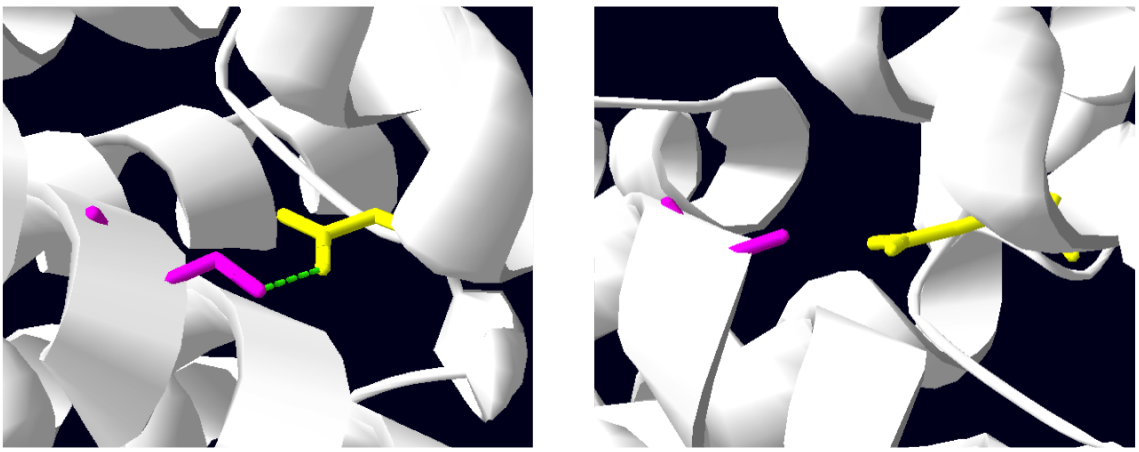

Figure 4.11: Swisspdb Viewer respresentation of the AQP4 amino acid sequance, with S52 residue mutated to S52D and the S80 Residue mutated to S80A - Orientations of mutated residue sidechains were found using Swisspdb Viewer, and then a short (50ps) molecular dynamics simulation was run to relax the mutated residue into their lowest energetic states. Image (A) S52D (yellow) with S80 wildtype (pink) which has hydrogen bonds forming (green hashed line). Image (B) shows that S80 has been mutated to S80A (pink residue), and the hydrogen bonds are no longer visible (no hashed green line)

it is unlikely that mutation of these residues is retarding a protein kinase phosphrylation event. This implies that the hydrogen bonds are causing a structural change in the folding of the AQP. These mutants were then investigated using linear dichroism, by over expressing the mutated and wildtype AQP4 protein and inserting it into a lipid bilayer. Linear dichroism is a technique which uses polarised light to produce an electromagnetic field which oscillates in only one plane. Using light parallel and perpendicular to this field enables the experimentalist to measure how much energy is absorbed in one dimension relative to the other. This methodology helps to identify how membrane proteins insert into lipid bilayers. However, on analysis, there was very little change in the absorption signal (data not shown). An explanation for this is that, even with an over expression profile of the protein there was insufficient expression of AQP4 in the samples selected most likely owing to the nature of transient transfection, meaning not all cells were expressing the GFP-tagged AQP4 protein. This work could be taken forward to investigate this interaction further by doing in-depth molecular modelling, to understand how AQP4 interacts with membranes, dimerises, and how the mutations at S52 may be altering the structure of the AQP4.

However, S276 has still been identified as a potential kinase phosphorylation site. Modelling of this would be very difficult as the available crystallographic structures have been truncated removing the tail part of the C-terminus, and thusly the S276 residue.

Up until now, this project had been investigating the role of GFP-tagged AQP4 and its mutants in a simulated experimental environment, using HEK 293 cells, however, to establish if this translocation, and functional swelling response to an extracellular change in tonicity, is a true reflection of how AQP4 reacts in astrocytes, the phenomenon needed to be observed in native cell lines. The next chapter will discuss how this was achieved and the results these endeavours yielded, and whether or not this model is physiologically relevant and a true reflection of AQP4's mechanistic response to changes in tonicity.

5

Physiological Relevance

Although it was crucial to first investigate the cellular responses to a change in tonicity in a model cell line such as HEK293, it can not be said to be of physiological relevance, as an astrocyte cell line, could express AQP4 differently, or have a different response to the change in tonicity. Therefore it was decided to try and transfect an astrocytic cell line with AQP4-GFP tagged constructs. Immortalised astrocyte cell line were transfected using the same protocol, and transfection reagents, TransFast. However, when analysed using laser induced confocal microscopy there was no visible fluorescence. This meant that the transfection was unsuccessful as there were no cells expressing AQP4-GFP tagged constructs. Therefore owing to the difficulty of transfecting the cell line, what other possible method could be utilised?

Endogenous AQPs in isolated rate primary astrocytes were visualised using a methodology called immunocytochemistry. This was a particularly tricky protocol to engineer as the confocal imaging requires that the cells are fixed on coverslips. For the cells to be fixed on a coverslip, they need to be perfused with paraformaldehyde and other solutions, all of which can alter the expression profile of AQP, due to a change in the extracellular tonicity. The protocol was modified and optimised to limit the effects of the change in extracellular tonicity, so that the correct expression profile was viewed and the time taken to do so

was recorded. The average time taken to translocate was often faster then the time taken to perfuse the cells with formaldehyde (cell fixing agent). Although it should be noted that a time analysis of the translocation protocol, was very difficult to formaly quantify while the water was added, this was owing to the Z-stack shifting and it taking time to alter the Z-stack back to the correct position. Following primary and FITC-conjugated secondary antibody washes, the cover slips were observed using confocal microscopy. This technique was successful, as you can see from the images published in our paper, (135). This experiment was then repeated with AQP4 which did yield a very faint confocal image, unfortunately it was too faint to visualise in a recordable image, however it was visible to the naked eye. The cells were fixed and therefore not living meaning the translocation and functional swelling response couldn't be observed, meaning only cells from the same subcultured population on different coverslips could be observed making the quantitative analysis very variable. With further optimisation the methodology could potentially be utilised to observe living immortalised astrocytes with endogenous AQP4, enabling a clear image of the translocation and functional swelling response to extracellular changes in tonicity.

Following these results, there was a connundrum, as to how to visualise AQP4 in astrocytic cells lines. Following discussions with a transfection specialist Mirus was suggested, as they had a new transfection reagent which was being reported as capable of transiently transfecting cell lines identified to be notoriously difficult to transfect. Researched suggested their new product TransIT 2020 would be capable of improving the transfection rate. The new transfection protocol, as detailed in the materials and methods, was performed with immortalised astrocytes observing the translocation and functional swelling response using laser induced microspectrometry, when the extracellular tonicity was altered from an isotonic to a hypotonic state.

As can be seen from figure 5.1, the transfection was successful, however, the confocal machine was damaged preventing us from being able to analyise the translocation response. High resolution full Z-stacked images, of the cell were

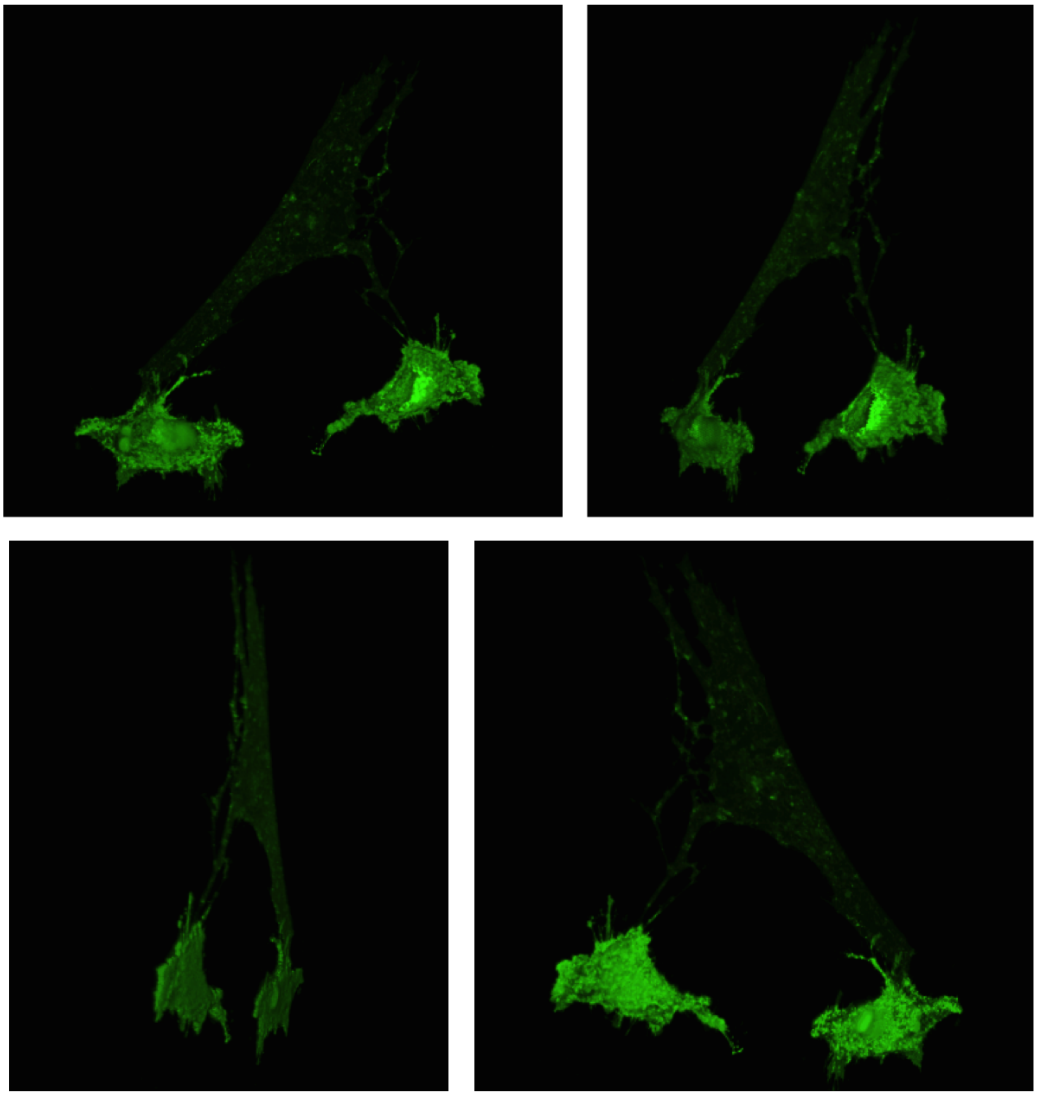

Figure 5.1: Regulation of hypotonicity-induced increase in cell volume by AQP4 translocation in Immortalised astrocytes. - Representative images shows an astrocyte with constitutively expressed AQP4-GFP tagged constructs following treatment with TransIt 2020

taken, which was usually somethingimpossible to do as the translocation time was much faster than the time needed to record an image such as this

Future work would be to repeat the transfection protocol and investigate the effects of translocation in immortalised astrocytes, as a response to a change in extracellular tonicity. We would then suggest investigating how this phenomenon, may be retarded by the mutagenesis of S52A, S52D, S80A, S80D, S52D/S80A, S276A, and S276D as well as repeating the inhibitor experiments with the immortalised astrocyte line. Understanding these better in an astrocyte cell line will enable further understanding concerning the mechanism by which AQP4 is translocated, which could potentially identify a drug target to retard the formation of cytotoxic oedemas.

5.1 Co-immunoprecipitation of HEK293 cells transfected with AQP4 WT, AQP4 S42D and AQP4 S80D

Although a possible mechanism based on the information we have found from analysis with inhibitors and mutants was derived, a better understanding as to whether any other proteins were binding to AQP4 as part of the translocation process was sensible to try and understand. This however proved very difficult in a model which was revearsable and quick. Co-immunoprecipitation was then used to identify any other proteins bound to AQP4. The protocol for co-iummunoprecipitation is detailed in the materials and methods. Figure 5.2 shows in the first column there are no bands, because there was no AQP4 present, so the antibodies could not bind to the AQP4 protein. However the other three columns showed slightly different results. S52D seems to have been divided into 4 bands, S80D on has 1 band at around 48kDa and AQP4 WT seems to have the same bands as S52 but they are a lot fainter aside from the band at approximately 48kDa which is significantly darker than the S52D mutant. An explanation of this is not that more proteins have bound to the AQP4, it just seems to be that we are observing the tetrameric, dimer, and monomer forms of the protein with

another band which, is very heavy and unidentifiable. For this information to be usful mass spectrometry analysis would be needed, which is a very specialised technique for proteins, and useful as part of a further study.

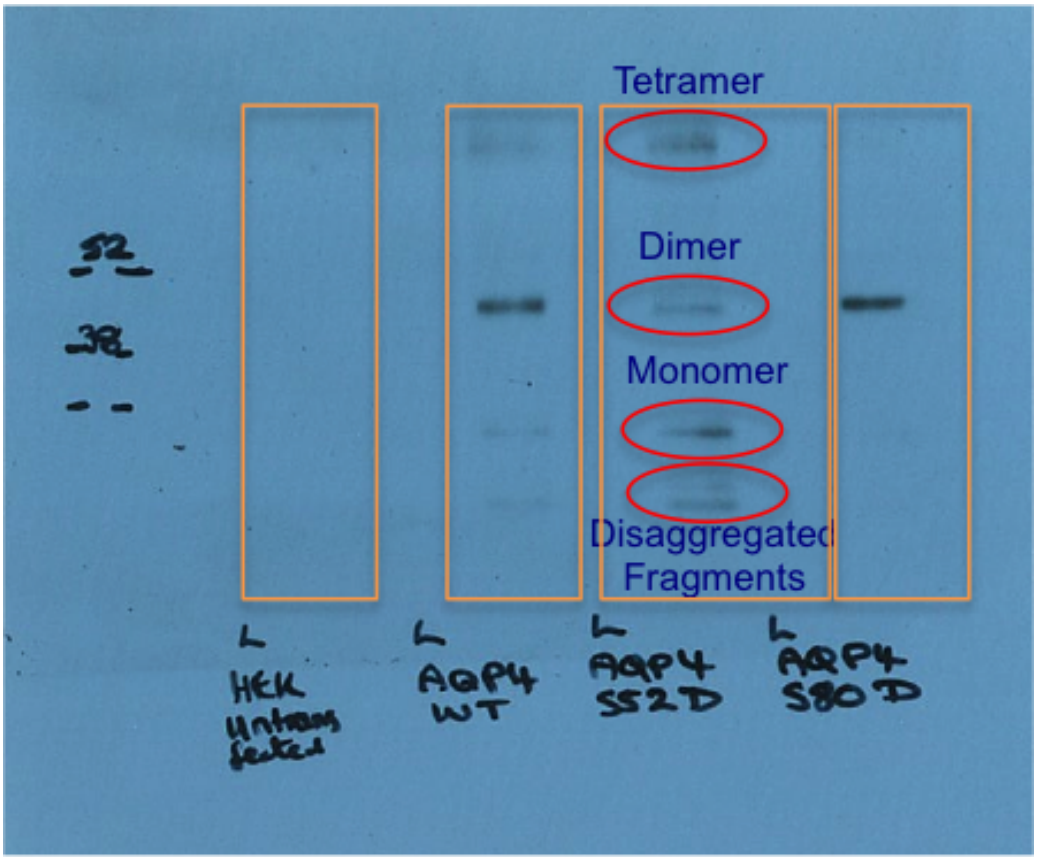

Figure 5.2: Western Blot of untransfected HEK293 with Transfected AQP4 WT, and 2 mutant AQP4, S52D and S80D. - This image shows the instability of AQP4 S52D in comparison to AQP4 wild type and AQP 280D, using untransfected HEK293

5.2 Nitrate and Nitrite Fluorometric Modified Greiss Assay

In the introduction and chapter 3, some aquaporins had been identified as potential nitrate and nitrite transporters. This is of particular interest as nitrate and nitrite are oxidative precursors for nitric oxide (a well known vasodilator), and it is well documented that tissues that are able to control and regulate the concentrations of nitrite and nitrate demonstrate better protection against hypoxic episodes, which can be directly linked to the formation of a cytotoxic oedema. To investigate this, a modified greiss assay published in nature protocols was used (122) which would enable analysis of nitrate and nitrite at very low concentrations. Initially this was done by transfecting all AQPs into HEK293 cell lines and measuring the levels, of nitrate and nitrite they uptake, following an incubation period. The results however, identified only one AQP to have any significant change from WT or control HEK293 cells, and that was AQP3 as shown in figure 5.3. This was initially a surprise as publications have identified AQP5, and AQP6 to potentially have a link to nitrate and nitrite transportation, however, AQP3 had been identified as an aquaglyceroporin, which could mean it was able to transport other small charged molecules and that it may not be selective to just transporting glycerol. Figure 5.3 shows the initial findings, and it was evident AQP3 had a marked increase in the amount of nitrite detected. However, when attempts were made to reproduce this experiment, it proved very difficult, the standard curves were rarely comparable, and concentrations were often too low to detect any fluorescence, even after months of trying to modify and optimise the nature protocol. An assumption was made that the water supply, although filtered using a milipore system, was unlikely to be able to reduce the high nitrate and nitrite content of UK water, and therefore was unable to distinguish the results from the background noise. Another reason could be that this experiment relied on transient transfection of HEK293, intrinsically this means that not all cells will have AQP4, and therefore the concentration of cells tested in the flurimeter may not have had sufficient AQP to demonstrate a marked increase in comparison. The protocol also required many washes, which caused cells to be

lost, and also for an osmotic equilibrium to be met.

It was therefore thought possible to be able to observe the cells under confocal microscopy to see if any cells exhibited a translocation response to a change in the concentration of extracellular nitrate and nitrite. The concentrations of nitrate and nitrite were varied from 20μM to 200μM, however there was no change in the FIP for any of the aquaporins.

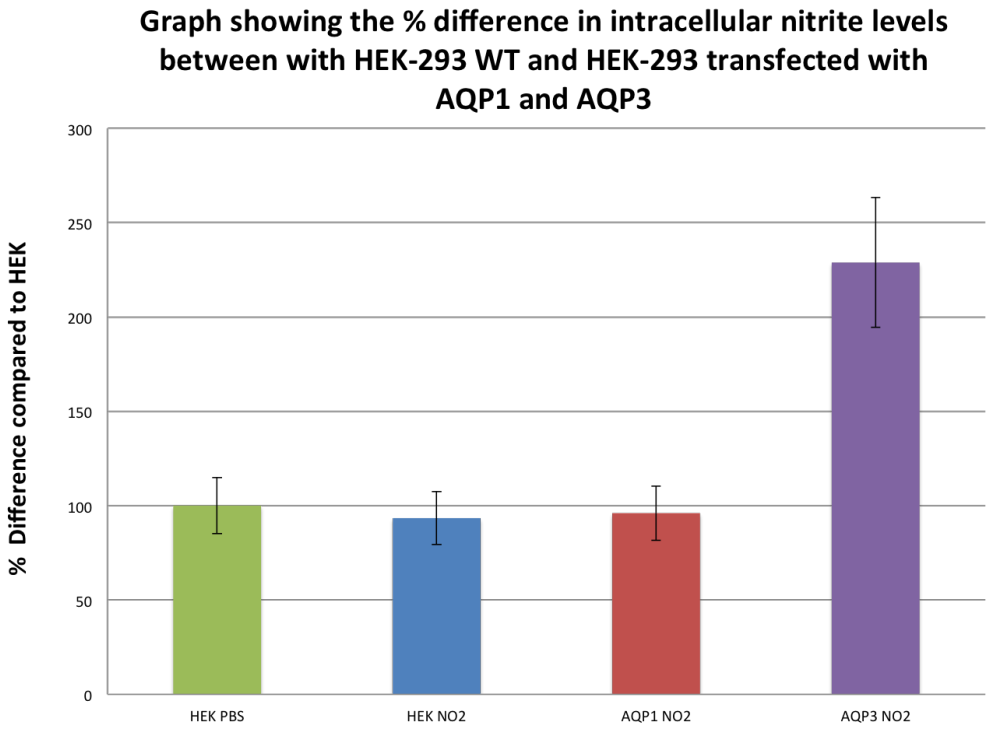

Figure 5.3: Uptake of nitrite into HEK293 cells transfected with AQP1 and AQP3, compared with HEK WT -

6

Discussion

This thesis has provided some very interesting developments and discoveries. We have characterised all known AQPs and were able to visualise their expression profiles and their response to extracellular changes in tonicity for AQP0, AQP1, AQP2, AQP3, AQP4, AQP5, and AQP12. This is useful to the wider scientific community as it gives insight into the subcellular localisation of these transporter proteins which can be found in a wide variety of tissue samples throughout the human body. This with further research and replication of our protocols will enable visualisation of these proteins and how they may be regulated to perform their individual roles in each tissue. For example, analysis of AQP3 and its function as an aquaglyceroporin can be better quantified using this visualisation technique, enabling more detailed research to be performed into its role within adipose cell lines, linking to diabetes (one of the largest causes of financial strains on Western health services).

We have also suggested a mechanism (figure 6.1) for the structure function of AQP4 as well as visualised and quantified its responses to changes in extracellular tonicities. This is a particularly interesting due to the discussion surrounding AQP4's involvement in the formation of a cytotoxic brain oedema. As we know AQP4 knockout mice demonstrated significant reduction in the pathological response in such disorders like acute cerebral ischemia (60), water intoxication (142)

(60) and traumatic brain injury. Our protocol, is a quick and easy methodology, which enables live observation of a cell's reaction to a change in extracellular tonicity, whilst also allowing visualisation of the expression profile of AQP4 as the external environment alters. These data coupled with Verkmann's findings using immunoprecipitation to identify expression profiles of AQP4 in astrocytic end feet, gives rise to evidence to support the relationship of AQP4 to the formation of a cytotoxic oedema

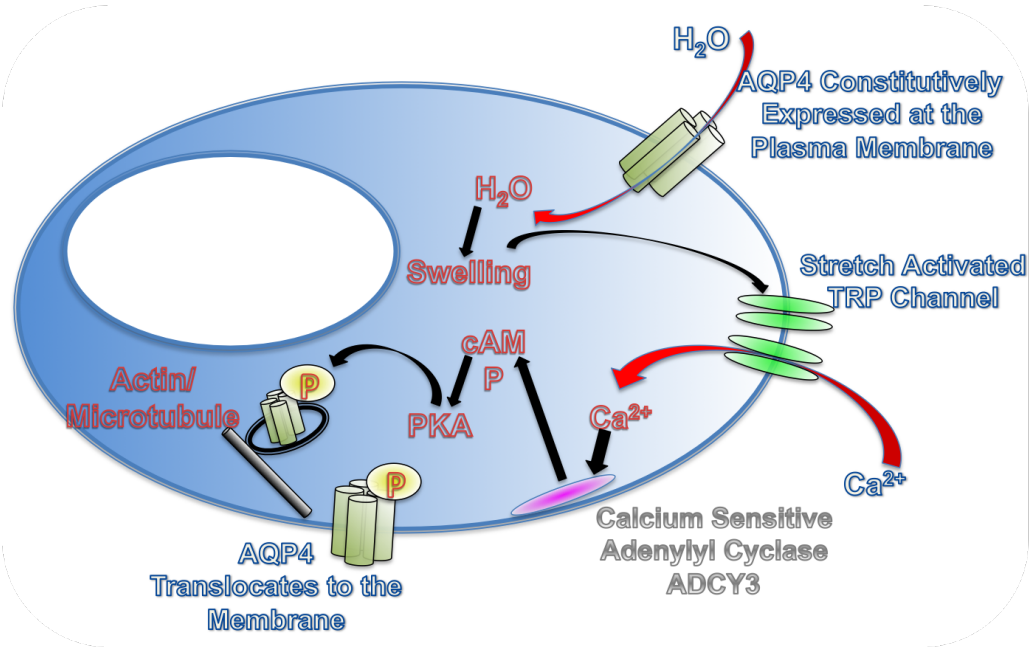

Figure 6.1: Schematic Representation of the AQP4 Translocation Activation Response to an Increase in Extracellular Hypotonicity - A model showing influx of water causes cell swelling that induces extracellular calcium entry leading to AQP4 translocation to the plasma membrane. This involved extracellular and intracellular calcium release, cytoskeletal filiamentation and activation of PKA.

Further research involving profiling libraries for known drugs that can cross the blood brain barrier (BBB) and disrupt a stage in the activation of AQP4, to translocate from an intracellular expression profile to a plasma membrane expres-

sion profile, could deliver real solutions to the formation of a cytotoxic oedema. For example a drug that can target the stretch activated TRP-channels, or inhibit the calcium influx mechanism, would prevent the translocation of AQP4 from the cytosol to the plasma membrane, which in turn prevents water building up on the brain in instotial pockets. This work can be made even more compelling by optimising the new and improved transfection protocol with TransIT 2020, so that more data can be collected in an immortalised astrocyte cell line, as this would give greater physiological relevance to the findings. However, if research were to be performed on tissue samples, a larger data sample would be required so as to give statistical significance to differences, negating the inherrent variance in the different tissues samples required for each treatment, making for a difficult comparison matrix.

Further interesting discoveries from this PhD have arisen due to the structural instability, and the retardation of the structure function response to a change in extracellular tonicity, for the AQP4 mutant S52D. Although it is clear that the S52 residue is not a phosphorylation site, the mutation of serine to aspartic acid and the hydrogen bonds formed between the polar head and the near by S80 residue, pose very interesting questions as to how this could prevent the translocation and potentially insertion of AQP4 into the plasma membrane. Although the Linear Dichroism experiment did not yield any results, further optimisation surrounding the technique could give the insight needed to understand if the mutant was preventing insertion into the plasma membrane. There is also an opportunity to model the mutant and its interaction with plasma membranes in more detail, using molecular modelling techniques. Although this is based on assumptions and leads you to an answer, it is still a very good method for focusing your work, as it may rule out more options initially than would have been possible just relying on experimental data. This information could then start to elucidate how AQP4 monomers dimerise, and insert into the membrane which as yet still remains a mystery. As we can see from the Western blot data that the S52D mutant seemed to exist in all states instead of its normal tetrameric state. This information could also prove useful and interesting as a drug target, however, the enclosed location

of S52 in the alpha helical twist 6.2, may prove difficult to access with a drug.

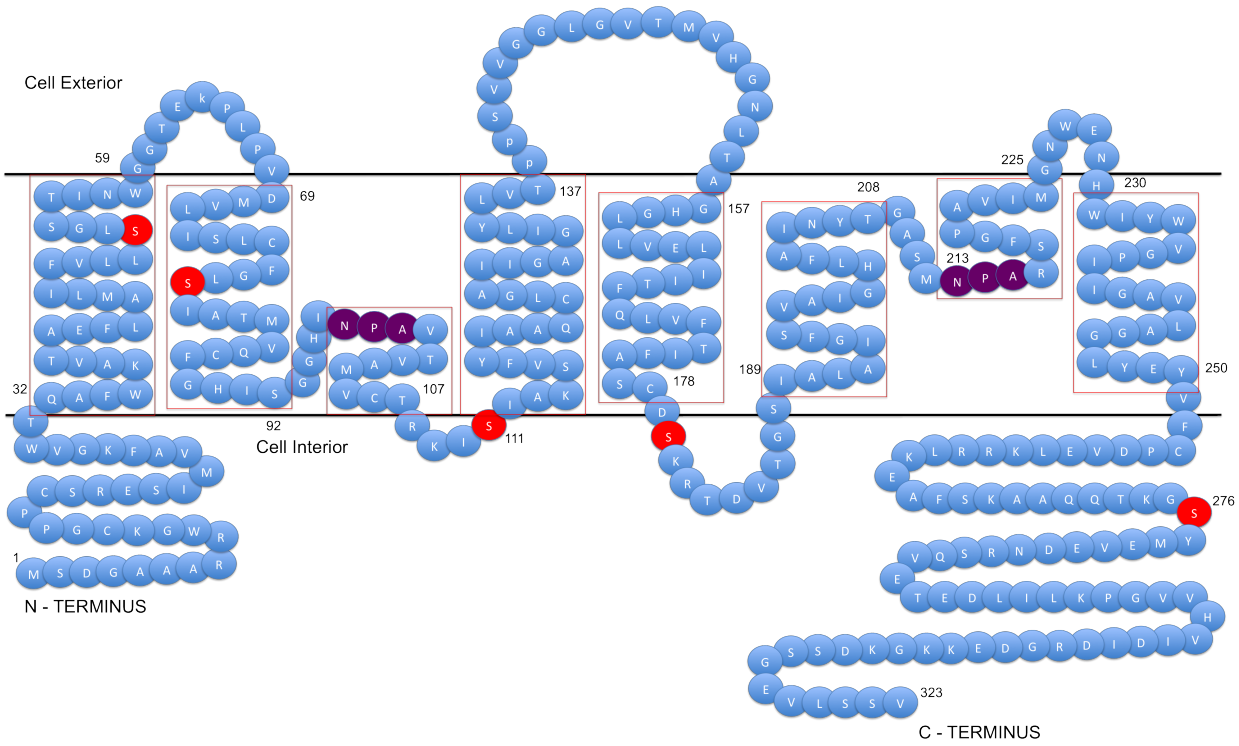

Figure 6.2: Primary Amino Acid Structure of AQP4 - Schematic representation of the primary amino acid structure of AQP4. The red coloured circles identify the PKA phosphorylation sites,(64).

As a result of the mutant analysis research we identified S276 to be a potential phosphorylation site (figure 6.2), however further modelling analysis is not currently possible, due to the truncated crytallographic structure meaning that S276 is not present. Therefore further research could be done to isolate a sequence based on the crystal structure without the N-terminal end being truncated, or statistical probabilities could be used to establish the most likely structure. S276D also did not seem constitutively expressed at the plasma membrane in an isotonic extracellular solution, however, if S276D was mimicking a phosphorylated AQP4 protein, we would expect AQP4 to appear to be constitutively expressed in the plasma membrane. The fact that it isn't, implies that it is not the only phospho-

rylation site required to activate AQP4 to translocate to the plasma membrane, however, it is essential. Further profiling of other potential phosphorylation site could be utilised to help identify the other phosphorylation sites involved.

In conclusion, this work has challenged the accepted published work and developed a quick and robust methodology for analysing and visualising, in real time, the effect of altering the extracellular tonicty, on the expression profile of AQPs. We have proposed a new mechanism for this translocation phenomenon in AQP4, and have evidenced its physiological relevance in astrocytes, for which we have now created a quick and robust methodology. We have published work, which has been credited by the F1000, and are currently in the process of writing another. We feel that this work has significantly impacted the development of this field, and will encourage further development, which in the future may identify a drug that can prevent the formation of a cytotoxic oedema.

References

[1] Donald DF Loo, Ernest M Wright, and Thomas Zeuthen. **Water pumps**. *The Journal of physiology*, **542**(1):53–60, 2002. 2

[2] Subrata Tripathi and Emile L Boulpaep. **Mechanisms of water transport by epithelial cells**. *Experimental Physiology*, **74**(4):385–417, 1989. 2

[3] Søren Nielsen, Chung-Lin Chou, David Marples, Erik Ilsø Christensen, Bellamkonda K Kishore, and Mark A Knepper. **Vasopressin increases water permeability of kidney collecting duct by inducing translocation of aquaporin-CD water channels to plasma membrane**. *Proceedings of the National Academy of Sciences*, **92**(4):1013–1017, 1995. 2

[4] Kristin Jäger, Dorothea Reh, Matthias Gebhardt, Ulrich Schaudig, Saadettin Sel, Lars Bräuer, and Friedrich Paulsen. **Expression Profile of Aquaporins in Human Nasolacrimal Duct Epithelium**. *Current eye research*, **35**(4):267–273, 2010. 2

[5] Carissa M Krane, James E Melvin, Ha-Van Nguyen, Linda Richardson, Jennifer E Towne, Thomas Doetschman, and Anil G Menon. **Salivary acinar cells from aquaporin 5-deficient mice have decreased membrane water permeability and altered cell volume regulation**. *Journal of Biological Chemistry*, **276**(26):23413–23420, 2001. 2

[6] MJ O'Donnell and SH Maddrell. **Paracellular and transcellular routes for water and solute movements across insect epithelia**. *Journal of Experimental Biology*, **106**(1):231–253, 1983. 2

[7] Seungho Choe, John M Rosenberg, Jeff Abramson, Ernest M Wright, and Michael Grabe. **Water permeation through the sodium-dependent galactose cotransporter vSGLT**. *Biophysical journal*, **99**(7):L56–L58, 2010. 5

[8] Gregory M Preston, T Piazza Carroll, William B Guggino, Peter Agre, et al. **Appearance of water channels in Xenopus oocytes expressing red cell CHIP28 protein**. *Science*, **256**(5055):385–387, 1992. 6

[9] Nicolas Guex and Manuel C Peitsch. **SWISS-MODEL and the Swiss-Pdb Viewer: An environment for comparative protein modeling**. *Electrophoresis*, **18**(15):2714–2723, 1997. 7

[10] Jochen S Hub, Helmut Grubmüller, and Bert L Groot. **Dynamics and energetics of permeation through aquaporins. What do we learn from molecular dynamics simulations?** *Aquaporins*, pages 57–76, 2009. 8

[11] Fatemeh Khalili-Araghi, James Gumbart, Po-Chao Wen, Marcos Sotomayor, Emad Tajkhorshid, and Klaus Schulten. **Molecular dynamics simulations of membrane channels and transporters**. *Current opinion in structural biology*, **19**(2):128–137, 2009. 8

[12] Bert L De Groot, Tomaso Frigato, Volkhard Helms, and Helmut Grubmüller. **The mechanism of proton exclusion in the aquaporin-1 water channel**. *Journal of molecular biology*, **333**(2):279–293, 2003. 8

[13] AS Verkman and Alok K Mitra. **Structure and function of aquaporin water channels**. *American Journal of Physiology-Renal Physiology*, **278**(1):F13–F28, 2000. 8

[14] Alan S Verkman. **Aquaporins at a glance**. *Journal of Cell Science*, **124**(13):2107–2112, 2011. 8

[15] Peter Francis, Jean-Ju Chung, Masato Yasui, Vanita Berry, Anthony Moore, M Keith Wyatt, Graeme Wistow, Shomi S Bhattacharya, and Peter Agre. **Functional impairment of lens aquaporin in two families with dominantly inherited cataracts**. *Human molecular genetics*, **9**(15):2329–2334, 2000. 9

[16] Alberto Ruiz and Dean Bok. **Characterization of the 3 UTR sequence encoded by the AQP-1 gene in human retinal pigment epithelium**. *Biochimica et Biophysica Acta (BBA)-Biomembranes*, **1282**(2):174–178, 1996. 9

[17] XUEJUN Li, HEMING Yu, and SS Koide. **The water channel gene in human uterus.** *Biochemistry and molecular biology international*, **32**(2):371, 1994. 9

[18] Thomas Walz, Barbara L Smith, Peter Agre, and Andreas Engel. **The three-dimensional structure of human erythrocyte aquaporin CHIP.** *The EMBO journal*, **13**(13):2985, 1994. 9

[19] Peter MT Deen, Marian AJ Verdijk, NVAM Knoers, Bé Wieringa, Leo AH Monnens, CH van Os, and BA van Oost. **Requirement of human renal water channel aquaporin-2 for vasopressin-dependent concentration of urine**. *Science-AAAS-Weekly Paper Edition-including Guide to Scientific Information*, **264**(5155):92–94, 1994. 9

[20] Nathalie Roudier, Pierre Ripoche, Pierre Gane, Pierre Yves Le Pennec, Geoff Daniels, Jean-Pierre Cartron, and Pascal Bailly. **AQP3 deficiency in humans and the molecular basis of a novel blood group system, GIL**. *Journal of Biological Chemistry*, **277**(48):45854–45859, 2002. 9

[21] Kenichi Ishibashi, Sei Sasaki, Fumiko Saito, Tatsuro Ikeuchi, and Fumiaki Marumo. **Structure and chromosomal localization of a human water channel (AQP3) gene**. *Genomics*, **27**(2):352–354, 1995. 9

[22] Toshio Ota, Yutaka Suzuki, Tetsuo Nishikawa, Tetsuji Otsuki, Tomoyasu Sugiyama, Ryotaro Irie, Ai Wakamatsu, Koji Hayashi, Hiroyuki Sato, Keiichi Nagai, et al. **Complete sequencing and characterization of 21,243 full-length human cDNAs**. *Nature genetics*, **36**(1):40–45, 2003. 9

[23] Daniela S Gerhard, L Wagner, EA Feingold, CM Shenmen, LH Grouse, G Schuler, SL Klein, S Old, R Rasooly, P Good, et al. **The status, quality, and expansion of the NIH full-length cDNA project: the Mammalian Gene Collection (MGC)**. *Genome research*, **14**(10b):2121, 2004. 9

[24] Baoxue Yang, Tonghui Ma, and AS Verkman. **cDNA cloning, gene organization, and chromosomal localization of a human mercurial insensitive water channel**. *Journal of Biological Chemistry*, **270**(39):22907–22913, 1995. 9

[25] Takumi Misaka, Keiko Abe, Kyoko Iwabuchi, Yuko Kusakabe, Masao Ichinose, Kazumasa Miki, Yasufumi Emori, and Soichi Arai. **A water channel closely related to rat brain aquaporin 4 is expressed in acid-and pepsinogen-secretory cells of human stomach**. *FEBS letters*, **381**(3):208–212, 1996. 9

[26] Tonghui Ma, Baoxue Yang, Wen-Lin Kuo, and AS Verkman. **cDNA cloning and gene structure of a novel water channel expressed exclusively in human kidney: evidence for a gene cluster of aquaporins at chromosome locus 12q13**. *Genomics*, **35**(3):543–550, 1996. 9

[27] Hiroshi Kuriyama, Shoko Kawamoto, Narihiro Ishida, Ikko Ohno, Shiro Mita, Yuji Matsuzawa, Kenichi Matsubara, and Kousaku Okubo. **Molecular cloning and expression of a novel human aquaporin from adipose tissue with glycerol permeability**. *Biochemical and biophysical research communications*, **241**(1):53–58, 1997. 9

[28] Nobuyuki Koyama, Kenichi Ishibashi, Michio Kuwahara, Naohiko Inase, Masahiko Ichioka, Sei Sasaki, and Fumiaki Marumo. **Cloning and functional expression of human aquaporin8 cDNA and analysis of its gene**. *Genomics*, **54**(1):169–172, 1998. 9

[29] Tobias Sjöblom, Siân Jones, Laura D Wood, D Williams Parsons, Jimmy Lin, Thomas D Barber, Diana Mandelker, Rebecca J Leary, Janine Ptak, Natalie Silliman, et al. **The consensus coding sequences of human breast and colorectal cancers**. *science*, **314**(5797):268–274, 2006. 9

[30] Kenichi Ishibashi, Michio Kuwahara, Yong Gu, Yujiro Tanaka, Fumiaki Marumo, and Sei Sasaki. **Cloning and functional expression of a new aquaporin (AQP9) abundantly expressed in the peripheral leukocytes permeable to water and urea, but not to glycerol**. *Biochemical and biophysical research communications*, **244**(1):268–274, 1998. 9

[31] Jesper V Olsen, Blagoy Blagoev, Florian Gnad, Boris Macek, Chanchal Kumar, Peter Mortensen, and Matthias Mann. **Global, in vivo, and site-specific phosphorylation dynamics in signaling networks**. *Cell*, **127**(3):635–648, 2006. 9

[32] Satoru Hatakeyama, Yutaka Yoshida, Tatsuo Tani, Yu Koyama, Kouei Nihei, Kazufumi Ohshiro, Jun-Ichi Kamiie, Eishin Yaoita, Takeyasu Suda, Katsuyoshi Hatakeyama, et al. **Cloning of a new aquaporin (AQP10) abundantly expressed in duodenum and jejunum**. *Biochemical and biophysical research communications*, **287**(4):814–819, 2001. 9

[33] Kenichi Ishibashi, Makoto Suzuki, and Masashi Imai. **Molecular cloning of a novel form (two-repeat) protein related to voltage-gated sodium and calcium channels**. *Biochemical and biophysical research communications*, **270**(2):370–376, 2000. 9

[34] Tetsuji Otsuki, Toshio Ota, Tetsuo Nishikawa, Koji Hayashi, Yutaka Suzuki, Jun-ichi Yamamoto, Ai Wakamatsu, Kouichi Kimura, Katsuhiko Sakamoto, Naoto Hatano, et al. **Signal sequence and keyword trap in silico for selection of full-length human cDNAs encoding secretion or membrane proteins from oligo-capped cDNA libraries**. *DNA Research*, **12**(2):117–126, 2005. 9

[35] Tomohiro Itoh, Tatemitsu Rai, Michio Kuwahara, Shigeru BH Ko, Shinichi Uchida, Sei Sasaki, and Kenichi Ishibashi. **Identification of a novel aquaporin, AQP12, expressed in pancreatic acinar cells**. *Biochemical and biophysical research communications*, **330**(3):832–838, 2005. 9

[36] Philip; Conner Alex.C Day, Rebecca E.; Kitchen. **Human aquaporins: Regulators of transcellular water flow**. *Biochimica et Biophysica Acta (BBA)-Biomembranes*, **1840**(5):1492–1506, May 2014. 10, 17

[37] P Agre, AM Saboori, A Asimos, and BL Smith. **Purification and partial characterization of the Mr 30,000 integral membrane protein associated with the erythrocyte Rh (D) antigen.** *Journal of Biological Chemistry*, **262**(36):17497–17503, 1987. 8

[38] Ali M Saboori, Barbara L Smith, and Peter Agre. **Polymorphism in the Mr 32,000 Rh protein purified from Rh (D)-positive and-negative erythrocytes**. *Proceedings of the National Academy of Sciences*, **85**(11):4042–4045, 1988. 8

[39] Bradley M Denker, BL Smith, FP Kuhajda, and P Agre. **Identification, purification, and partial characterization of a novel Mr 28,000 integral membrane protein from erythrocytes and renal tubules.** *Journal of Biological Chemistry*, **263**(30):15634–15642, 1988. 11

[40] Kiyohide Fushimi, Shinichi Uchida, Y Hara, Yukio Hirata, Fumiaki Marumo, Sei Sasaki, et al. **Cloning and expression of apical membrane water channel of rat kidney collecting tubule**. *Nature*, **361**(6412):549–552, 1993. 11

[41] Sei Sasaki. **Aquaporin 2: From its discovery to molecular structure and medical implications**. *Molecular Aspects of Medicine*, 2012. 11, 13

[42] Yumi Yamashita, Keiji Hirai, Yoshifumi Katayama, Kiyohide Fushimi, Sei Sasaki, and Fumiaki Marumo. **Mutations in sixth transmembrane domain of AQP2 inhibit its translocation induced by vasopression**. *American Journal of Physiology-Renal Physiology*, **278**(3):F395–F405, 2000. 11

[43] Søren Nielsen, Jørgen Frøkiær, David Marples, Tae-Hwan Kwon, Peter Agre, and Mark A Knepper. **Aquaporins in the kidney: from molecules to medicine**. *Physiological Reviews*, **82**(1):205–244, 2002. 11

[44] PETER H Baylis. **Osmoregulation and control of vasopressin secretion in healthy humans**. *American Journal of Physiology-Regulatory, Integrative and Comparative Physiology*, **253**(5):R671–R678, 1987. 11

[45] GL Robertson. **Physiology of ADH secretion.** *Kidney international. Supplement*, **21**:S20, 1987. 11

[46] Daniel G Bichet et al. **Nephrogenic diabetes insipidus.** *The American journal of medicine*, **105**(5):431, 1998. 11

[47] Kiyohide Fushimi, Sei Sasaki, and Fumiaki Marumo. **Phosphorylation of serine 256 is required for cAMP-dependent regulatory exocytosis of the aquaporin-2 water channel**. *Journal of Biological Chemistry*, **272**(23):14800–14804, 1997. 11, 82

[48] TOSHIYA Katsura, CORINNE E Gustafson, DENNIS A Ausiello, and DENNIS Brown. **Protein kinase A phosphorylation is involved in regulated exocytosis of aquaporin-2 in transfected LLC-PK1 cells**. *American Journal of Physiology-Renal Physiology*, **272**(6):F816–F822, 1997. 11, 66, 82

[49] EJ Kamsteeg, I Heijnen, CH Van Os, and PMT Deen. **The subcellular localization of an aquaporin-2 tetramer depends on the stoichiometry of phosphorylated and nonphosphorylated monomers**. *The Journal of cell biology*, **151**(4):919–930, 2000. 11

[50] Goro Nishimoto, Marina Zelenina, Dailin Li, Masato Yasui, Anita Aperia, Søren Nielsen, and Angus C Nairn. **Arginine vasopressin stimulates phosphorylation of aquaporin-2 in rat renal tissue**. *American Journal of Physiology-Renal Physiology*, **276**(2):F254–F259, 1999. 11

[51] Marina Zelenina, Birgitte Mønster Christensen, Johan Palmér, Angus C Nairn, Søren Nielsen, and Anita Aperia. **Prostaglandin E2 interaction with AVP: effects on AQP2 phosphorylation and distribution**. *American Journal of Physiology-Renal Physiology*, **278**(3):F388–F394, 2000. 11

[52] Jason D Hoffert, Trairak Pisitkun, Guanghui Wang, Rong-Fong Shen, and Mark A Knepper. **Quantitative phosphoproteomics of vasopressin-sensitive renal cells: regulation of aquaporin-2 phosphorylation at two sites**. *Proceedings of the National Academy of Sciences*, **103**(18):7159–7164, 2006. 11

[53] Robert A Fenton, Hanne B Moeller, Jason D Hoffert, Ming-Jiun Yu, Søren Nielsen, and Mark A Knepper. **Acute regulation of aquaporin-2 phosphorylation at Ser-264 by vasopressin**. *Proceedings of the National Academy of Sciences*, **105**(8):3134–3139, 2008. 13

[54] Jason D Hoffert, Jakob Nielsen, Ming-Jiun Yu, Trairak Pisitkun, Stephen M Schleicher, Soren Nielsen, and Mark A Knepper. **Dynamics of aquaporin-2 serine-261 phosphorylation in response to short-term vasopressin treatment in collecting duct**. *American Journal of Physiology-Renal Physiology*, **292**(2):F691–F700, 2007. 13

[55] Hua Jenny Lu, Toshiyuki Matsuzaki, Richard Bouley, Udo Hasler, Quan-Hong Qin, and Dennis Brown. **The phosphorylation state of serine 256 is dominant over that of serine 261 in the regulation of AQP2 trafficking in renal epithelial cells**. *American Journal of Physiology-Renal Physiology*, **295**(1):F290–F294, 2008. 13

[56] Luke Xie, Jason D Hoffert, Chung-Lin Chou, Ming-Jiun Yu, Trairak Pisitkun, Mark A Knepper, and Robert A Fenton. **Quantitative analysis of aquaporin-2 phosphorylation**. *American Journal of Physiology-Renal Physiology*, **298**(4):F1018–F1023, 2010. 13

[57] Hanne B Moeller, Mark A Knepper, and Robert A Fenton. **Serine 269 phosphorylated aquaporin-2 is targeted to the apical membrane of collecting duct principal cells**. *Kidney international*, **75**(3):295–303, 2008. 13

[58] Hanne B Moeller, Nanna MacAulay, Mark A Knepper, and Robert A Fenton. **Role of multiple phosphorylation sites in the COOH-terminal tail of aquaporin-2 for water transport: evidence against channel gating**. *American Journal of Physiology-Renal Physiology*, **296**(3):F649–F657, 2009. 13

[59] Jonathan M Crane and Alan S Verkman. **Determinants of aquaporin-4 assembly in orthogonal arrays revealed by live-cell single-molecule fluorescence imaging**. *Journal of cell science*, **122**(6):813–821, 2009. 13

[60] Geoffrey T Manley, Miki Fujimura, Tonghui Ma, Nobuo Noshita, Ferda Filiz, Andrew W Bollen, Pak Chan, and AS Verkman. **Aquaporin-4 deletion in mice reduces brain edema after acute water intoxication and ischemic stroke**. *Nature medicine*, **6**(2):159–163, 2000. 13, 22, 68, 123, 124

[61] Marios C Papadopoulos and AS Verkman. **Aquaporin-4 gene disruption in mice reduces brain swelling and mortality in pneumococcal meningitis**. *Journal of Biological Chemistry*, **280**(14):13906–13912, 2005. 13

[62] Marios C Papadopoulos, Geoffrey T Manley, Sanjeev Krishna, and AS Verkman. **Aquaporin-4 facilitates reabsorption of excess fluid in vasogenic brain edema**. *The FASEB journal*, **18**(11):1291–1293, 2004. 14

[63] Orin Bloch, Marios C Papadopoulos, Geoffrey T Manley, and AS Verkman. **Aquaporin-4 gene deletion in mice increases focal edema associated with staphylococcal brain abscess**. *Journal of neurochemistry*, **95**(1):254–262, 2005. 14

[64] Papadopoulos Marios C Verkman, Alan S. **Aquaporin water channels in the nervous system**. *Nature Reviews Neuroscience*, **14**:216–277, April 2013. 14, 96, 126

[65] Jiang Li, Rajkumar V Patil, and AS Verkman. **Mildly abnormal retinal function in transgenic mice without Müller cell aquaporin-4 water channels**. *Investigative ophthalmology & visual science*, **43**(2):573–579, 2002. 14

[66] Jiang Li and AS Verkman. **Impaired hearing in mice lacking aquaporin-4 water channels**. *Journal of Biological Chemistry*, **276**(33):31233–31237, 2001. 14

[67] Daniel C Lu, Hua Zhang, Zsolt Zador, and AS Verkman. **Impaired olfaction in mice lacking aquaporin-4 water channels**. *The FASEB Journal*, **22**(9):3216–3223, 2008. 14

[68] Devin K Binder, Xiaoming Yao, Zsolt Zador, Thomas J Sick, Alan S Verkman, and Geoffrey T Manley. **Increased seizure duration and slowed potassium kinetics in mice lacking aquaporin-4 water channels**. *Glia*, **53**(6):631–636, 2006. 14

[69] Jennifer M Carbrey, Linhua Song, Yao Zhou, Masafumi Yoshinaga, Aleksandra Rojek, Yiding Wang, Yangjian Liu, Heidi L Lujan, Stephen E DiCarlo, Søren Nielsen, et al. **Reduced arsenic clearance**

and increased toxicity in aquaglyceroporin-9-null mice. *Proceedings of the National Academy of Sciences*, **106**(37):15956–15960, 2009. 14

[70] B Wu and E Beitz. **Aquaporins with selectivity for unconventional permeants**. *Cellular and Molecular Life Sciences*, **64**(18):2413–2421, 2007. 14

[71] Hiroyasu Tsukaguchi, Chairat Shayakul, Urs V Berger, Bryan Mackenzie, Sreenivas Devidas, William B Guggino, Alfred N van Hoek, and Matthias A Hediger. **Molecular characterization of a broad selectivity neutral solute channel**. *Journal of Biological Chemistry*, **273**(38):24737–24743, 1998. 14

[72] T Ma, M Hara, R Sougrat, J M Verbavatz, and A S Verkman. **Impaired stratum corneum hydration in mice lacking epidermal water channel aquaporin-3**. *J Biol Chem*, **277**(19):17147–17153, May 2002. 15

[73] M Hara, T Ma, and A S Verkman. **Selectively reduced glycerol in skin of aquaporin-3-deficient mice may account for impaired skin hydration, elasticity, and barrier recovery**. *J Biol Chem*, **277**(48):46616–46621, Nov 2002. 15

[74] M Hara and A S Verkman. **Glycerol replacement corrects defective skin hydration, elasticity, and barrier function in aquaporin-3-deficient mice**. *Proc Natl Acad Sci U S A*, **100**(12):7360–7365, Jun 2003. 15

[75] Mariko Hara-Chikuma, Eisei Sohara, Tatemitsu Rai, Masahito Ikawa, Masaru Okabe, Sei Sasaki, Shinichi Uchida, and AS Verkman. **Progressive Adipocyte Hypertrophy in Aquaporin-7-deficient Mice ADIPOCYTE GLYCEROL PERMEABILITY AS A NOVEL REGULATOR OF FAT ACCUMULATION**. *Journal of Biological Chemistry*, **280**(16):15493–15496, 2005. 15

[76] Toshiyuki Hibuse, Norikazu Maeda, Tohru Funahashi, Kaori Yamamoto, Azumi Nagasawa, Wataru Mizunoya, Ken Kishida, Kazuo Inoue, Hiroshi Kuriyama, Tadashi Nakamura, et al. **Aquaporin 7 deficiency is associated with development of obesity through activation of**

adipose glycerol kinase. *Proceedings of the National Academy of Sciences of the United States of America*, **102**(31):10993–10998, 2005. 15

[77] Norikazu Maeda, Toshiyuki Hibuse, and Tohru Funahashi. **Role of aquaporin-7 and aquaporin-9 in glycerol metabolism; involvement in obesity**. *Aquaporins*, pages 233–249, 2009. 15

[78] SHIZUO Hatashita, JUNPEI Koike, TADAO Sonokawa, and SHOZO Ishii. **Cerebral edema associated with craniectomy and arterial hypertension.** *Stroke*, **16**(4):661–668, 1985. 20

[79] CharlesS Houston and John Dickinson. **Cerebral form of high-altitude illness**. *The Lancet*, **306**(7938):758–761, 1975. 20

[80] John W Severinghaus. **Hypothetical roles of angiogenesis, osmotic swelling, and ischemia in high-altitude cerebral edema**. *Journal of Applied Physiology*, **79**(2):375–379, 1995. 20

[81] MD Yoichi Katayama and T Kawamata. **Edema fluid accumulation within necrotic brain tissue as a cause of the mass effect of cerebral contusion in head trauma patients**. In *Brain Edema XII*, pages 323–327. Springer, 2003. 21

[82] AW Unterberg, J Stover, B Kress, and KL Kiening. **Edema and brain trauma**. *Neuroscience*, **129**(4):1019–1027, 2004. 21, 22

[83] Erlend A Nagelhus, Yoshiyuki Horio, Atsushi Inanobe, Akikazu Fujita, Finn-m Haug, Søren Nielsen, Yoshihisa Kurachi, and Ole Petter Ottersen. **Immunogold evidence suggests that coupling of K+ siphoning and water transport in rat retinal Müller cells is mediated by a coenrichment of Kir4. 1 and AQP4 in specific membrane domains**. *Glia*, **26**(1):47–54, 1999. 22

[84] S Saadoun, MC Papadopoulos, and S Krishna. **Water transport becomes uncoupled from K+ siphoning in brain contusion, bacterial meningitis, and brain tumours: immunohistochemical case review**. *Journal of clinical pathology*, **56**(12):972–975, 2003. 22

[85] Zsolt Vajda, Michael Pedersen, Ernst-Martin Füchtbauer, Karin Wertz, Hans Stødkilde-Jørgensen, Endre Sulyok, Tamás Dóczi, John D Neely, Peter Agre, Jørgen Frøkiær, et al. **Delayed onset of brain edema and mislocalization of aquaporin-4 in dystrophin-null transgenic mice**. *Proceedings of the National Academy of Sciences*, **99**(20):13131–13136, 2002. 22

[86] Anthony Marmarou. **Pathophysiology of traumatic brain edema: current concepts**. In *Brain Edema XII*, pages 7–10. Springer, 2003. 22

[87] Egon MR Doppenberg, Sung C Choi, and Ross Bullock. **Clinical trials in traumatic brain injury: lessons for the future**. *Journal of neurosurgical anesthesiology*, **16**(1):87–94, 2004. 22

[88] Anthony Marmarou, JG Dunbar, and A Marmarou. **Modulation of aquaporin-4 water transport in a model of TBI**. In *Brain Edema XII*, pages 261–263. Springer, 2003. 22

[89] Hajime Arima, Naoki Yamamoto, Kazuya Sobue, Fuminori Umenishi, Toyohiro Tada, Hirotada Katsuya, and Kiyofumi Asai. **Hyperosmolar mannitol stimulates expression of aquaporins 4 and 9 through a p38 mitogen-activated protein kinase-dependent pathway in rat astrocytes**. *Journal of Biological Chemistry*, **278**(45):44525–44534, 2003. 22

[90] Jérôme Badaut, Lorenz Hirt, Cristina Granziera, Julien Bogousslavsky, Pierre J Magistretti, and Luca Regli. **Astrocyte-specific expression of aquaporin-9 in mouse brain is increased after transient focal cerebral ischemia**. *Journal of Cerebral Blood Flow & Metabolism*, **21**(5):477–482, 2001. 22

[91] Jérôme Badaut, François Lasbennes, Pierre J Magistretti, and Luca Regli. **Aquaporins in Brain: Distribution, Physiology, and Pathophysiology**. *Journal of Cerebral Blood Flow & Metabolism*, **22**(4):367–378, 2002. 22

[92] J Badaut, JF Brunet, L Grollimund, MF Hamou, PJ Magistretti, JG Villemure, and Luca Regli. **Aquaporin 1 and aquaporin 4 expres-**

sion in human brain after subarachnoid hemorrhage and in peritumoral tissue. In *Brain Edema XII*, pages 495–498. Springer, 2003. 22

[93] Naoki Yamamoto, Kazuya Sobue, Masataka Fujita, Hirotada Katsuya, and Kiyofumi Asai. **Differential regulation of aquaporin-5 and-9 expression in astrocytes by protein kinase A**. *Molecular brain research*, **104**(1):96–102, 2002. 22

[94] John E Rash, Thomas Yasumura, C Sue Hudson, Peter Agre, and Søren Nielsen. **Direct immunogold labeling of aquaporin-4 in square arrays of astrocyte and ependymocyte plasma membranes in rat brain and spinal cord**. *Proceedings of the National Academy of Sciences*, **95**(20):11981–11986, 1998. 22

[95] Steven Allender, Vito Peto, Peter Scarborough, Anna Boxer, and Mike Rayner. **Coronary heart disease statistics**. 2012. 23

[96] Joy Adamson, Andy Beswick, and Shah Ebrahim. **Is stroke the most common cause of disability?** *Journal of Stroke and Cerebrovascular Diseases*, **13**(4):171–177, 2004. 23

[97] Michael Thain, Michael Hickman, Michael Abercrombie, CJ Hickman, and Minnie Louie Johnson Abercrombie. *The Penguin dictionary of biology*. Penguin Books, 1994. 23

[98] Intercollegiate Stroke Working Party. *National clinical guideline for stroke*. Royal College of Physicians of London, 2012. 23

[99] R Luengo-Fernandez, J Leal, and AM Gray. **UK research expenditure on dementia, heart disease, stroke and cancer: are levels of spending related to disease burden?** *European journal of Neurology*, **19**(1):149–154, 2012. 23

[100] A Aggarwal, P Aggarwal, M Khatak, and S Khatak. **Cerebral ischemic stroke: sequels of cascade**. *Int J Pharm Bio Sci*, **1**, 2010. 24

[101] I Lizasoain, A Cardenas, O Hurtado, C Romera, J Mallolas, P Lorenzo, J Castillo, and MA Moro. **Targets of cytoprotection in acute**

ischemic stroke: present and future. *Cerebrovascular Diseases*, **21**(Suppl. 2):1–8, 2006. 24

[102] Wade S Smith. **Pathophysiology of focal cerebral ischemia: a therapeutic perspective**. *Journal of vascular and interventional radiology*, **15**(1):S3–S12, 2004. 24

[103] Taku Sugawara, Miki Fujimura, Nobuo Noshita, Gyung Whan Kim, Atsushi Saito, Takeshi Hayashi, Purnima Narasimhan, Carolina M Maier, and Pak H Chan. **Neuronal death/survival signaling pathways in cerebral ischemia**. *NeuroRx*, **1**(1):17–25, 2004. 24

[104] Jin-Moo Lee, Margaret C Grabb, Gregory J Zipfel, Dennis W Choi, et al. **Brain tissue responses to ischemia**. *Journal of Clinical Investigation*, **106**(6):723–731, 2000. 24

[105] Peter Lipton. **Ischemic cell death in brain neurons**. *Physiological reviews*, **79**(4):1431–1568, 1999. 25

[106] Anthony Lau and Michael Tymianski. **Glutamate receptors, neurotoxicity and neurodegeneration**. *Pflügers Archiv-European Journal of Physiology*, **460**(2):525–542, 2010. 25

[107] Kuniyasu Niizuma, Hidenori Endo, and Pak H Chan. **Oxidative stress and mitochondrial dysfunction as determinants of ischemic neuronal death and survival**. *Journal of neurochemistry*, **109**(s1):133–138, 2009. 25

[108] Elżbieta Salińska, Wojciech Danysz, and Jerzy W Łazarewicz. **The role of excitotoxicity in neurodegeneration**. *Folia Neuropathol*, **43**(4):322–339, 2005. 25

[109] Stuart A Lipton. **Failures and successes of NMDA receptor antagonists: molecular basis for the use of open-channel blockers like memantine in the treatment of acute and chronic neurologic insults**. *NeuroRx*, **1**(1):101–110, 2004. 25

[110] Pierre J Magistretti and Igor Allaman. **Brain energy metabolism**. In *Neuroscience in the 21st Century*, pages 1591–1620. Springer, 2013. 25

[111] DavidG Nicholls. **Spare respiratory capacity, oxidative stress and excitotoxicity**. *Biochemical Society Transactions*, **37**(6):1385, 2009. 25

[112] Joaquín Jordán, Tomás Segura, David Brea, Maria F Galindo, and José Castillo. **Inflammation as therapeutic objective in stroke**. *Current pharmaceutical design*, **14**(33):3549–3564, 2008. 25

[113] Shyam S Sharma. **Emerging neuroprotective approaches in stroke treatment**. *Current Research & Information on Pharmaceutical Sciences*, **4**:8–12, 2003. 25

[114] Pak H Chan. **Reactive oxygen radicals in signaling and damage in the ischemic brain**. *Journal of Cerebral Blood Flow & Metabolism*, **21**(1):2–14, 2001. 25

[115] Leonardo Pantoni, Cristina Sarti, and Domenico Inzitari. **Cytokines and cell adhesion molecules in cerebral ischemia experimental bases and therapeutic perspectives**. *Arteriosclerosis, thrombosis, and vascular biology*, **18**(4):503–513, 1998. 25

[116] Alexander G Nikonenko, Lidija Radenovic, Pavle R Andjus, and Galyna G Skibo. **Structural features of ischemic damage in the hippocampus**. *The Anatomical Record*, **292**(12):1914–1921, 2009. 25

[117] Mia von Euler, Olof Bendel, Tjerk Bueters, Johan Sandin, and Gabriel von Euler. **Profound but transient deficits in learning and memory after global ischemia using a novel water maze test**. *Behavioural brain research*, **166**(2):204–210, 2006. 25

[118] Richard E Hartman, Jin M Lee, Greg J Zipfel, and David F Wozniak. **Characterizing learning deficits and hippocampal neuron loss following transient global cerebral ischemia in rats**. *Brain research*, **1043**(1):48–56, 2005. 25

[119] Howard S Kirshner, José Biller, and Alfred S Callahan. **Long-term therapy to prevent stroke**. *The Journal of the American Board of Family Practice*, **18**(6):528–540, 2005. 25

[120] Salvatore Cuzzocrea, Emanuela Mazzon, Giuseppina Costantino, Ivana Serraino, Laura Dugo, Giusy Calabrò, Giovanni Cucinotta, Angela De Sarro, and AP Caputi. **Beneficial effects of n-acetylcysteine on ischaemic brain injury**. *British journal of pharmacology*, **130**(6):1219–1226, 2000. 25

[121] Dong Hyun Kim, Byung Hoon Yoon, Yong-Won Kim, Seungjoo Lee, Bum Young Shin, Ji Wook Jung, Hyoung Ja Kim, Yong Sup Lee, Jae Sue Choi, Sun Yeou Kim, et al. **The seed extract of Cassia obtusifolia ameliorates learning and memory impairments induced by scopolamine or transient cerebral hypoperfusion in mice**. *Journal of pharmacological sciences*, **105**(1):82–93, 2007. 25

[122] Andreas K et al Nussler. *Fluometric measurement of nitrite/nitrate by 2,3-diaminonapthalene*, **1** of *1754-2189*. Nature Publishing Group, 2006. 59, 120

[123] Laura C. Green et al. *Analysis of Nitrate, Nitrite and [15N]nitrate in biological fluids*, **126** of *131-138*. Elsevier, 1982. 59

[124] J Gao, H Yu, Q Song, and X Li. **Establishment of HEK293 cell line expressing green fluorescent protein-aquaporin-1 to determine osmotic water permeability**. *Anal Biochem*, **342**(1):53–58, Jul 2005. 61

[125] R Horsefield, K Nordén, M Fellert, A Backmark, S Törnroth-Horsefield, A C Terwisscha van Scheltinga, J Kvassman, P Kjellbom, U Johanson, and R Neutze. **High-resolution x-ray structure of human aquaporin 5**. *Proc Natl Acad Sci U S A*, **105**(36):13327–13332, Sep 2008. 61

[126] Z Han and R V Patil. **Protein kinase A-dependent phosphorylation of aquaporin-1**. *Biochem Biophys Res Commun*, **273**(1):328–332, Jun 2000. 61

[127] F García, A Kierbel, M C Larocca, S A Gradilone, P Splinter, N F LaRusso, and R A Marinelli. **The water channel aquaporin-8 is mainly intracellular in rat hepatocytes, and its plasma membrane insertion is stimulated by cyclic AMP**. *J Biol Chem*, **276**(15):12147–12152, Apr 2001. 61

[128] H Yasui, M Kubota, K Iguchi, S Usui, T Kiho, and K Hirano. **Membrane trafficking of aquaporin 3 induced by epinephrine**. *Biochem Biophys Res Commun*, **373**(4):613–617, Sep 2008. 61

[129] P M Deen, M A Verdijk, N V Knoers, B Wieringa, L A Monnens, C H van Os, and B A van Oost. **Requirement of human renal water channel aquaporin-2 for vasopressin-dependent concentration of urine**. *Science*, **264**(5155):92–95, Apr 1994. 62

[130] S Nielsen, C L Chou, D Marples, E I Christensen, B K Kishore, and M A Knepper. **Vasopressin increases water permeability of kidney collecting duct by inducing translocation of aquaporin-CD water channels to plasma membrane**. *Proc Natl Acad Sci U S A*, **92**(4):1013–1017, Feb 1995. 62, 66

[131] M T Conner, A C Conner, J E Brown, and R M Bill. **Membrane trafficking of aquaporin 1 is mediated by protein kinase C via microtubules and regulated by tonicity**. *Biochemistry*, **49**(5):821–823, Feb 2010. 62, 80, 89, 91

[132] K Fushimi, S Sasaki, T Yamamoto, M Hayashi, T Furukawa, S Uchida, M Kuwahara, K Ishibashi, M Kawasaki, and I Kihara. **Functional characterization and cell immunolocalization of AQP-CD water channel in kidney collecting duct**. *Am J Physiol*, **267**(4 Pt 2):573–582, Oct 1994. 66

[133] T Saito, S E Ishikawa, S Sasaki, N Fujita, K Fushimi, K Okada, K Takeuchi, A Sakamoto, S Ookawara, T Kaneko, F Marumo, and T Saito. **Alteration in water channel AQP-2 by removal of AVP stimulation in collecting duct cells of dehydrated rats**. *Am J Physiol*, **272**(2 Pt 2):183–191, Feb 1997. 66

[134] Janne Lebeck. **Metabolic impact of the glycerol channels AQP7 and AQP9 in adipose tissue and liver**. *Journal of molecular endocrinology*, pages JME–13, 2014. 73, 74

[135] Matthew T Conner, Alex C Conner, Charlotte E Bland, Luke H J Taylor, James E P Brown, H Rheinallt Parri, and Roslyn M Bill.

Rapid aquaporin translocation regulates cellular water flow: mechanism of hypotonicity-induced subcellular localization of aquaporin 1 water channel. *J Biol Chem*, **287**(14):11516–25, Mar 2012. 79, 116

[136] ET AL ALBERTS, BRUCE. *Molecular Biology of the Cell*, **139-194.** Garland, New York, 1994. 79, 85

[137] DONALD VOET, JUDITH G VOET, AND CHARLOTTE W PRATT. **Fundamentals of biochemistry**. *Chap. V, Wiley & Sons, Chichester*, page 515, 1999. 82

[138] TIMOTHY A DUNN, DANIEL R STORM, AND MARLA B FELLER. **Calcium-dependent increases in protein kinase-A activity in mouse retinal ganglion cells are mediated by multiple adenylate cyclases**. *PloS one*, **4**(11):e7877, 2009. 91

[139] CATHERINE E. CREELEY. **Alcohol-induced apooptosis of oligodendrocytes in the fetal macaque brain**. *Acta Neuropathalogica Communications*, page 1:23, 2013. 91

[140] **Triggering the interferon response: the role of IRF-3 transcription factor** [online]. 96

[141] NICOLAS PEITSCH, MANUEL C; GUEX. **SWISS-MODEL and the Swiss-Pdb Viewer: An environment for comparative protein modeling**. *Electrophoresis*, **18**:2714–2723, 1997. 106

[142] ZSOLT; VERKMAN A.S YANG, BAOXUE; ZADOR. **Glial Cell Aquaporin-4 Overexpression in Transgenic Mice Accelerates Cytotoxic Brain Swelling**. *Journal of Biological Chemistry*, **283**(15280-15286), 2008. 123